MULTI PHOTON ABSORPTION PROCESSES INDUCED BY ULTRA-FAST LIGHT PULSES

im Fachbereich Physik der
Freien Universität Berlin
eingereichte Dissertation
von

Baidaa Khalifa Hamed

Berlin, 11 September 2015

Die in vorliegender Dissertation dargestellte Arbeit wurde in der Zeit zwischen Januar 2011 und August 2015 im Fachbereich Physik an der Freien Universität Berlin unter Betreuung von Prof. Dr. K. Heyne durchgeführt.

Erstgutachter: Prof. Dr. K. Heyne

Freie Universität Berlin

Zweitgutachterin: Prof. Dr. Ulrike Alexiev

Freie Universität Berlin

Date of the defence: 11 September 2015

Table of Contents

Acknowledgement

The great pyramid can only be made by great efforts, which are represented by great persons who supported me during my journey for learning.

Firstly, I would like to express my sincere gratitude to my supervisor Prof. Dr. Karsten. Heyne for his support, motivation, guidance as well as his immense scientific experience. Which facilitated many difficulties for me without his guidance and persistent help this thesis would not have been possible.

I owe a special thanks to Dr. Valeri Kozich for his infinite patience, guidance and from the initial to the final level of this research. He was like shining light in the dark road. Guiding me all the way.

My sincere thanks also go to Theodore von Haimberger for his support by programing and design of programs during the course of this research. My gratitude also goes to our group members.

I would like to thank Dr. Hazim Dway Al-Khuzai for his help in image-processing.
I would like to thank DAAD (German Iraqi Academic Exchange) for financial support, many people have been a part of my graduate education and I am highly grateful to all of them.

Last but not least I would like to thank my family: my loving mother from her I brought strength. My affectionate father who cared for me a lot. My husband for supporting me spiritually throughout writing this thesis and my life in general. And my precious son Amin who gave me a great motive to keep studying and be what I'm now.

For all I mention above …all love and respect

List of Figures

Abbreviations

TPA	*Two-photon absorption*
SPA	*Single-photon absorption*
TPEF	*Two-photon excited fluorescence*
OPA	*Optical parametric amplifier*
DFG	*Difference frequency generation*
SHG	*Second harmonic generation*
GVM	*Group velocity mismatch*
PDT	*Photodynamic therapy*
FWHM	*Full width at half maximum*
DMSO	*Dimethyl sulfoxide*
Mix	*Mixture solvent*

CHAPTER 1

Introduction

Two-photon absorption has attracted considerable interest in optics, biological and medical investigations where technologies, such as ultrashort pulse characterization [1-10], frequency up-conversion lasing [11-13], two-photon excitation microscopy [14-17], three-dimensional (3D) ultrahigh density optical data storage [18-20], 3D microfabrication [21,22], activating photosensitizers in photodynamic therapy (PDT) [23-25] and optical power limiting [26-28] are used.

The development of mode-locked ultrafast lasers in the 1990 provided a source of extremely high peak intensity light pulses that facilitate instantaneous two-photon processes. Also, there appeared an increasing demand for efficient two-photon absorbers, especially chromophores that are compatible with new technological and biological applications.
For example, PDT with two-photon excitation has an advantage due to the longer laser wavelength employed resulting in lower absorption and scattering by human tissues than visible light. This enables increased penetration of exciting light into a human body and can be used for two-photon excitation of biologically relevant molecules deep inside of the tissues. Then the advantage can be gained by two-photon absorption -based photodynamic therapy, which uses excitation by light of a drug inside of the body as a first step of photophysical and photochemical processes leading to tumor destruction. The use of near-IR light for two-photon excitation of photosensitizers can greatly increase the efficiency of PDT.

The ultimate success of any of the two-photon-based applications critically depends on the efficiency of the two-photon absorption, in particular, on the value of intrinsic nonlinear cross section. So far, two-photon absorption properties of only a limited number of molecules have been known. Lack of reliable spectroscopic data has been holding back the search for new

efficient two-photon absorbers. In particular, almost no information has been available on two-photon absorption properties of biologically relevant tetrapyrrolic molecules.

In this respect, study of the two-photon absorption properties of organic molecules, especially those compatible with biological and medical applications, is of great importance. Compounds of the tetrapyrrole type perform several crucial functions in nature, such as oxygen transportation (breathing), photosynthesis, etc. They have found considerable interest in this respect as they already play a strong role as photosensitizers in PDT [29] and due to the fact that some of them exhibit high two-photon absorption cross-sections [30]. For these reasons, a comprehensive investigation of the two-photon absorption properties of tetrapyrroles is rather important.

Here we present a comparative investigation of the two-photon excitation of six photosensitizers of the porphyrin type: 5,10,15,20-tetrakis (m-hydroxyphenyl) porphyrin (m-THPP), chlorin 5,10,15,20-tetrakis (m-hydroxyphenyl) chlorin (m-THPC, Foscan, temoporfin), palladium 5,10,15,20-tetrakis (3-hydroxyphenyl)-porphyrinato-palladium-(II) (m-THPP-PD), 5,15-Bis-(4-carboxphenyl)-10,20-dihexyl-porphyrin (m-TCP-PD), Al(tpfc)py_1 and Al(tpfc)py_2 type 5,10,15 tris (pentafluorophenyl) corrole in the spectral range of 1.04–1.45 μm.

We also paid attention to the polarization effect. We measured the two-photon absorption cross-sections for linear and circular polarized exciting pulses. The polarization effects can reveal important information about photophysical properties of the organic compounds. It can provide information about the angle between dipole moments, symmetry of excited states.

We did image-processing for applications, it can be seen in Appendix A.

Finally, it has been studied the influence of solvents on the two-photon absorption process and it has been found that the TPA cross section increases with increasing the polarity of solvents.

CHAPTER 2

Two-Photon Processes

2.1 Introduction to the Two-Photon Absorption

The phenomenon of two-photon absorption (TPA) was first predicted by Göppert-Mayer in 1931[31]. Thirty years later, the first experiments on TPA were done by Kaiser and Garret. They illuminated a europium-doped crystal (CaF_2) [32] containing Eu^{2+} ions, demonstrating the existence of two-photon excitation.

Two-photon absorption is a nonlinear process in which two photons of identical or different frequencies are simultaneously absorbed by the same species exciting the molecule from one state (usually the ground state) to a higher energy electronic state. The difference in the energy between the two involved states of the molecule is equal to the sum of the two photons energies. The energy of both photons which absorbed by the molecule is:

$$h\nu_1 + h\nu_2 = E \qquad (2.1)$$

where h is the Plank constant, ν_i is the frequency of the i-th absorbed photon, E is the transition energy.

As it shown in Fig.2.1 (a), there is no real intermediate level populated in this process, both photons are absorbed simultaneously through a virtual level, while in (b), the stepwise two photon process can be divided into two distinctive single photon processes. Every level is physically populated, which can be registered by means of transient spectroscopy. The next level in the sequence is populated only after the previous one.

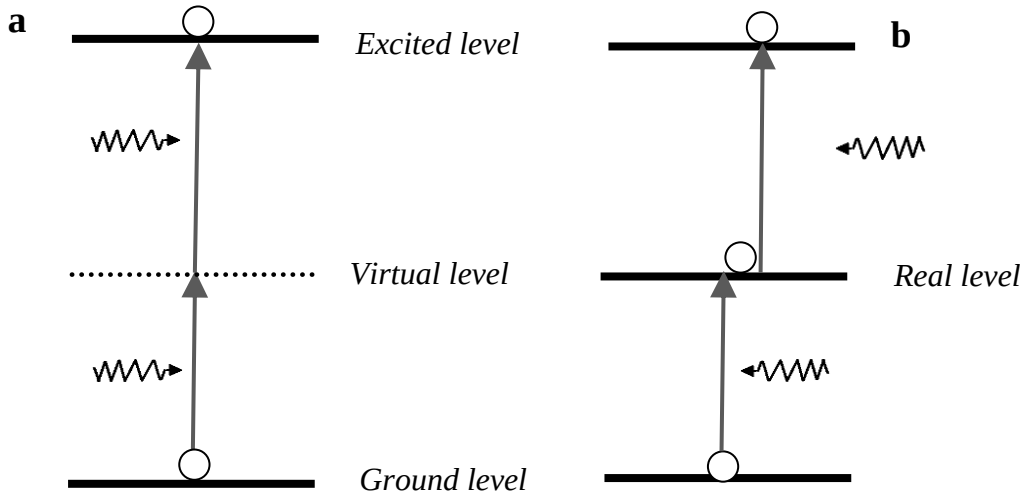

Figure 2.1 *Graphical representations of a simultaneous and a stepwise two photon absorption. (a) Simultaneous two photon process. (b) Stepwise two photon process.*

The magnitude of the two-photon absorption is proportional to the square of the light intensity. It is a nonlinear process. Single photon absorption is a linear process since it is related linearly to the intensity of light. This is a major difference between one and two-photon absorption. In TPA two photon of twice the wavelength-half of the energy combine to provide the energy needed for the transition. In two-photon absorption there is no need for an intermediate state to populate before arriving at the final state. Instead of this intermediate state, the electron is excited to a virtual state (Fig.2.1a.) allowed by quantum mechanics. Note, that this effect is completely different from stepwise absorption, in which case there are real intermediate levels involved that are populated (Fig.2.1b). The virtual state is accessible when the molecules absorb the first photon. For TPA to occur a basically simultaneous absorption of two photons take place via a virtual state in a medium. Thus TPA is a third order nonparametric process, the selection rules for TPA process are different from that of single-photon absorption [33]. The TPA is an interesting spectroscopic tool because of the applicable parity selection rules which differs from those of single photon absorption (SPA), as for example in the case of centrosymmetric molecules. Single photon transitions are allowed only between states of different parity, i.e. ungerade ↔ gerade. whereas two-photon transitions are permitted

between states of the same parity, i.e. gerade ↔ gerade and ungerade ↔ ungerade. Since the ground level is usually of gerade parity, TPA simplifies the investigation of excited gerade parity levels that are usually very difficult to access by ordinary linear absorption spectroscopy. Consequently, TPA spectroscopy greatly increases our understanding of molecular properties. Therefore, it opens up the possibility of probing transitions which are inaccessible under single-photon excitation [34-36].

Some of the properties that make TPA attractive for practical applications are: the excitation of the molecules selectively in a small volume $\sim \lambda^3$, and the beam initiating the TPA has a longer in comparison with the SPA wavelength and it penetrates deeper in the tissue.

Two-photon absorption is a nonlinear process which means that the transmittance of the material depends on the light intensity and this is of particular interest to various applications such as optical data storage [37, 38], fluorescence imaging [39], up converting lasing [40, 41], activating photosensitizers in photodynamic therapy (PDT) [42-45] optical power limiting [46], two-photon microscopy [47] and two-photon induced biological caging studies [48], three-dimensional (3D) ultrahigh density optical data storage [49-51], 3D microfabrication [52-56], and optical power limiting [57-59].

These applications exploit the important features of TPA which is the access to the highly energetic excited states by using comparatively low energy photons and the quadratic dependence of the absorption process. Due to the quadratic dependence of the TPA process, spatial selectivity is obtained by using focused beam.

In these applications, especially in photodynamic therapy (PDT), which will be explained in details in chapter 4, and two photon fluorescence microscopy, the aim is to achieve deeper penetration into the biological tissues. The near-IR light, which is typically used for two-photon excitation, is scattered and absorbed by human tissues much less than is visible light. This enables deeper penetration of the exciting light into the human body and can be used for two-photon excitation of biologically relevant molecules deep inside tissues. As a consequence, TPA-based fluorescence microscopy that employs excitation of near-IR light

provides imaging of the tissues of magnitude an order deeper than one-photon confocal fluorescence microscopy using visible light.

Two-photon excitation of photosensitizers using the near-IR light can greatly increase the efficiency of PDT because using excitation of a photosensitizer molecule inside the body as a first step of photophysical and photochemical processes leading to tumor damage, whereas the single photon absorption based PDT can treat only tumors which either sit close to the surface or are accessible by endoscope.

In the visible region of the spectrum the use of two photon absorption in the optical power limiting has a major importance for the protection of the eyes [60]. Until today a large number of studies about photosensitizers which takes advantage of the conventional single photon absorption phenomenon have been published. However, very few studies have been devoted to evolving photosensitizers which absorbs two-photon simultaneously [61]. Another application of the TPA is microfabrication. It utilizes the two photon absorption mechanisms and has attracted attention recently [62].

One of the important application areas of the TPA technique is two-photon microscopy. It was first introduced by the German scientist Winfried Denk [63]. Two-photon microscopy is useful because at a longer wavelength, less scattering occurs than at the shorter wavelengths [63-65].

To provide diffraction-limited 3D resolution, one can effectively confine two-photon excitation to the small focal volume by focusing laser light in a two-photon absorbing medium, This is particularly important for 3D microfabrication, high-density 3D optical data storage and two-photon fluorescence microscopy. The excitation wavelength in a two-photon transition is typically much longer and well separated from the fluorescence wavelength. This greatly facilitates the registration of two-photon fluorescence, because fluorescence and excitation photons can be easily separated by filters. Two-photon fluorescence is also employed to readout high density 3D optical data storage. Unconverted fluorescence permits lasing at new wavelengths where single photon pumping is inefficient.

The quadratic dependence of TPA on the excitation light intensity can be used to limit optical power. An ideal power limiter allows the light of low intensity to propagate without absorption, while high intensity light is strongly attenuated. Moreover, the immediate response of TPA can provide for effective cutoff even in the femtosecond time scale. Quadratic dependence of TPA on the excitation intensity allows measurements of cross-correlation functions or second order intensity autocorrelation and is used for short laser pulse characterization.

The final success of any of the applications which is based on two-photon absorption crucially depends on the efficiency of TPA, particularly, on the value of its nonlinear cross section (σ_2). Until now, the properties of TPA have been studied and known only for a limited number of molecules in adequate detail. The search for new efficient two-photon absorbers has been held back due to the lack of reliable spectroscopic data. Almost no information has been available on the properties of TPA of biologically relevant tetrapyrrolic compounds (porphyrins, chlorins, bacteriochlorins, and so on).

The study of the TPA properties of organic molecules, in particular those which apply to medicine and biology applications, is of great interest. As example, tetrapyrrolic molecules perform many critical functions in nature, such as oxygen transport (breathing), photosynthesis, etc. They are widely used in TPA-based PDT. For these reasons, an extensive spectroscopic investigation of the TPA properties of tetrapyrroles molecules is needed.

2.2 Methods for Measuring TPA Cross-Sections

The methods for determining the two photon cross-section were outlined by Alberta, Xu and Webb [61-64]. Two photon cross-sections of organic molecules can be measured by several techniques. The most common techniques are two-photon absorption (TPA) and two photon excited fluorescence (TPEF). Measuring the TPA cross-section is based on the measurement of the change in the transmittance when the pump beam intensity is varied.

In the TPEF experiments the integral efficiency of fluorescence induced due to TPA is measured. The two-photon-excited fluorescence signal is proportional to the TPA.

Measuring the absorption is a simpler experimental setup than that required for fluorescence measurements. But saturation, excited-state absorption and photo-bleaching can restrict the accuracy of the absorption measurements.

For both methods high pump power is required. Typically for these purposes Ti:Saphire laser systems and OPAs with ultra-short pulses are used.

2.2.1 Two-Photon Excited Fluorescence

Early observations of fluorescence were described by Bernardino de Sahagun. Sahagún studied fluorescence in 1560 and Nicolas Monardes in 1565 [66]. A fluorescent molecule is a molecule which has absorbed thermal energy or photons in a certain range of wavelengths. It becomes excited after absorbing light. An outer electron will jump from the ground state to the excited singlet or triplet state. Upon returning from the electronic excited state to the electronic ground state, it emits light at a different wavelength. The excited molecules may lose energy through a non-radiative process to reach the lowest vibrational level of the excited state. Fluorescence is then the radiative loss of energy as a photon is emitted from a molecule in the excited state returning to the ground state. Since a non-radiative loss of energy occurs between the absorption and subsequent fluorescence, the emitted photon is of lower frequency and a longer wavelength, than the absorbed photon producing a red shift between the absorbance and fluorescence spectra. However, when the absorbed electromagnetic radiation is intense, it is possible for molecule to absorb two photons, this two-photon absorption lead to emission of radiation having a shorter wavelength than the absorbed radiation. The emitted radiation may also be of the same wavelength as the absorbed radiation, termed “resonant fluorescence” [67].

The main disadvantage of fluorescence-based methods is that the molecules must fluoresce. In some cases, especially concerning fluorescence emitting molecules, fluorescence efficiency measurements can be more sensitive than the measurements of the change of transmission (nonlinear transmittance-based method).

The fluorescence quantum yield gives the collection efficiency of the fluorescence process. It is defined as the ratio of the number of photons emitted to the number of photons absorbed [68, 69].

$$\emptyset = \frac{number\ of\ the\ emitted\ photons}{number\ of\ the\ absorbed\ photons}$$

The TPEF cross section is linearly proportional to the TPA cross section, with the constant of proportionality being the fluorescence quantum efficiency (η_2) of the fluorescence molecule:

$$\sigma_{TPE} = \sigma_2 \eta_2 \qquad (2.2)$$

Two-photon cross section is determined using Albota, et al method [67, 70]. The number of the absorbed photons as a function of time N(t) in the focal volume of strongly focused illumination is related to the number of fluorescence photons per unit time F(t) [61, 62]:

$$\mathrm{F(t)} = \frac{1}{2}\,\emptyset\,\eta_2 \mathrm{N(t)} \qquad (2.3)$$

The $\frac{1}{2}$ factor accounts for the fact that two photons are being absorbed for every one photon emitted as fluorescence. The time averaged fluorescence emission < F(t) > can be measured experimentally with the spectrometer. When the incident optical field is in the form of pulses, the time-averaged fluorescence detected can be expressed as:

$$< F(\mathrm{t}) > \approx \frac{1}{2}\,\emptyset\,\eta_2 \sigma_2 \mathrm{C}\,\frac{\mathrm{g_p}}{\mathrm{f\,T}}\,\frac{8 < P(t) >^2}{\frac{\pi\lambda}{\mathrm{n}}} \qquad (2.4)$$

In equation (2.4) *C* is the concentration (in mole per cubic centimeters), *n* is the refractive index of the sample, < P(t) > is the time-averaged laser source power (in photons per second), λ is the excitation wavelength, T is the full width at half-maximum (FWHM) of the excitation pulse, and f is the pump pulse repetition rate. $\mathrm{g_p}$ is dimensionless and depends on the pulse

shape. The TPEF cross section, defined here as $\sigma_2\eta_2$ can thus be related to experimental variables by use of equation (2.4). It follows then that σ_2 is:

$$\sigma_2 = \frac{2 < F(t) >}{\eta_2 \emptyset\, C} \frac{f_T}{g_p} \frac{\pi\lambda}{8n < P(t)^2 >} \tag{2.5}$$

Equations (2.4) and (2.5) are not sufficient to determine σ_2 if the collection efficiency $\emptyset$ is not known for the experimental setup. The use of a reference standard with a known value of $\sigma_2(\lambda)$ allows the unknown σ_2 to be calculated as the ratio of the two individual equations:

$$\frac{< F(t) >_{ref}}{< F(t) >_{unkn}} = \frac{\emptyset_{ref}\eta_{2ref}\sigma_{2ref}C_{ref} < P_{ref}(t) >^2 n_{ref}}{\emptyset_{unkn}\eta_{2unkn}\sigma_{2unkn}C_{unkn} < P_{unkn}(t) >^2 n_{unkn}} \tag{2.6}$$

Solving for $\sigma_2$we get,

$$\sigma_{2unkn}(\lambda)\eta_{2unkn} = \frac{\emptyset_{ref}\eta_{2ref}\sigma_{2ref}C_{ref}}{\emptyset_{unkn}C_{unkn}} \frac{< P_{ref}(t) >^2 < F(t) >_{unkn}}{< P_{unkn}(t) >^2 < F(t) >_{ref}} \frac{n_{ref}}{n_{unkn}} \tag{2.7}$$

Two photon absorption cross-section σ_2 is mostly expressed in Goppert-Mayer unit (GM), where [1 GM = 10^{-50} (cm^4s / photon)]. The organic molecules have small values of TPA cross sections, typically of the order 10 GM.

The accuracy of two photon absorption cross section obtained from TPEF experiment does not depend on the pulse width [63]. Since the TPEF experiment is performed with a dilute solution, a very small amount of material is needed. This technique has limitation, that the molecules must have a photoluminescence feature which can be handled by measuring the secondary photochemical process, like the generation of the luminescence from the singlet oxygen which is generated by the energy transfer from the triplet excited state of the material, and this is achieved by TPA.

It is important to note that the error in the determination of the two photon absorption cross section are commonly more than 10 %, even if the experiments are carefully performed at the best of conditions [65].

In our work we used Fluorescence-based method simultaneously with nonlinear transmittance-based method, so called open aperture z-scan.

2.2.2 Open Aperture Z-Scan Technique

The Z-scan technique was introduced by Sheik-Bahae et al. [71, 72]. It works on the principle of moving the sample under investigation along the laser beam. The transmittance changes as the sample is moved along the beam axis. This is because of the different pump intensities that the sample experiences, dependent on the sample position (z) relative to the focus ($z = 0$). The transmitted light through the sample power as function of the sample position is measured. The two nonlinear parameters which can be determined are the sample's nonlinear absorption coefficient and the nonlinear index of refraction. To measure the nonlinear refraction index an aperture is place in front of the detector measuring the transmitted light. This makes the measurements sensitive to beam spreading or focusing and related to the transformation of phase distortion into amplitude distortion. The medium with nonlinear refractive index causes an additional depending on z, focusing (at positive n) or defocusing (at negative n) of the beam. Since our work deals with the nonlinear absorption, open aperture z-scan experiment is used. It is used to calculate the nonlinear absorption parameter directly from the transmittance measurements. The basic set up can be seen in Fig2.2. In order to tune the excitation wavelength, we used a home built optical parametric amplifier. It is described in details in chapter three.

As there are some differences in definition of the TPA cross section [73], we first present the definitions and approximations for the quantitative estimations we use. The TPA in a sample is described by the following differential equation:

$$dI/d\iota = -\beta I^2 \qquad (2.8)$$

where I is the intensity, ι is the distance in the sample and β is the two-photon absorption coefficient.

The two-photon absorption coefficient β is related to the cross section σ_2 as [74- 75]:

$$\sigma_2 = \beta h\nu / N_A d \tag{2.9}$$

where $h\nu$ is the exciting photon energy, N_A is the Avogadro constant, d is the concentration of the TPA molecule in solution [76,77]. For weak absorption and a sample thin in comparison to Rayleigh range (z_R), we can expand the solution of Eq.(2.8) in a series and take only the first terms. The actual quantity of interest in the open-aperture z-scan experiment is the average transmitted power as a function of the sample position. For this we can integrate over the transverse coordinates to obtain the instantaneous transmitted power and then integrate over the duration of the pulse. The transmitted power in these approximations as a function of the sample-position z with respect to the focal point distance is given by:

$$T(z) = 1 - \frac{\beta I_0 L}{2\left(1 + \left({}^{z}/_{z_R}\right)^2\right)} \tag{2.10}$$

where I_0 is the incident laser intensity on the Gaussian beam-axis at the waist, L is the sample thickness. From the fit of the *T(z)* curve the nonlinear absorption coefficient β and the cross section σ_2 is obtained.

In Fig.2.2 we show an experimental scheme. The laser beam is focused into the sample with lens L_1. To collect the signal on the probe detector D_1, we used lens L_2. We measured both the fluorescence intensity and the change in the transmittance by also collecting the fluorescence signal with the lenses L_3 and L_4 on detector D_3.

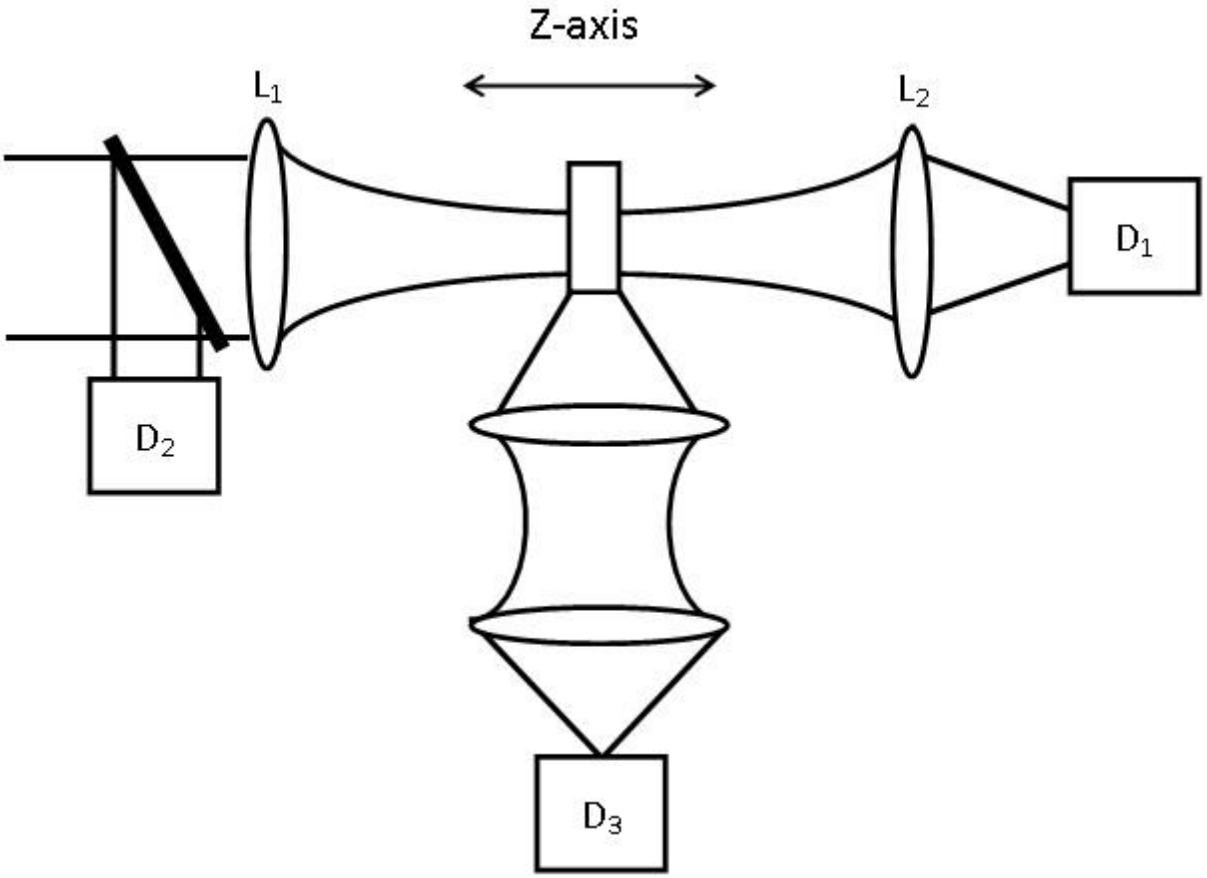

***Figure 2.2**: Scheme of open-aperture z-scan measurements. D_1, D_2 and D_3 are photodiodes, L_1, L_2, L_3 and L_4 are lenses.*

CHAPTER 3

Optical Parametric Amplifiers

3.1 Principles of Optical Parametric Amplifier

The most widely used methods to generate a high-power and widely tunable light, is the optical parametric amplifier (OPA).

Femtosecond optical parametric amplifier has become a well-known device and is the most widespread source of tunable femtosecond pulses since the early days of laser development [78, 79]. OPAs can provide high output energies, broad frequency stability and are simple to operate. The availability of high-intensity lasers has enabled the use of OPA for a large number of applications, ranging from time-resolved studies to high-resolution spectroscopy, especially, in the field of ultrafast spectroscopy [80]. OPA systems are usually optimized for either the shortest possible pulse duration or for maximum output and wavelength stability. They provide pulse energies from picojoules to milli-joules [81].

Femtosecond OPA can produce pulse energies up to the 100mJ level [82]. In addition, OPAs has the ability to generate pulses significantly shorter than the pump pulses, exploiting the broad band gain available in the parametric interaction. In fact ultra-broadband pulses have been obtained with durations down to approximately 5 fs in the visible [83] and 15 fs in the IR [84]. These contain only a few optical cycles of the carrier frequency.

The process of optical parametric amplification (OPA) resembles difference frequency generation (DFG). It involves incidence of two waves with frequencies ω_p and ω_s in the nonlinear medium and the light at the frequency ω_i is generated ($\omega_i = \omega_p - \omega_s$). If the wave at ω_p is intense, the amplification at ω_s occurs as a result of the interaction. The beam at

frequency ω_p is referred to as the pump beam, ω_s will be signal or seed beam, and ω_i will be the idler beam. Therefore, the energy conservation law simply transforms to:

$$\omega_p = \omega_s + \omega_i \tag{3.1}$$

Similarly, in terms of wavelengths we have:

$$\frac{1}{\lambda_p} = \frac{1}{\lambda_s} + \frac{1}{\lambda_i} \tag{3.2}$$

It should also satisfy the momentum conservation

$$k_p = k_s + k_i \tag{3.3}$$

The division of the energy between the signal and idler photons is adjustable, so an OPA provides a tunable source of femtosecond pulses.

In principle, the signal frequency to be amplified can vary from$(\omega_p/2)$, which is the so-called degeneracy condition (when $\omega_s = \omega_i$) to ω_p, correspondingly, the idler can vary from $(\omega_i/2)$ to zero (when $\omega_s = \omega_p$). In our OPA the pump at 400nm, generated a signal beam from 545 nm to 666 nm. However, in practice not all the wavelengths that satisfy the energy conservation law can be generated. The absorption at the infrared wavelengths in the crystal cuts the range.

3.2 Phase Matching

Phase matching in nonlinear optics describes conservation of energy and momentum. The most common procedure to achieve phase matching is to make use of the birefringence of crystals. Birefringence is the dependence of the refractive index on the polarization of the optical radiation. Not all crystals display birefringence; in particular crystals belonging to the cubic crystal system are optically isotropic and thus not phase-matchable. Glasses and amorphous materials are also non-birefringent.

Birefringent crystals have different indices of refraction for different wave polarizations, the orientation of the wave vector can be changed by exploiting a medium's birefringence. The quantum mechanical momentum of a photon, ħ*k*, is related to the wave vector $\vec{k}$, $\vec{k} = \left(\frac{n\omega}{c}\right)\hat{s}$. The index of refraction for each beam depends on several factors, including the incidence angle of the beams relative to the crystal axes, the propagation directions within the crystal, the polarizations of each beam in a birefringent medium, and the temperature of the medium.

When using a collinear geometry, only the incidence angle and play a role. The reason that phase matching is of such critical importance in nonlinear optics can be understood by considering dispersion. In nonlinear optics, energy is shared among multiple waves and the interacting waves are at multiple frequencies. Dispersion will cause the waves to travel through the nonlinear medium at different speeds. The interactions will take place until the waves physically separate because of dispersion. However, birefringent optical media will have waves with one polarization travel at one speed while waves with the other polarization will travel with another speed. Selecting the polarization of the waves and their direction of travel, the waves can be made to move at the same speed through the medium. This significantly increases the interaction length between the waves, and drastically increases the output power achievable after such an interaction.

The perfect phase-matching condition for the wave vectors k_s, k_i and k_p of signal, idler and pump, $\Delta k = k_p - k_s - k_i = 0$, is often difficult to achieve because the refractive index of materials shows an effect known as normal dispersion; i.e. the refractive index increases with frequency. As a result the condition for perfect phase matching with collinear beams is:

$$n_p = \frac{n_i\omega_i}{\omega_p} + \frac{n_s\omega_s}{\omega_p} \tag{3.4}$$

In femtosecond OPAs, and negative uniaxial crystals ($n_e < n_o$), the pump is polarized along the extraordinary direction. If signal and idler beams have the same ordinary polarization (perpendicular to that of the pump beam) the phase matching is called type I ($o_i + o_s = e_p$) where i is the idler with ordinary polarization, s is the signal with extraordinary polarization and p is the pump with extraordinary polarization. If one of the two generated beams is

polarized parallel to the pump beam, that is type II phase-matching, either the signal ($e_s + o_i = e_p$) or idler ($o_s + e_i = e_p$) can have extraordinary polarization. Both types of phase-matching can be used and have their specific advantages. Usually the phase matching is achieved by adjusting the angle θ_m between the wave-vector $\vec{k}$ of the propagation beam and the optical axis of the nonlinear crystal (angular phase-matching) (Fig.3.1), or by changing the refractive index by adjusting the temperature of the nonlinear crystal (temperature phase matching). The value of refractive index can be calculated through the relation:

$$\frac{1}{n_e(\theta_m)^2} = \frac{sin^2\theta_m}{n_z^2} + \frac{cos^2\theta_m}{n_o^2} \tag{3.5}$$

where, n_z is the principal value of the extraordinary refractive index. Note that $n_e(\theta_m)$ is equal to the value of n_z when θ_m=90º, and when θ_m=0, n_e is equal to n_o. Phase matching is achieved by adjusting the angle θ_m to obtain the value of $n_e(\theta_m)$ for which the condition $\Delta k = 0$ is satisfied. Phase matching allows us to select the desired wavelength.

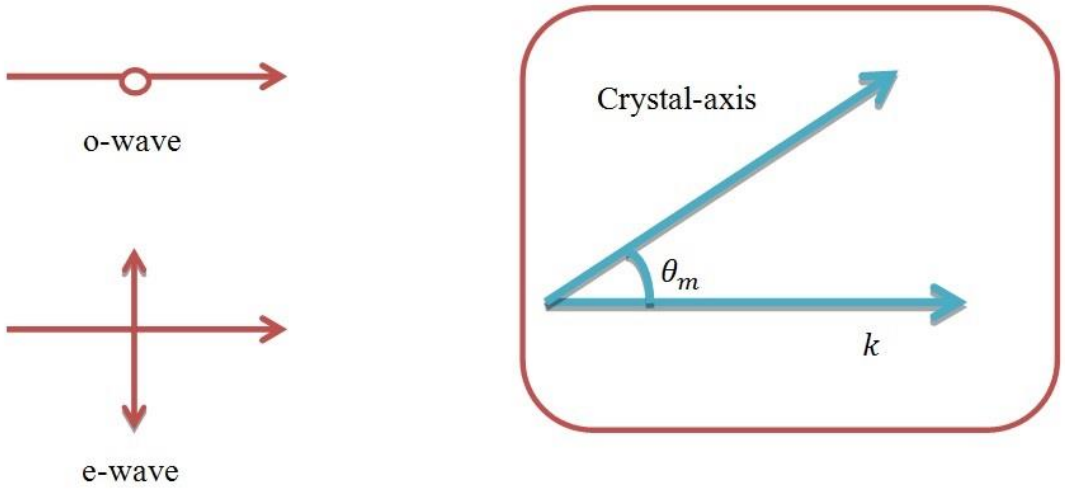

Figure 3.1: *Schematics of the process in a non-linear crystal. The terms ordinary "o" and extraordinary "e" are used to describe the two beams within the crystal, The polarization o-wave comes out of the page and the polarization vector of the e-wave is in the plane of the page.*

Unfortunately, phase matching does not simultaneously ensure matching of the three group velocities. The highest parametric conversion efficiency of ultrashort pulses is achieved when the phase-matching condition is accompanied by matching of the group velocities of the interacting pulses, especially in nonlinear crystals with large dispersion.

3.3 Group Velocity Dispersion

Dispersion can be described as the change in the group velocity with frequency and plays an important role in ultrafast optics. As a pulse propagates in a dispersive medium, the frequency-dependent velocity will modify the pulse envelope, often resulting in an increase of the pulse duration and/or a degradation of the pulse quality (e.g. creation of satellite pulses).

The three pulses propagate in the nonlinear crystal with different group velocities, $v_g = \frac{d\omega}{dk}$. With the slowly varying amplitude approximation and neglecting the pulse lengthening due to the second or high order dispersion (which is good approximation in the 100fs range), we obtain the following equations [85]:

$$\frac{dA_i}{dz} + \frac{1}{v_{gi}} \frac{dA_i}{dt} = -j \frac{\omega_i \mathrm{d}_{\mathrm{eff}}}{n_i c_0} A_s^* A_p \exp(-j\Delta kz) \qquad (3.6a)$$

$$\frac{dA_s}{dz} + \frac{1}{v_{gs}} \frac{dA_s}{dt} = -j \frac{\omega_s \mathrm{d}_{\mathrm{eff}}}{n_s c_0} A_i^* A_p \exp(-j\Delta kz) \qquad (3.6b)$$

$$\frac{dA_p}{dz} + \frac{1}{v_{gp}} \frac{dA_p}{dt} = -j \frac{\omega_p \mathrm{d}_{\mathrm{eff}}}{n_p c_0} A_s A_i \exp(j\Delta kz) \qquad (3.6c)$$

where A_p, A_s and A_i are the pulse envelopes of the pump, signal and idler respectively. $\mathrm{d}_{\mathrm{eff}}$ is the nonlinear optical coefficient, which relates to $x^{(2)}$ and depends on the propagation direction and polarization of the beams in the nonlinear material. Eq. (3.6) also neglects third order effects (self- and cross-phase modulation). By transforming them to a frame of reference

that is moving with the group velocity of the pump pulse $\tau = t - \frac{z}{v_{gp}}$) we obtain the equations:

$$\frac{dA_i}{dz} + \left(\frac{1}{v_{gi}} - \frac{1}{v_{gp}}\right)\frac{dA_i}{d\tau} == -j\frac{\omega_i \mathrm{d}_{\mathrm{eff}}}{n_i c_0} A_s^* A_p \exp(-j\Delta kz) \qquad (3.7a)$$

$$\frac{dA_s}{dz} + \left(\frac{1}{v_{gs}} - \frac{1}{v_{gp}}\right)\frac{dA_s}{d\tau} == -j\frac{\omega_s \mathrm{d}_{\mathrm{eff}}}{n_s c_0} A_i^* A_p \exp(-j\Delta kz) \qquad (3.7b)$$

$$\frac{dA_p}{dz} == -j\frac{\omega_p \mathrm{d}_{\mathrm{eff}}}{n_p c_0} A_s A_i \exp(j\Delta kz) \qquad (3.7c)$$

Eq. (3.7) have been simplified and there are some important parameters in ultrashort parametric amplification, which are related to the group velocity mismatch (GVM) between the interaction pulses. Particularly, GVM limits the interaction length between the pump and the amplified (signal or idler) pulse over which the parametric amplification takes place, while GVM between idler and signal beams limits the phase matching bandwidth. The beneficial interaction length for parametric interaction is defined as the propagation length after which the signal (or the idler) pulse separates from the pump in the absence of gain, and it is quantified by the pulses splitting length. It is expressed as:

$$l_{jp} = \frac{\tau}{\delta_{jp}}, \ldots\ldots j = i, s \qquad (3.8)$$

where $\delta_{j,p} = \frac{1}{v_{gi}} - \frac{1}{v_{gp}}$ is the GVM between pump and signal or idler and τ is the pump duration. The pulse splitting length becomes shorter for decreasing pulse durations. The GVM depends on the phase-matching type, the crystal type, and the pump wavelength. Because of the greater dispersion in the visible region, GVM becomes larger in the visible region. GVM effects can be neglected for crystal lengths shorter than the pulse splitting length. But GVM plays a critical role for crystal lengths longer than or comparable to the pulse splitting length, and Eq. (3.7) must be solved numerically to properly account for it.

δ (i,p) and δ (s,p) can have different signs. When δ (i,p) δ (s,p)> 0, both idler and signal pulses walk away from the pump in the same direction so that the gain quickly decreases for the propagation distances longer than the pulse splitting length and finally saturates. On the other hand, when δ (i,p) δ (s,p)< 0, idler and signal pulses move in the opposite direction with respect to the pump pulse; in this way both idler and signal pulses tend to stay localized under the pump pulse and the gain grows exponentially, even for crystals whose lengths exceed of the pulse splitting length in the case of a collinear configuration. For this situation we assume that perfect phase matching, $\Delta k = 0$, is achieved for a given signal frequency ω_s and for the corresponding idler frequency, ω_i ($\omega_i = \omega_p - \omega_s$). If the signal increases to a certain value, $\Delta\omega$ to $\omega_s+\Delta\omega$, by energy conservation Eq. (3.3), the idler frequency decreases to $\omega_i-\Delta\omega$. We can thus take a Taylor expansion to first order in the wave-vector mismatch. This wave-vector mismatch can be approximated to the first order as:

$$\Delta k = \Delta k_0 - \frac{\partial k_s}{\partial w_s}\Delta w - \frac{\partial k_i}{\partial w_s}\Delta w \qquad (3.9)$$

Since $\partial w_s = -\partial w_i$, and $\Delta k_0 = 0$, we obtain the following:

$$\Delta k = -\frac{\partial k_s}{\partial \omega_s}\Delta\omega + \frac{\partial k_i}{\partial \omega_i}\Delta\omega = \left(\frac{1}{v_{gi}} - \frac{1}{v_{gs}}\right)\Delta\omega \qquad (3.10)$$

A large GVM difference between idler and signal waves considerably decreases the phase matching bandwidth. A large gain bandwidth can be expected in the case of group velocity matching between signal and idler ($v_{gs} = v_{gi}$), the group velocities of signal and idler, and thus the phase matching bandwidth, are set. The gain coefficient depends on:

(i) The pump intensity,
(ii) The signal and idler wavelengths, λ_s and λ_i.
(iii) The nonlinear coefficient d_{eff} .
(iv) The refractive indices at the three interacting wavelength.

3.4 Home-Build Optical Parametric Amplifier

There are several types of femtosecond optical parametric amplifier schemes which have been reported, but there are only a few basic principles underlying their respective implementations.

Femtosecond OPA is pumped for example either with the fundamental (800 nm) or with the second-harmonic (400 nm), both emanating from a regeneratively amplified modelocked Ti:Sapphire laser. Pumping with the fundamental can generate new frequencies in the IR. Pumping in the visible/blue can generate frequencies in the visible region. Standard systems typically run at 1 kHz repetition rate and generate pulses at the wavelength longer than λ=0.8 μm with 0.5 - 1 mJ pulse energy and durations ranging from 50 to 150 fs. However, the OPA could also be pumped at a higher repetition rate such as 250 kHz but with lower output energy levels of 5 to 10 μJ [86].

The optical parametric amplification process consists of interaction between a weak signal beam with a strong pump beam. At the first stage of an OPA, the generated initial beam is called the seed beam. A nonlinear optical material is required to generate the seed beam.

There are two common techniques, which have been used to generate seed beams: parametric super fluorescence and white-light continuum generation. After generating the seed beam, the pump and the seed pulses are combined in a suitable nonlinear crystal, in a first parametric amplification stage. In the second stage, the signal beam can be further amplified.

In this section we describe a home-built femtosecond optical parametric amplifier as the source of ultra-short spectrally tunable pulses. The scheme of our experimental setup is shown in Fig.3.7. The OPA is pumped by a mode-locked Ti:sapphire laser (CPA-2001, Clark-MXP, Inc.) delivering ~150 fs pulses of 0.5 mJ energy at a repetition rate of 1 kHz.

The total average power available is ~540 mW. The laser beam at the fundamental frequency is divided into two parts, using beam splitter BS1. About 160 mW (30% of the power) goes to first OPA-stage and about 380 mW (70%) is reflected to serve as a pump for the second OPA-stage.

There are three *key* elements in an OPA: the pump beam, the seed and the nonlinear crystal where the interaction takes place. Another important issue is the type of interaction, i.e. collinear or noncollinear, as well as the type of phase matching (Type I or Type II).

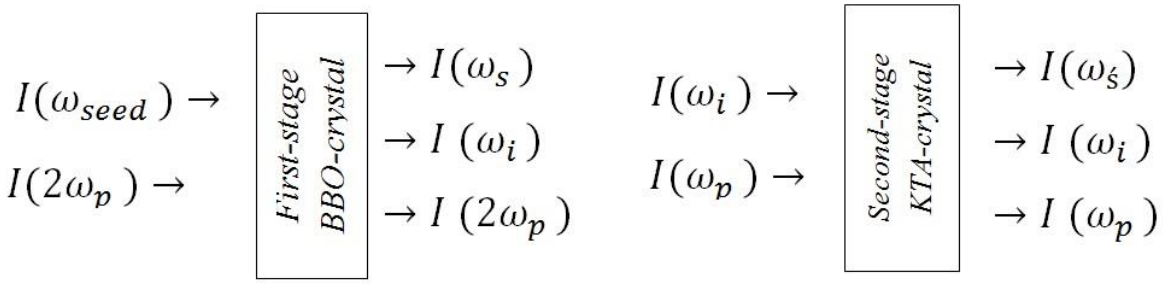

Figure 3.2: *Two-stages OPA,* ω_p*:* ω_{pump} *,* ω_s *:* ω_{signal} *,*ω_i *:* ω_{idler} *,* $\omega_{ś}$*:* $\omega_{IR\ signal}$

Our set-up is arranged collinearly. The first OPA-stage is pumped by the second harmonic $I(2\omega_p)$ of the Ti:sapphire laser. We seed with the generated white-light ($I(\omega_{seed})$) which has a wide spectrum. The direction of the polarization vector of the seed beam is horizontal and the second harmonic pump beam has a polarization vector oriented vertically to the seed. The pump and seed beams interact in the BBO-crystal to generate a short wavelength beams called signal $I(\omega_s)$ in the range of $666 - 560\ nm$ and a long wavelength beam called idler $I(\omega_i)$ in the range of $1000 - 1400\ nm$. The idler is amplified in the second OPA-stage with the pump beam (at the fundamental wavelength) in the KTA-crystal. An amplified idler beam $I(\omega_i)$ and longer wavelength (IR-range) $I(\omega_{ś})$ are generated.

The First Stage of OPA

The fundamental power, which comes from BS_1 is focused with L_1 lens ($f = 1000\ mm$) and is once again divided by another beam splitter, BS_2, into two parts. We chose the second harmonic of the Ti: Sapphire laser system as the pump for the first OPA stage.

Part of the fundamental beam (95%) about 154 mW is frequency-doubled in a BBO-crystal 6x6x2 mm^3, (θ=29.2º) by second harmonic generation (SHG). The second harmonic light (at 388 nm) is used to pump the first OPA stage. By changing the angle between the crystal-plane and the incident pump beam, an optimum of SHG can be achieved. By choosing the appropriate angle, we get a 388 nm beam with a power of approximately 14.5 mW.

A nonlinear optical material is required to generate a seed beam with broad spectrum (see Fig.3.4). In our OPA we used white-light continuum generation in a sapphire plate to get the seed beams. A small fraction of the fundamental beam of 8 mW (5%) is used to produce a white light continuum which has a broad spectrum.

We used sapphire plate for white-light generation because sapphire plates are more resistant to degradation than fused silica plates. The super continuum generation in sapphire remains stable for appreciable durations. This can be attributed to its high thermal conductivity and low absorption in the UV [85].

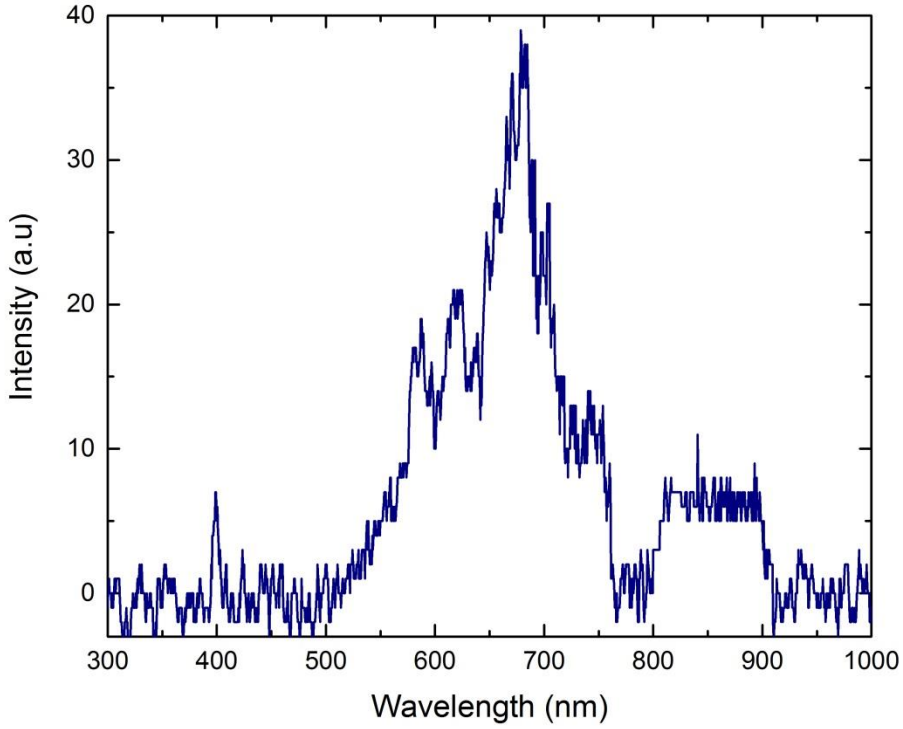

Figure 3.4: *Spectrum of super continuum pulses generated in a 2 mm thick sapphire plate, A SP700 was used to block the fundamental at 775 nm.*

The light is focused in a 2 mm thick sapphire plate. Two lenses L_2 and L_3 with focal distances $f = 20\ mm$, are used to focus the beam to a required intensity for the generation of white light, and collimate the white light beam. As a result of self-phase modulation, a large spectral broadening takes place. By adjusting the focal length of the lens and the opening diameter of diaphragm, the process is optimized: stability, wavelength range and spatial shape. Thus, the seed is formed to be amplified in the nonlinear crystal. For the parametric gain a nonlinear crystal needs to satisfy the following requirements:

Small linear and nonlinear absorption at the operating wavelengths, high laser-induced damage threshold. The high transparency in the UV region and damage threshold to laser-induced damage makes the beta barium borate crystal β-BaB_2O_4(BBO) [87] suitable in many cases as a frequency conversion tool.

The pump and the seed pulses are overlapped using the dichroic mirror DM_1 highly reflective ($R < 99\%$) for the pump and highly transmitting ($T < 90\%$) for the seed beam, and overlap in the BBO crystal of 6x6x2 mm^3 size and cut at the angle of θ=29.2º.

We have used type I phase matching interaction ($o_s + o_i = e_p$) in a first parametric amplification stage (Fig.3.5).

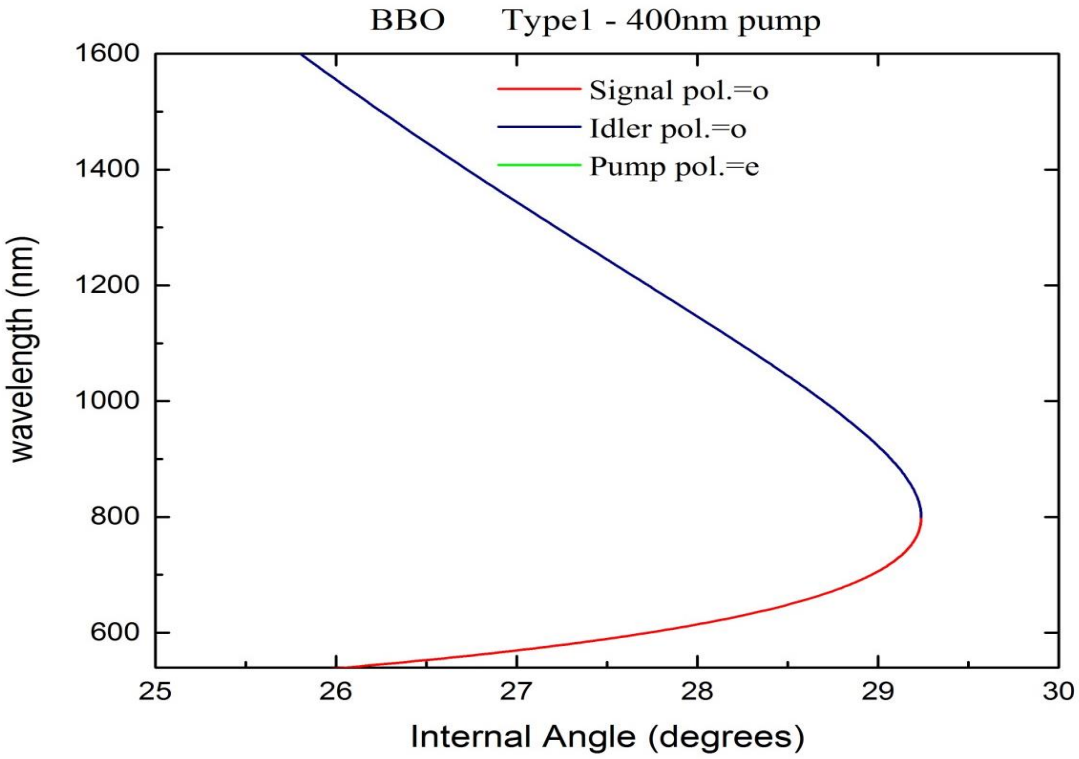

Figure 3.5: *Phase-matching conditions for type I BBO crystal with a pump wavelength of 400 nm, using SNLO program.*

As seen in Fig3.5 the phase-matching angle varies in the range 26.5 - 28.5 degree to get wavelengths from 1000 to 1450 nm.

The pump is focused into the crystal using L4 lens ($f = 250mm$). We took care not to exceed 10 GW/cm^2 intensity in order not to damage crystal. Its damage threshold is 35 GW/cm^2. The

BBO crystal is close to the focal point of the lens but still far enough from it to avoid optical parametric super- luminescence. The seed and pump relative timing must be adjusted by a delay line to achieve temporal overlap and compensate the differences in the beams' paths. The spatial overlap between the pump and seed beams is adjusted by using pinholes PN_1 before and PN_2 after the crystal. The optical amplification can only occur if the pump and seed light pulses overlap in both space and time. The spot size of the pump beam in the nonlinear crystal is varied and is chosen to achieve the highest possible gain without causing optical damage of the crystal, or inducing third-order nonlinear effects that would cause beam distortion or breakup.

By choosing a crystal orientation, the phase matching condition for the desired signal and idler wavelengths can be reached. The amplification is controlled using the portable fiber spectrometer of OceanOptics5.

The output of the first OPA stage (signal plus idler powers) has the power in the range of 0.3 – 0.8 mW.

The Second Stage of OPA

The second OPA stage is pumped at the fundamental wavelength of the Ti:Sapphire laser 775 nm I(ω_p) , and is seeded by the idler wave $I(\omega_i)$ generated in the first OPA stage. The pump and the seed beams have both horizontal polarizations. For the amplification process, we have KTA crystal of type II. This crystal needs the pump and the signal beams to be polarized perpendicularly. We change the polarization of the pump beam. The polarization of the pump beam is rotated on 90 degree using a λ/2-plate to a vertical polarization.

The pump beam is focused with L_6 lens ($f = 1000\, mm$) in the crystal, seed beam (with horizontal polarization) from the first gain stage is focused with lens L_5 ($f = 175\, mm$) and reflected by a second dichroic mirror DM_2 (HR 770-820 and HT 870-8000 nm) to overlap with the pump of power 380 mW in potassium titanyle arsenate ($KTiOAsO_4$), or KTA crystal 7x7x5 mm^3 ($\theta = 38.4^{\circ}, \varphi = 0$).

We have used type II phase matching ($o_s + e_i = e_p$) (Fig.3.6). We have used KTA crystal because of relatively large nonlinear optical and electro-optical coefficients, wide angular bandwidth and small walk-off angle, and high damage threshold.

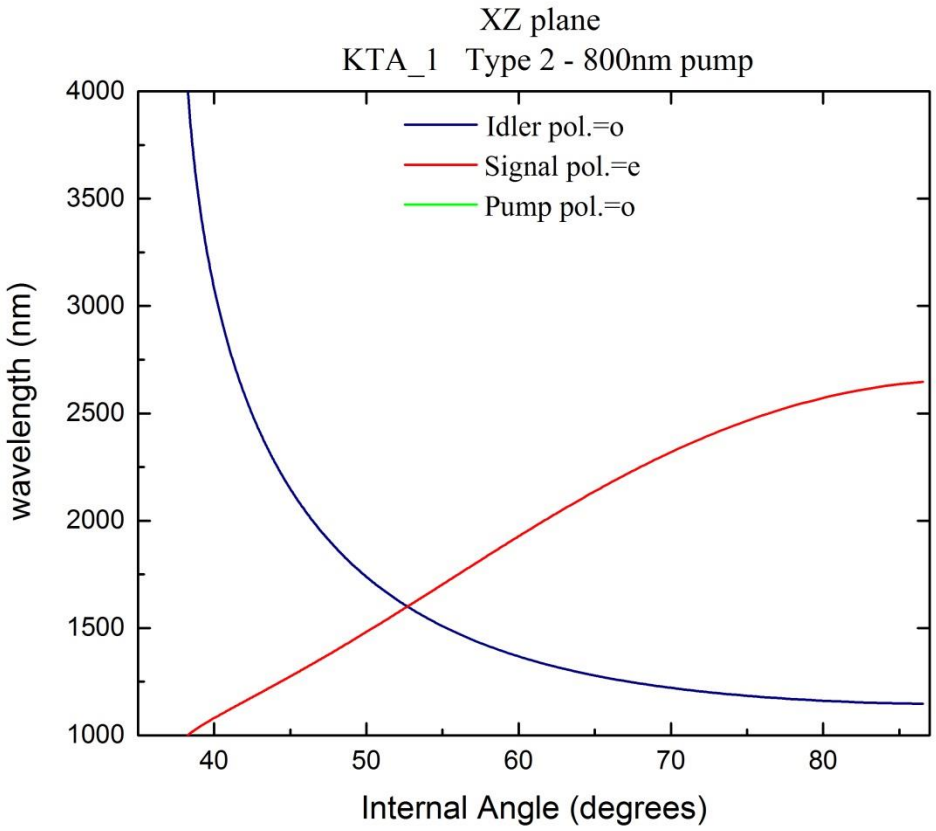

Figure 3.6: *Phase-matching conditions for: type II KTA crystal with a pump wavelength of 800 nm, using SNLO program.*

In the KTA-crystal at angle from 38.4 to 55.5 degrees a beam at wavelength range of 1000 - 1450 nm is amplified.

The temporal overlap is adjusted in both stages by manual delay lines DL_1 and DL_2 respectively, equipped with a micro screw.

Finally, the idler beam is reflected with the golden mirror M_3. The optimizing of the two stages is controlled with an InGaAs detector, which is sensitive in the range of 700 -1800 nm.

We have used SNLO software, to get specific data concerning nonlinear crystals. SNLO is public domain software developed at Sandia National Laboratories. From the SNLO software one can get phase-matching information for large number of nonlinear crystals, as well as effective nonlinear coefficients, group velocities, and birefringence [88].

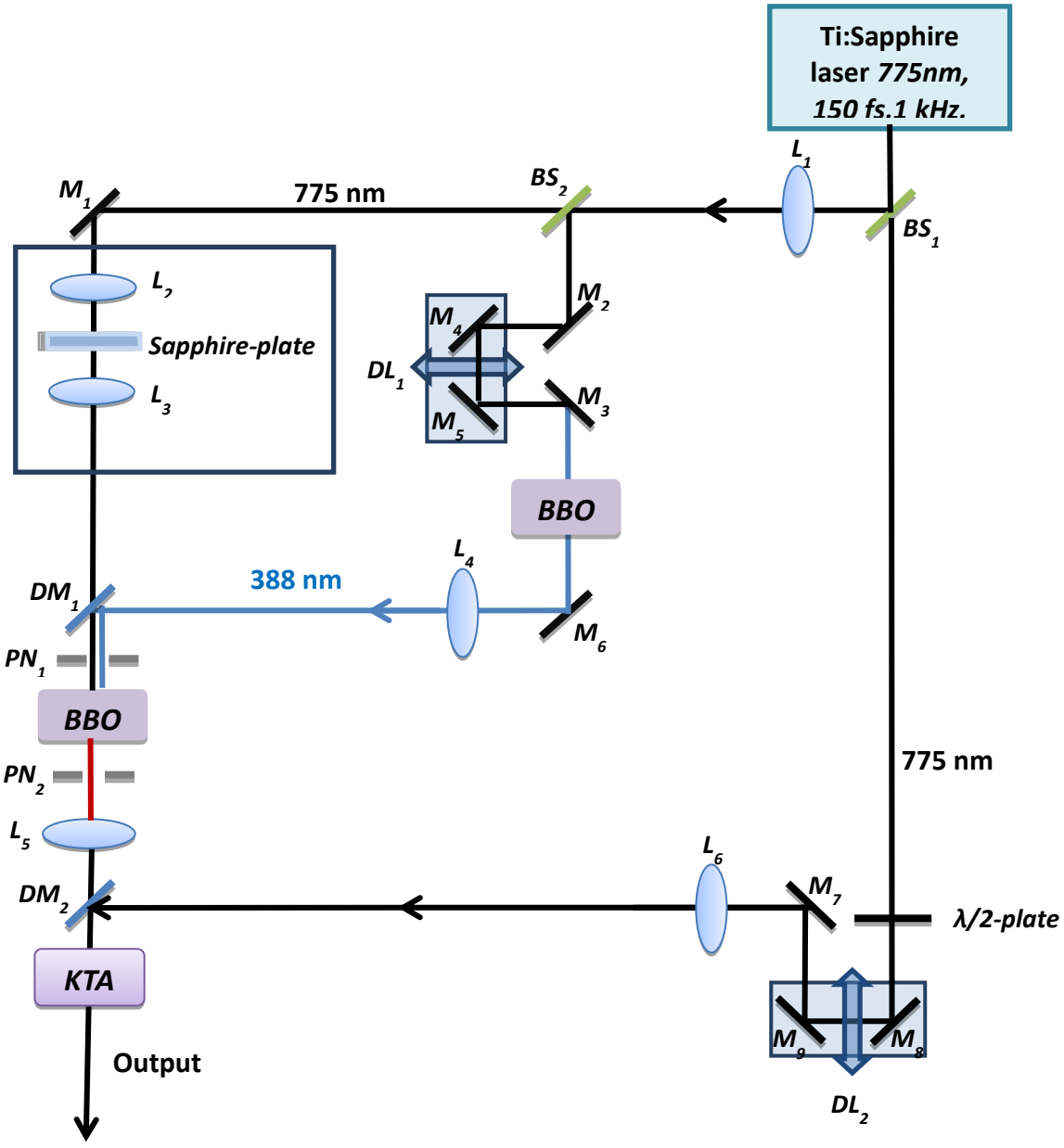

Figure 3.7: *Sketch of the experimental set-up of the two OPA stages. BS:Beam-splitter, DM: dichroicmirror, L: lenses, M: mirrors.*

Spectra of Amplified Signal after the First and Second Stages

We recorded the spectra of the generated beams after the first OPA-stage. The signal beam, for example, is generated at 630 nm and the idler beam in this case has 1050 nm wavelength. The idler beam at 1050 nm is further amplified in the second OPA-stage, as shown in Fig.3.8. The spectrometer is sensitive up to 1.1 μm.

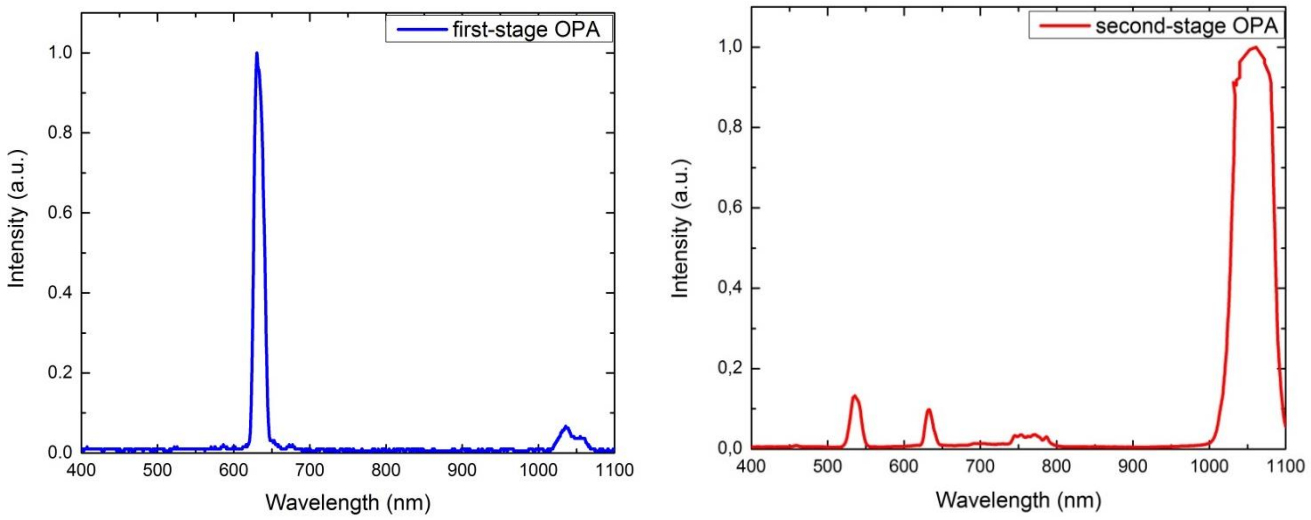

(a) **(b)**

Figure 3.8: *(a) Spectra of signal and idler beams generated after the first amplification stage, (b) spectra of the amplified idler beam after the second OPA stage. The spectra have been normalized.*

In order to control and check the wavelength of the amplified idler beam from the second OPA-stage, the second-harmonic generation was used. The frequency was doubled with a BBO-crystal. The second harmonic spectra of the output idler beam are shown in Fig. 3.9.

Figure 3.9: *Spectra of the second harmonic of output pulses measured after the second OPA-stage.*

OPA Performance

The idler beam has pulse energy in the range 10-35 μJ, and the wavelengths in the range of 1040-1450 nm. The pulse-width is measured with an autocorrelator of APE GmbH. The principle of the autocorrelation measurements is non-collinear generation of the second harmonic. The intensity autocorrelation function is given by:

$$A(\tau) = \int_{-\infty}^{+\infty} I(t)I(t-\tau)dt \qquad (3.11)$$

where t is the time, τ is the delay between two pulses and I is the intensity.

For Gaussian pulse shape, the pulse duration is $1/\sqrt{2}$ from the autocorrelation full width at half-maximum (FWHM). FWHM pulse-width of 100-125 fs is obtained assuming a Gaussian pulse-shape (Fig.3.10).

The wavelength we measure with a NIR / MIR spectrometers. The spectral width of the output idler beam is typically about 15 nm.

A long pass filter FGL850S is used to cut off the pulse at fundamental wavelength. A variable neutral density filter is used to keep photon flux used in the experiment of the same power at different wavelengths.

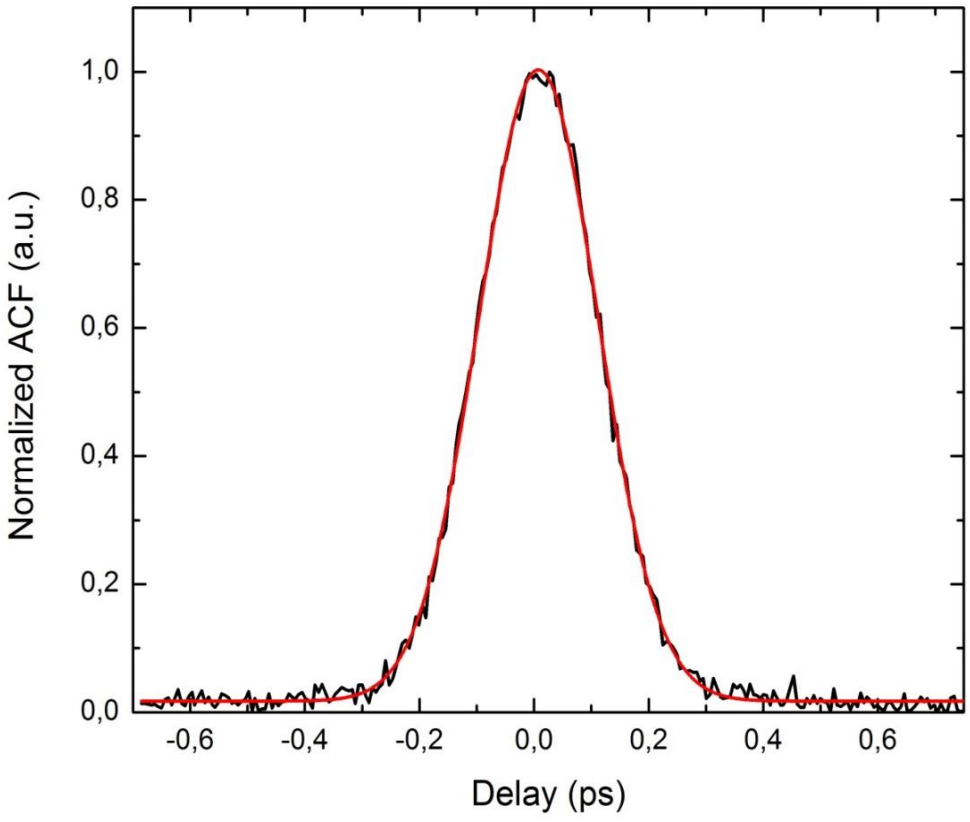

Figure 3.10: *The autocorrelation function, at λ= 1150 nm. It is fitted by Gaussian with FWHM of about 122 fs.*

The output power from the second OPA-stage versus the wavelengths is presented in Fig. 3.11. The power was measured with the powermeter in the range of 1040-1450 nm. The maximum power achieved is around 1225 nm. We used a pin-hole to cut the signal beam and measure only the idler one.

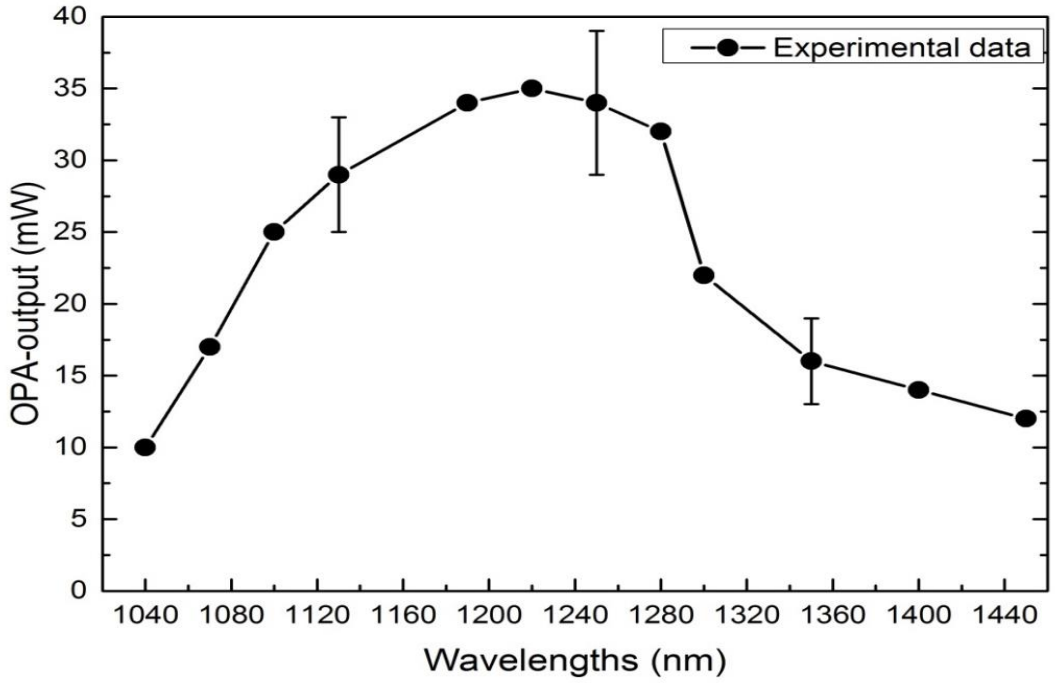

Figure 3.11: *OPA output power versus wavelengths at a repetition rate of 1 kHz.*

CHAPTER 4

Some Applications of the TPA

4.1 Excitation of Photosensitizers and Initiation of Photochemical Reactions

The molecules that we study here belong to photosensitizer. A photosensitizer (a *chromophore*) is a photosensitive molecule that localizes preferentially in certain kinds of cells and/or tissues, and absorbs light in a specific wavelength interval thus starting a photochemical reaction. There are many different photosensitizers, but many of them share the same photochemical reaction. Many new compounds have been synthesized in an attempt to create better photosensitizers [89]. They are called the second generation photosensitizers. One of the second-generation photosensitizers' features is the large absorption coefficients at longer wavelengths and thus, a photodynamic therapy (PDT) treatment with any of these compounds would require lower doses of drug and light for efficacy (performance). The photosensitizers of interest to us are those which could be used in PDT.

Photodynamic therapy has emerged in recent years as a novel approach and is one of the most promising treatments for malignant and non-malignant diseases. It has gained a lot of attention. PDT is used in such fields as oncology, ophthalmology, dermatology, cardiology [90, 91] and atherosclerotic illnesses such as coronary artery diseases [92].

The treatment is based on a photodynamic reaction, which is a chemical reaction initiated by light irradiation. This reaction can be used to selectively treat diseased cells. Three components are required to perform photodynamic therapy, which are combined to induce cellular and tissue illumination at a specific wavelength. The first factor of PDT is oxygen. The second factor involves the administration of light of a specific wavelength. In this chapter the third required element photosensitizer is studied.

The PDT can be done with one-photon or two-photon excitation. The main disadvantage of single photon PDT is the limited penetration depth of the visible light into the tissue. It is possible to overcome this problem by using two-photon excitation with near-infrared (IR) light [93]. Deeper penetration has been achieved. In this work, we are concentrated on two-photon excitation of photosensitizers.

The motivation of our study is the importance of TPA information. The main classes of photosensitizer are synthetic porphyrin, phthalocyanines, naphthalocyanines, chlorins, bacteriochlorins, porphycenes, azaporphyrins, and expanded porphyrins such as texaphyrins. Compounds of the tetrapyrrole type have found considerable interest in PDT with two-photon excitation as they already play an important role as photosensitizers in PDT [94]. Some of them have high two-photon absorption cross-sections. Tetrapyrrolic compounds (porphyrins, chlorins, bacteriochlorins, and so on) are widely present in nature and play very important role in different biological processes. For example, porphyrin-type molecules are the critical part of hemoglobin and myoglobin, which are the proteins transporting and storing oxygen. Chlorophyll, a derivative of chlorin, is found in green plants. It plays the central role in plant photosynthesis. Bacteriochlorophyll is used for the same purpose in photosynthetic bacteria. Owing to the great importance of the tetrapyrrolic molecules in biological processes, a great deal of attention has been paid to the study of their spectroscopic, physical, chemical, and biophysical properties. Tetrapyrrolic molecules have attracted attention also from a rather different direction, due to their potential applications in various areas of technology including photonics. For example, particular spectroscopic and linear absorption properties of tetrapyrroles have inspired research in the area of synthetic light harvesting antennasystems [95-97], holographic data storage [94,98,99-103], molecular scale electronic components [104-107], and PDT [108-110]. Recently, growing interest to the nonlinear optical properties of organic materials has prompted a new wave of investigation of tetrapyrrolic molecules. In particular, tetrapyrroles are of great interest to nonlinear optics applications like electro optical signal processing, power limiting, and molecular scale electronic components. On the other hand, there are a few investigations of the TPA properties of tetrapyrroles. Lack of reliable data on TPA properties of tetrapyrroles is in contrast with the large number of possible multiphoton-based applications. Moreover, if one wants to increase efficiency of two-photon

excitation, almost total lack of data about TPA properties of tetrapyrrolic molecules makes it exceedingly difficult to judge what values of TPA cross sections can be expected after their modification. Therefore, a systematic study of TPA properties of the tetrapyrroles leading to the guidelines defining steps necessary for their TPA enhancement is of great practical importance.

To explain the mechanism of the PDT, the photochemical reaction of the most common porphyrin-based photosensitisers ProtoporhyrinIX (PpIX) will be taken as an example. When PpIX absorbs light for example at 635 nm, the molecule will be excited to the first excited single state S_1 (Fig.4.1). This absorption band or energy level is called the Q-band. From this state the molecule can be transferred to the lowest triplet state (T_1) even though this inter-system crossing is spin-forbidden. This is possible because the small energy difference between the states makes the quantum yield for the transition high enough. The next relaxation of the molecule from the triplet state to the singlet ground state (S_0) is also a spin-forbidden inter-system crossing with a low transition probability. Hence, the lifetime of the triplet state is relative long (of the order of milliseconds), and gives the sensitizer time to interact with surrounding molecules.

In PDT the light is used at a specific wavelength to activate the photosensitizer, which has accumulated in a tumor or affected tissue, into its triplet state. The energy of the triplet state of photosensitizers can effectively be transferred to the oxygen molecule and this transfer of the energy gives rise to generation of singlet oxygen [111]. This cytotoxic singlet oxygen causes direct chemical damage to the malignant tissues and to atherosclerotic plaque. The combination of the interaction between light and drug must give rise to a targeted delivery of the cytotoxic effect [91], to make the PDT effective. Singlet oxygen production is an important issue for PDT and requires a sufficiently high energy of the triplet state of the sensitizer. The following is an example for the photodynamic effect. In mechanistic terms the process appears to depend primarily on singlet oxygen production, leading to a photoreaction, thus:

$$P(S_0) \xrightarrow{h\nu} P(S_1) \xrightarrow{ISC} P(T_1) \qquad (4.1)$$

$$T_1) + {}^3O_2 \rightarrow P(S_0) + {}^1O_2 \qquad (4.2)$$

${}^1O_2$ → results in membrane damage and cell death)

(where P is photosensitizer, S_0 is the ground singlet state, and S_1 is the first excited singlet state, T_1 = first excited triplet state, ${}^3O_2$ = ground state triplet oxygen, and ${}^1O_2 = {}^1\Delta_G$ singlet oxygen), so that the quantum yield of singlet oxygen formation is a significant parameter.

There are two types of PDT reactions. Type I reaction, a radical is formed, which may directly or indirectly induce cell damage. Radical processes occur concomitantly, but appear generally to play a less important role in cellular damage [112].The energy of the excited molecule (the sensitizer) is transferred to another molecule via electron transfer or hydrogen abstraction.

In the other type of reactions, Type II, the cell death is caused by the very reactive singlet oxygen. These reactions involve a process where the photosensitizer is relaxed from its triplet state to its singlet ground state, simultaneously as oxygen is excited from its triplet ground state to its singlet state (also a spin-forbidden inter-system crossing).

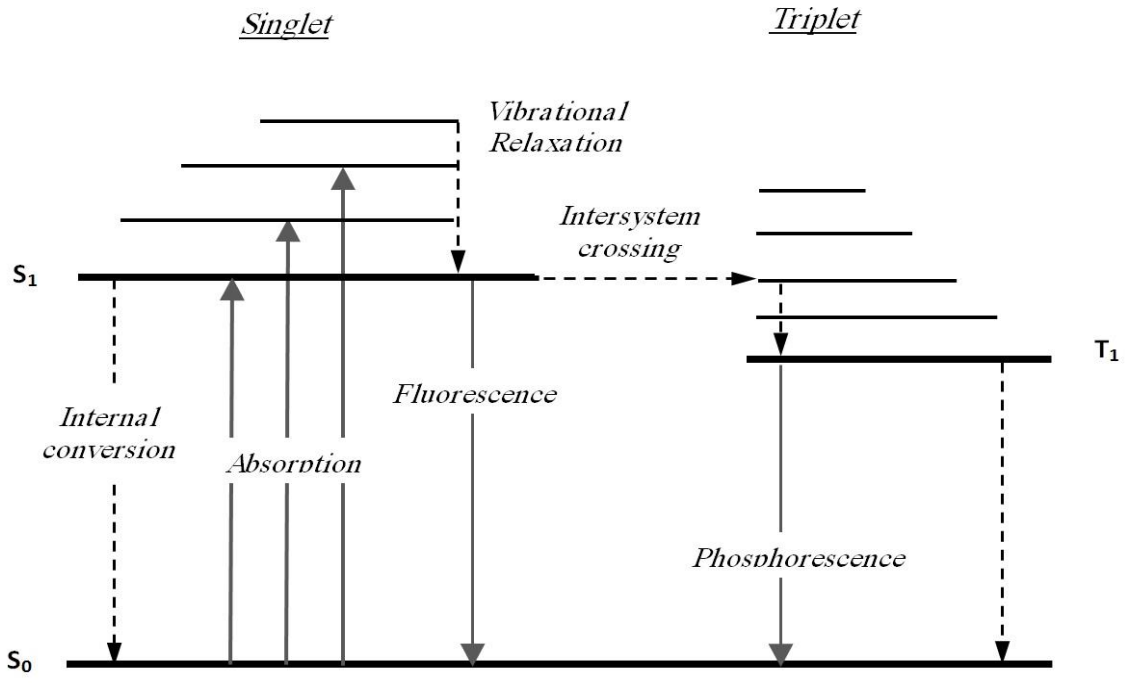

Figure 4.1: *Jablonski diagram.* ***S₀,*** *and* ***S₁*** *are singlet electronic levels,* ***T₁,*** *is triplet electronic levels.*

Fig.4.1 showing the possible photophysical processes in organic molecules. Excited state absorption is possible from both singlet and triplet levels. Fluorescence takes place between levels with the same multiplicity, i.e. S → S or T → T, phosphorescence takes place between levels with different multiplicity, i.e. T → S or S → T. Since radiation transition between levels with different multiplicity is forbidden, the efficiency of the phosphorescence is lower than efficiency of the fluorescence. The efficiency of radiation less processes between excited energy levels is very high so that fluorescence usually takes place only from the first excited singlet level $S_1 \rightarrow S_0$, phosphorescence takes place from the first triplet level $T_1 \rightarrow S_0$. Examples of fluorescence and phosphorescence between other energy levels are extremely rare and even if they do occur, the quantum yield of such processes is very small.

4.2 TPA in Tetrapyrrolic Molecules

Given the significance of the tetrapyrrolic molecules, there are a rather limited number of prior studies of their intrinsic TPA. Particularly, it was found that two-photon cross sections of aluminum phthalocyanine and chlorophyll at λex = 1064 nm are $\sigma_2 = 12.7\ GM$ [113], and $\sigma_2 = 8\ GM$ [114], respectively. For protoporphyrin IX the following values were reported: $\sigma_2 = 0.7\ GM$ at λex= 760 nm, $\sigma_2 = 0.9\ GM$ at λex = 770 nm, $\sigma_2 = 0.6\ GM$ at λex = 780 nm, and $\sigma_2 = 2\ GM$ at λex =790 nm [115]. More recently, a number of TPA cross section measurements were performed for several metalloporphyrins doped into boric acid glass [116]. The measured cross-sections were in the range 25 – 114 GM [117,118]. There are reported TPA spectra of several tetrapyrroles, but without giving absolute values of σ_2. From these experimental studies, one can see that the two photon cross sections of tetrapyrroles are rather small, typically less than 100 GM. Larger cross sections ($\sigma_2 \approx 100 - 1000\ GM$) are required to advance TPA applications of tetrapyrrolic molecules.

J. Rodriguez et al. [119] studied excited state absorption of a large group of porphyrins. H. Gratz and A. Penzkofer [120] investigated $S_1 \rightarrow S_n$ excited state absorption of meso-tetraphenylporphyrin in the wavelength range λ = 250 – 450 nm with respect to the ground state. Strong increase of $S_1 \rightarrow S_n$ absorption was revealed when going to shorter wavelengths.

The first clinical results for m-THPC have appeared in 1991 [115]. The photophysical properties of the porphyrin, m-THPP has been described earlier [121]. Also investigations of the two-photon excitation of the photosensitizer m-THPC at about 800 nm have already been reported [122, 123].

4.2.1 Porphyrins and Derivatives

In this section we give a brief description of the porphyrins and related compounds [124]. The attention paid to porphyrins and related compounds (tetrapyrrolic molecules) can be explained, first by their technological applications, and second by their significance for life on earth. The presence of these molecules is fundamental to our life. Tetrapyrrolic molecules play critical role in the processes like photosynthesis by plants and bacteria, oxygen transportation and storage inside animals (including humans).

Fig.4.2a presents the chemical structure of porphyrin. It consists of four pyrrole rings linked by methine bridges forming a porphyrin macrocycle. The porphyrin macrocycle is a hetero-aromatic system containing 22 π-electrons, 18 of which form a conjugated ring. It means that these electrons are not bound to some specific atom in the porphine but rather delocalized within the macrocycle. The macrocycle is very stable and, as a result, it was chosen by nature to carry out different important functions. By adding different substituents to periphery of the basic macrocycle and/or by introducing metals into the center of the macrocycle one can obtain different types of porphyrins. For example, porphyrin containing iron in the center of their macrocycle is called heme and is found widely in biophysics.

The typical UV-visible absorption spectrum of a porphyrin shows its strongest absorption peak at the Soret band at about 420 nm, accompanied by a weaker absorption bands in the visible up to about 640 nm (Q-bands) (Fig.4.2b). The rich visible absorption spectrum of the porphyrins leads to their strong coloration. Many of the porphyrin molecules solutions have intense red color. For example, the color of the blood is produced by the oxygen-transporting porphyrins. In fact, the word porphyrin is derived from the Greek word “porphyra”, meaning purple.

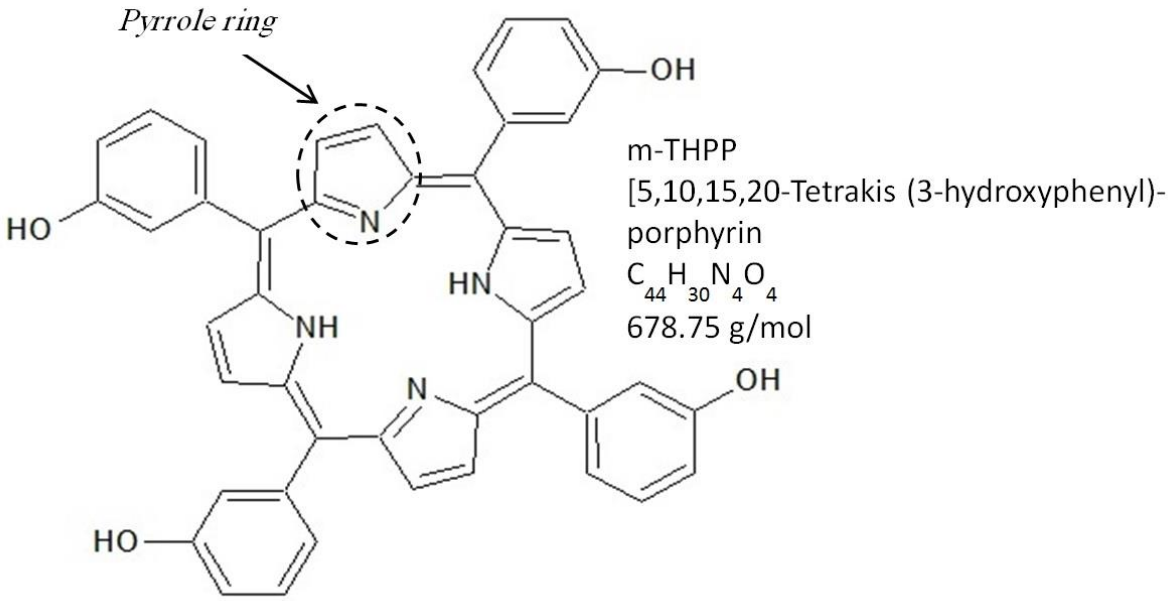

(a)

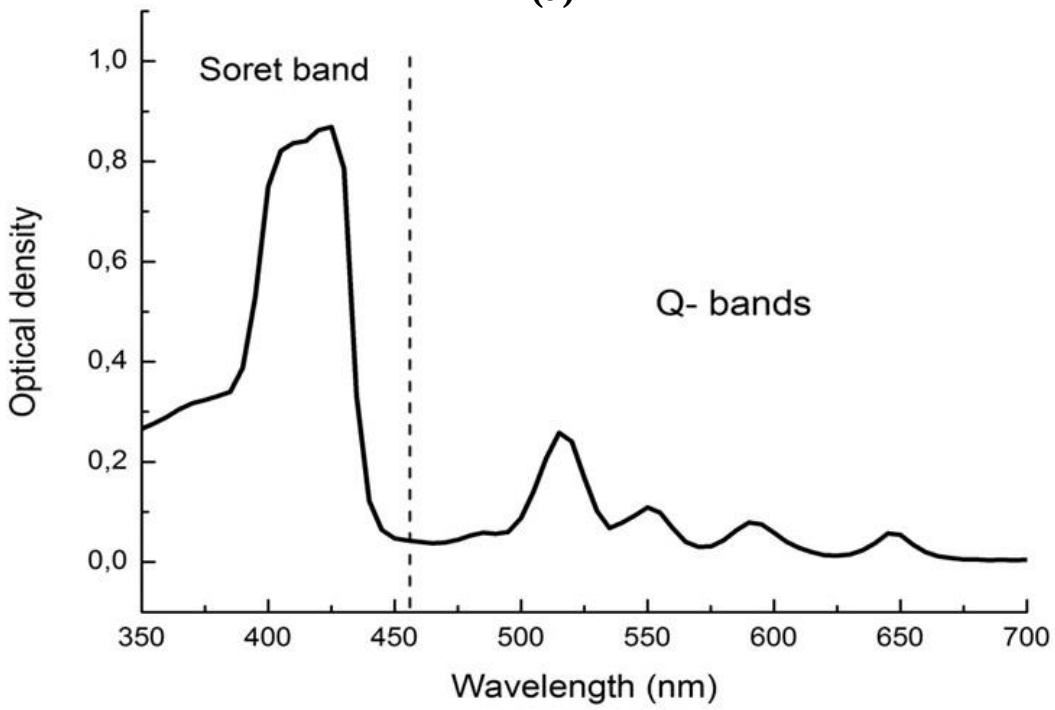

(b)

Figure 4.2: *(a) Chemical structure of porphine. A pyrrole ring is highlighted with a dashed oval. (b) Linear absorption spectrum of porphyrin molecules.*

In order to improve/ or modify the porphyrins, reducing of the pseudoolefinic b,b'-double bonds is possible by adding a metal ion to the center of the ring or by adding of a functional group to the periphery.

The reduction of one or more of pseudoolefinic b,b'-double bonds in the pyrrole rings of the porphyrin to a single bond produce a class of porphyrin derivatives called chlorin-type tetrapyrrole (Fig.4.3).

As a result, the symmetry of the molecule imparts distinct changes to its optical absorption properties [125, 126]. So, the absorption peak shifts to the red spectrum (650nm), which gives chlorin a green color like chlorophyll (magnesium-containing chlorins). They are the central photosensitive pigments in chloroplasts in plants and are involved in photosynthesis. The green color of chlorin gives plants their color.

Another photosensitizer was produced by substituting the two hydrogen atoms in the center of porphyrin ring with palladium. This leads to formation of m-THPP-pd (Fig.4.4).

Finally, by oxidation of two OH groups on opposite sides of the molecule (at the meso-bridge-carbon position) and adding also two hexyl chain groups, we get m-TCP-PD (Fig.4.4).

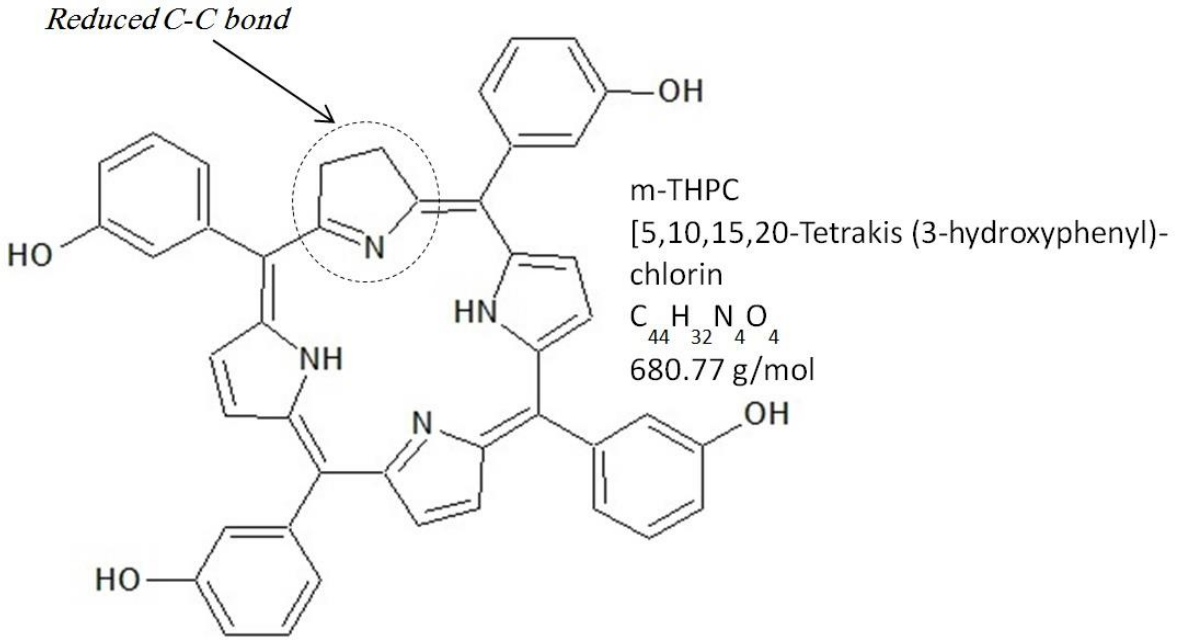

(a)

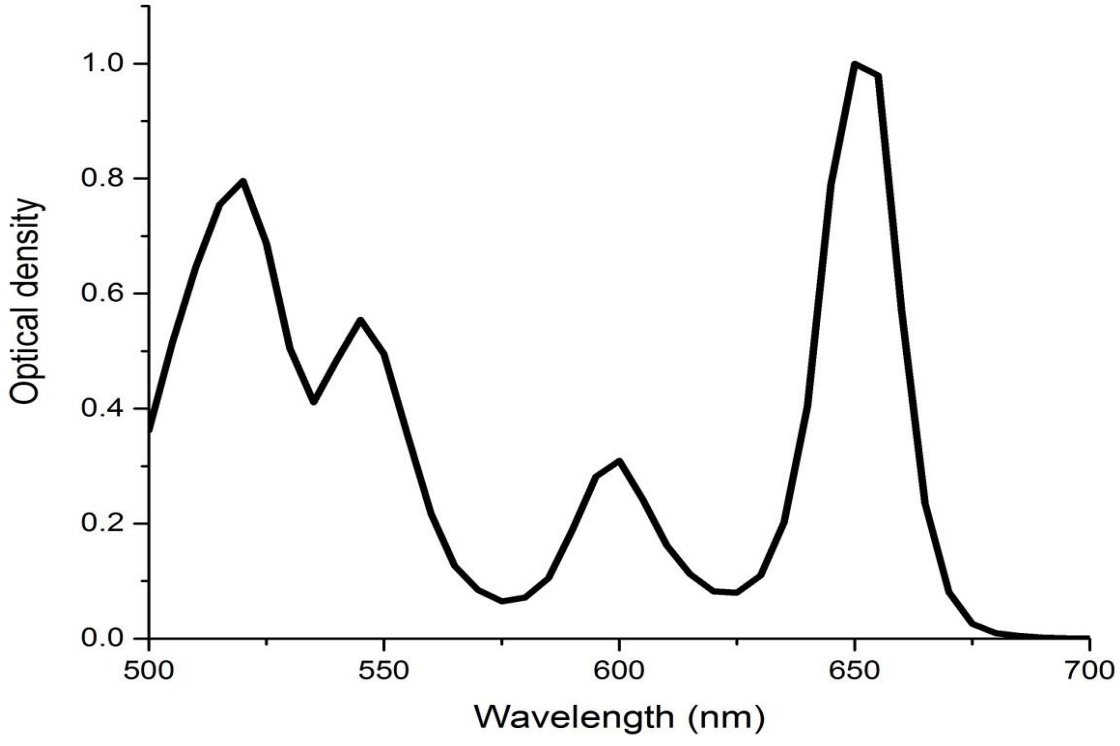

(b)

Figure 4.3: *a) Chemical structure of chlorin. A dashed oval is used to highlight structural difference between the porphine and the chlorin molecule. b) Linear absorption spectrum of chlorin molecule.*

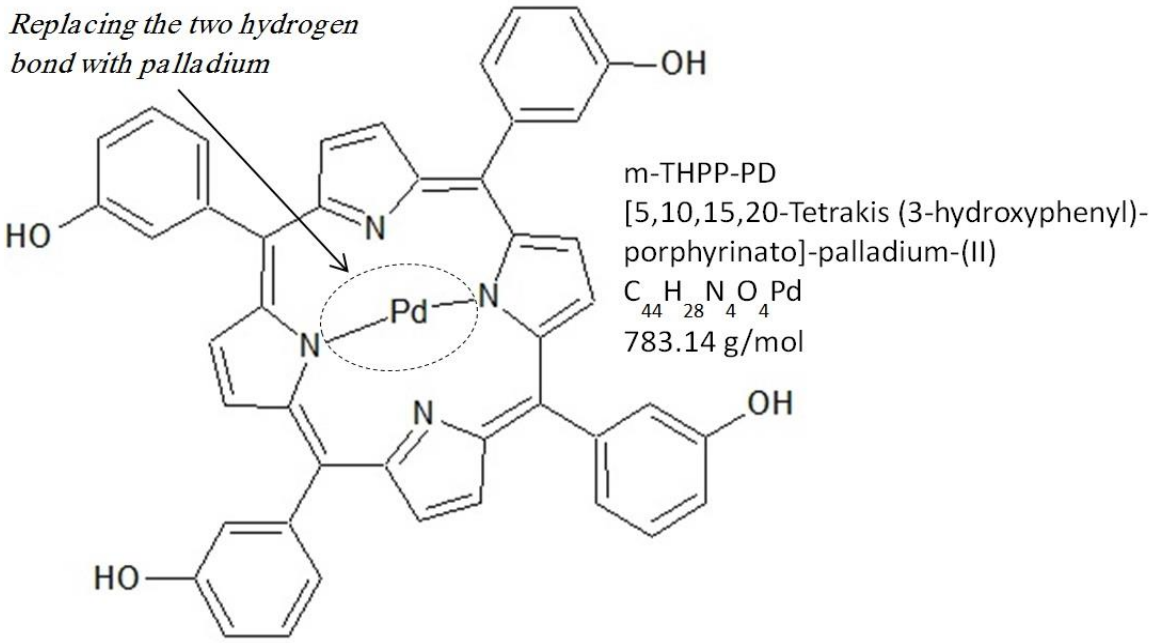

(a)

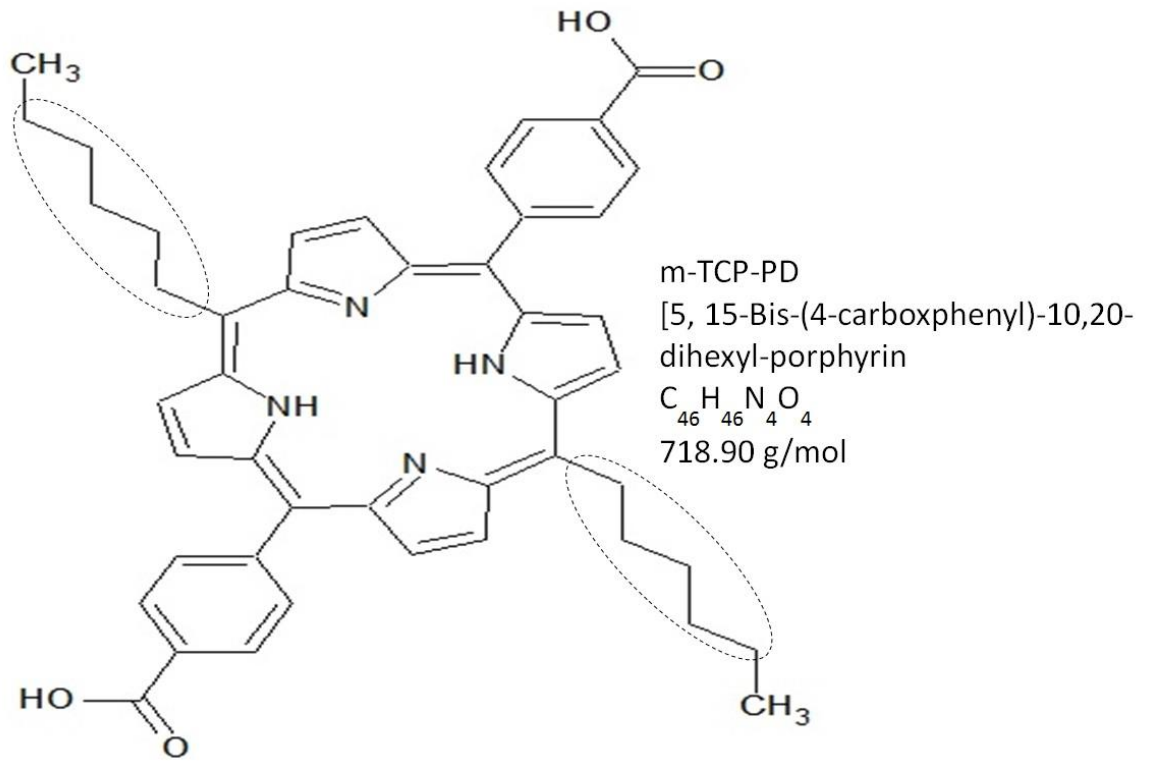

(b)

Figure 4.4: *Chemical structures of (a) m-THPP-PD and (b) m-TCP-PD. Dashed ovals are used to highlight structural differences between the porphine and these two molecules.*

4.2.2 Corroles

Corroles are tetrapyrrolic molecules. They are essentially slightly contracted analogs of porphyrins, by lacking one carbon atom in one of the methyne bridges of porphyrin ring. In spite of the lower symmetry, these structures preserve strong conjugation throughout the tetrapyrrolic macrocycle. They were first reported by Johnson and Kay in 1965 [127]. Corroles were the product of a many step synthetic scheme, finally formed by the photocyclization of a,c-biladienes. While this last step was simple, with 20-60% yields, the route to a,c-biladienes was far from easy. Indeed, the overall reaction from readily available starting materials to corrole was a multi-step synthesis, with poor yields in many of the reaction steps.

Therefore, while corroles have been known for more than 40 years, research in this field was progressing slowly, until the discovery of new synthetic method in 1999 by two groups working independently. Researches in this area really started to expand thereafter [128]. Indeed, the field of corrole research was basically non-existent prior to the development of these new methodologies. Many of the interesting properties of corroles were investigated by different groups. One particular corrole 5,10,15- tris (pentafluorophenyl) corrole, synthesized by the group of Zeev Gross, has been shown to stabilize four formal oxidation states of chromium, Cr(III, IV, V, IV) [129].

Since the synthesis of corroles became easier, the field of corrole has greatly expanded. A quick search of the literature reveals that of all the papers published on corroles in the 40 years since Johnson and Kay's initial publication, almost three-quarters have come out in the last five years.

One of their remarkable properties is the ability to stabilize metal ions in higher oxidation states, such as iron (IV), cobalt (IV), and cobalt (V) [130, 131]. Corroles are very versatile toward substitution and metallation reactions, corroles with varying solubility properties, are useful in many different applications. Some of these corroles form very tight conjugates with proteins, opening up possibilities for use in biological systems [132, 133]. The physical chemistry of corroles has recently emerged as an independent area of research [134–136].

These properties open up potential for using corroles in many applications, including such diverse areas as cancer diagnosis and treatment (PDT), and solar cell research. It is becoming clear that they are a very important class of molecules. A fundamental understanding of the properties of these new molecules is needed. In many respects, in comparison with porphyrins, the corroles exhibit several interesting properties, such as higher fluorescence quantum yield, larger Stokes shift, absence of phosphorescence and increased extinction in the red part of the spectrum. These aromatic tetrapyrrolic macrocycles simultaneously show a strong conjugation and a lowered symmetry, which are both the key properties for the enhancement of TPA. In fact, it has been noted that lowering the symmetry of a molecule, especially if this leads to a large difference in permanent dipole moments between the excited and ground states, augments the TPA [137–141].

We did the TPA cross-sections measurements in the range 1040-1450 nm. Also we investigated the lowest electronic transitions of the Q-band of hexacoordinated aluminum(III) 5,10,15-tris(pentafluorophenyl) corrole molecules, Al(tpfc) and Al(tpfc)(py)2 [142-145] (Fig.4.5).

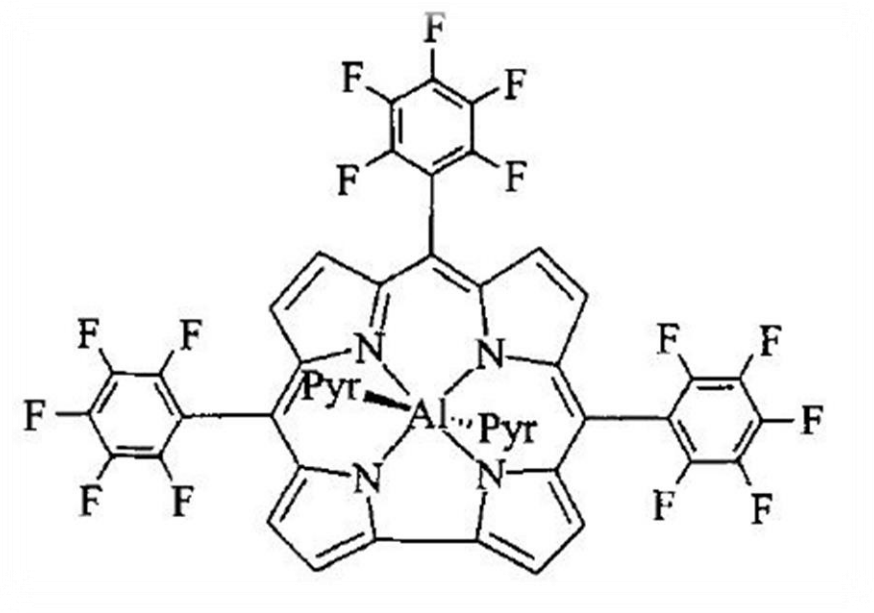

(a)

(b)

Figure 4.5: *(a) Chemical structures of aluminum corrol with two pyridine Al(tpfc)(py)$_2$, (b) Linear absorption spectrum, of Al(tpfc)(py)$_1$ (blue) and of Al(tpfc)(py)$_2$ molecules(red).*

CHAPTER 5

Experimental Measurements of the TPA Cross-Sections

5.1 Set-up Description

The experiments are carried out with short pulses of the mode-locked Ti:sapphire laser (CPA-2001, Clark-MXP, Inc.) having full-width at half-maximum (FWHM) pulse-length of 150 fs at the fundamental wavelength of 775 nm. Ti:sapphire laser is used for TPA measurements as well as to pump our home-build OPA. The tuning range of the OPA with a pulse-width of 100–125 fs is from 1040 to 1450 nm.

The experimental scheme is shown in Fig.5.1. A half-wave (λ/2)-plate and a linear polarizer are used to control the laser energy at the fundamental wavelength, while a variable neutral density filter was used to control the intensity at different wavelengths of the OPA .

The pump beam is focused into the sample with a 75 cm or 40 cm focal length lens (L_1) for the fundamental and the OPA beam, respectively. By splitting the laser beam with a beam splitter BS, 70% of the laser energy is used for the absorption measurements. The change in the transmittance is measured with the photodiode D_1 (probe detector). The reflected part of the beam (about 30%) is detected by photodiode D_2 (reference detector). D_2 is used to diminish the influence of the laser fluctuations by taking the ratio of the signals of the probe and reference detectors. The fluctuations are because of the change in the spatial and temporal profiles of the laser pulse. L_4 lens with focal length of 10 cm is used to collect the signal on the probe detector.

Photodiode D_3 is used to measure the fluorescence intensity simultaneously with the change in the transmittance. L_2 and L_3 lenses with focal length of 2.5 cm each are used to collect the fluorescence signal on detector D_3. A short pass filter FBS750 nm is used to cut off the light of the fundamental wavelength.

The detectors D_1 and D_2 are high-speed photodetectors DET 10C/M sensitive in the range of 700-1800 nm with 10 ns rise time. D_3 is FDS100 photodiode, sensitive in the range of 350-1100 nm. It has active area of 3.6 mm x 3.6 mm and 10 ns rise time.

The amplifiers of the signals from photodiodes are of type DLPCA-D-S4 from Femto, Messtechnik GmbH. The amplifiers are of the integrate-and-hold type. Time delay is used for resetting the amplifiers and to trigger the data acquisition.

The sample is scanned through the focal point using a motorized translation stage (model M-505-6PD) Physik Instrumente (PI) GmbH & Co.KG, which has a minimum step-size of 0.249 μm.

A sample is excited by means of two-photon absorption. Depending on the required wavelength, either the Ti-sapphire laser beam, or the beams from the optical parametric amplifier in the range 1.04-1.45 μm are used. The diameter of the laser beam is about 1 cm for the Ti:sapphire laser (fundamental) and 0.5 cm for the optical parametric amplifier. One needs the following parameters to describe the laser beam: beam waist, excitation wavelength, pulse duration, average intensity of the excitation light, and the repetition rate of the laser pulses.

The sample is moved along the axis of the beam. Due to the change in the intensity we have a change in the two-photon absorption and as a consequence a change in the transmittance of the sample. Knowledge of the transmittance versus sample position allows determining TPA cross-section. The transmitted power measurement and sample movement could be controlled simultaneously. To do this, programs were written in Visual C++ and Labview.

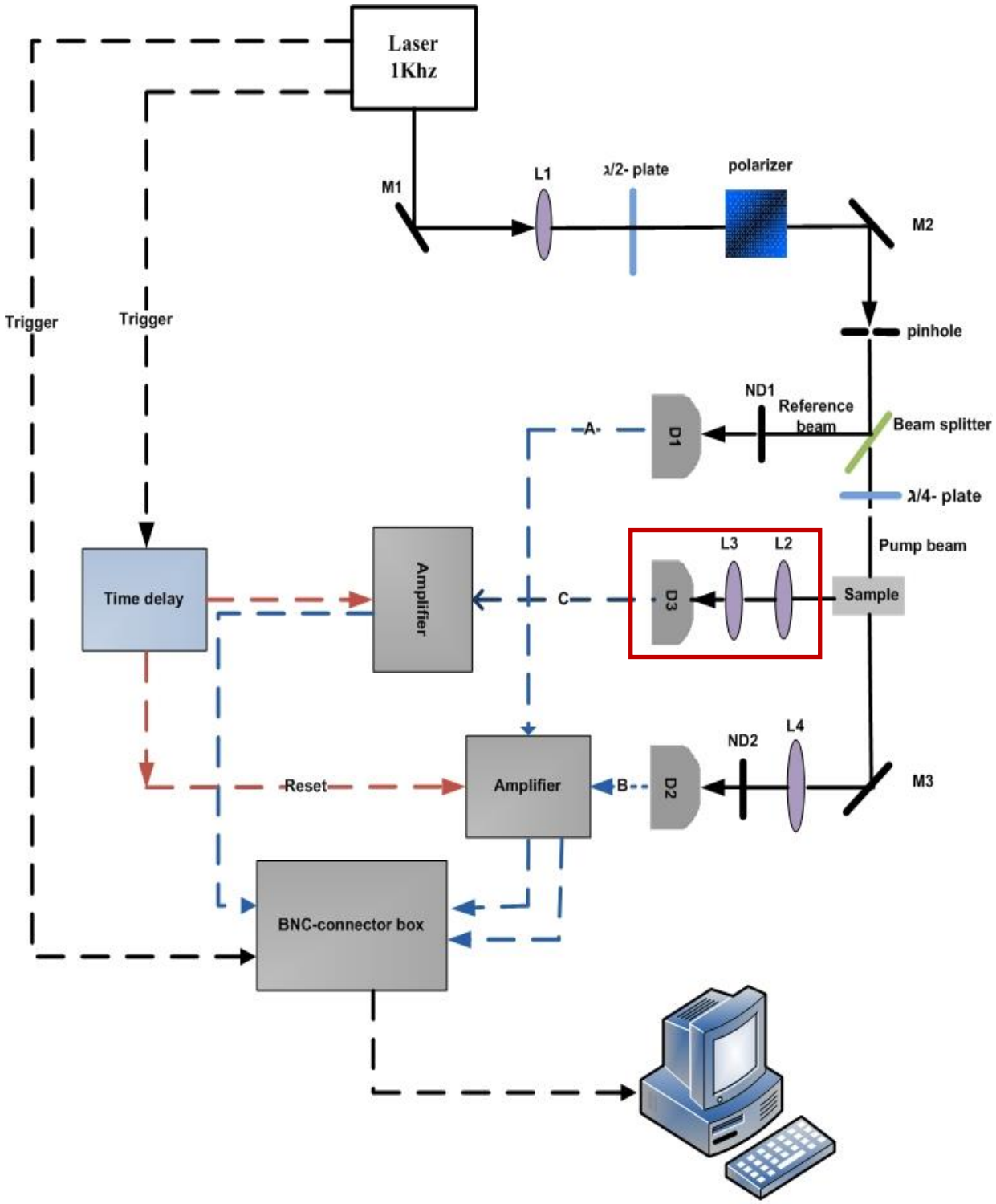

Figure 5.1: *Experimental setup for fluorescence (marked in red) and two-photon absorption measurements, D_1, D_2, and D_3 are photodiodes, ND_1 and ND_2 are neutral density filters, L_1, L_2 and L_3 are lenses.*

A pump beam waist ω_o is measured with a scanning knife-edge method, by taking the distance between the knife-edge positions (Fig.5.2) where 90% and 10% of the maximum power are transmitted. This beam size w (z) at the knife position is given by [146]:

$$w(z) \cong 0.78.\,(x_{10\%} - x_{90\%})$$

Fig.5.2 (a) shows scanning knife-edge power profile of the beam at 1050 nm. The blue circles are the normalized experimental data points and the red curve is the fit of the data. The determined beam waist is in the range from 0.1 to 0.14 mm at wavelengths of 1040 - 1450 nm (OPA). This corresponds to a Rayleigh parameter of $z_R = \pi w_o^2 / \lambda$ = about 30 - 40 mm. w_o is about 0.08 mm at the focal plane of the lens giving a Rayleigh range about 26 mm at 775 nm.

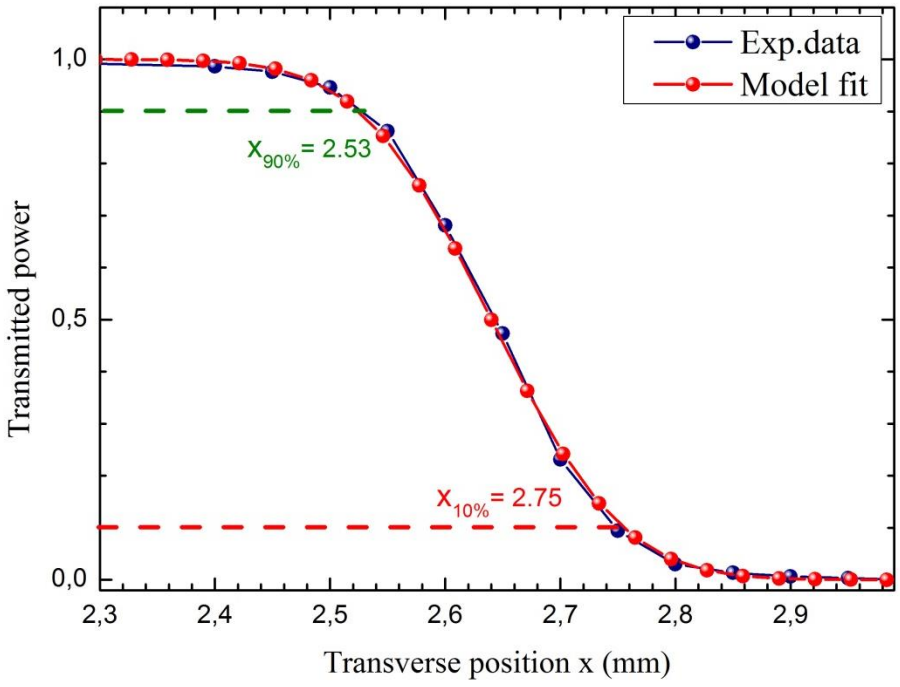

(a)

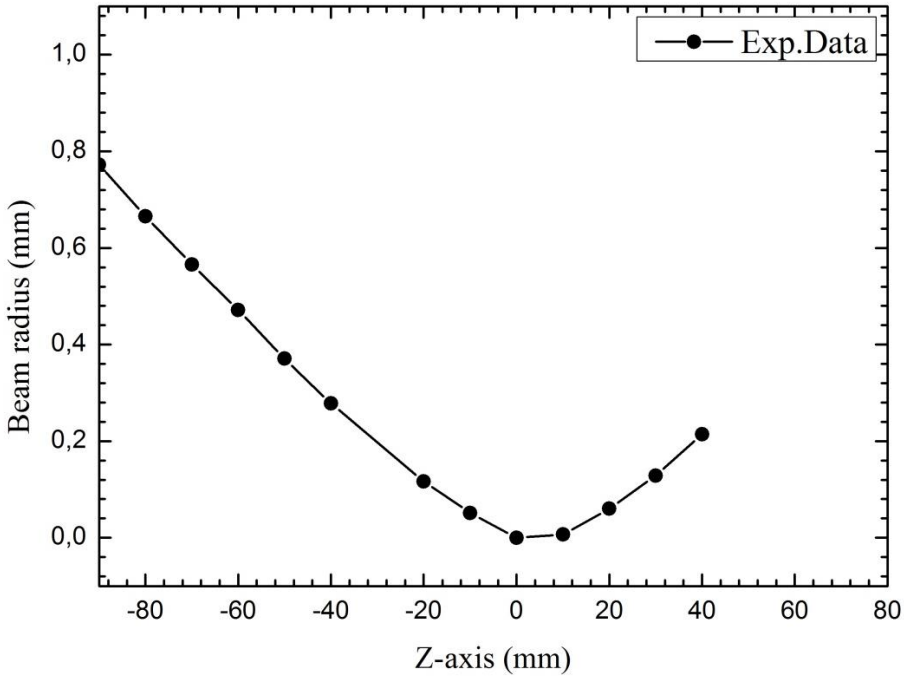

(b)

Figure 5.2: *(a) Measured transmitted power profile of the Ti:sapphire laser beam. (b) Measured radius of the laser beam near the focus.*

Fig.5.2 (b) shows the beam radius of the focused laser beam at different z-positions. These measurements show that, the intensity profile of the beam is rather well described as Gaussian one.

As alternative, we could check the size of the beam waist from the measured transmittance curves. We use the width of these curves at the half of the maximum of transmission changes. As we have quadratic dependence of the transmission changes on the pump beam intensity, then:

$$\frac{I_{1/2(FWHM)}}{I_o} = \frac{1}{\sqrt{2}} \qquad (5.1)$$

Taking into account that for a Gaussian beam

$$b = 2Z_R = 2\frac{\pi w_o^2}{\lambda} \tag{5.2}$$

$$I = \frac{I_0}{1 + (\frac{2z}{b})^2} \tag{5.3}$$

We get

$$b = \frac{2z}{\sqrt{\sqrt{2} - 1}} = \frac{2z}{0.6} \tag{5.4}$$

where b is the confocal parameter, z is the distance as shown in Fig.5.3. I_o is the maximum intensity, $I_{1/2}$ is the intensity at the half transmittance change. The values from such estimation correspond to the knife-edge method.

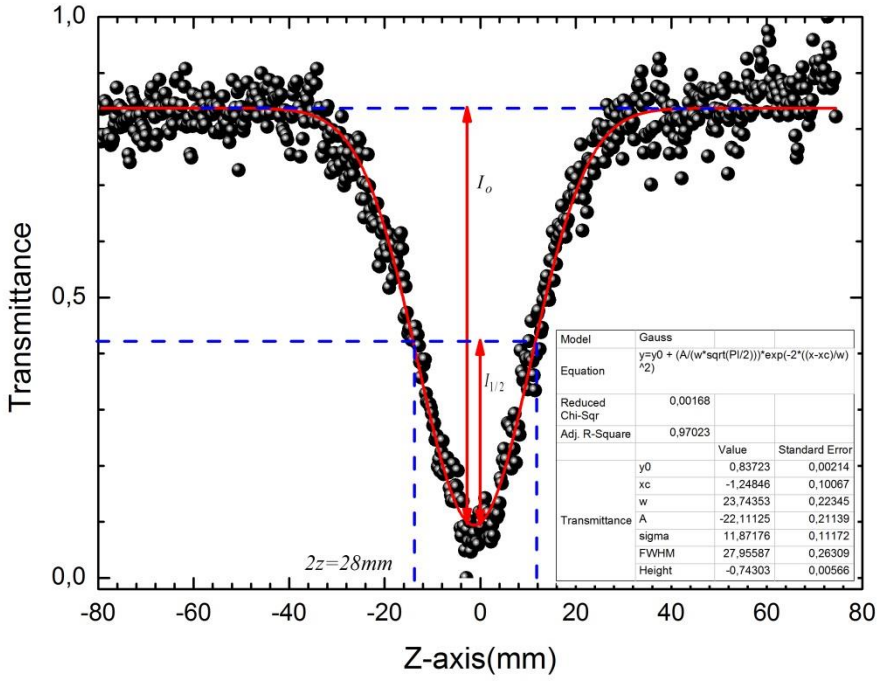

Figure 5.3: *Change in the transmittance for R6G in DMSO solvent.*

Experimental limitations one can expect from the fact that large excitation intensities, required for TPA, may lead to undesired side-effect such as Raman scattering, self-phase modulation, white light continuum generation and others. Strong side-effects can easily mask the TPA.

The calibration of our system was done with Rhodamine-6G, Rhodamine B (RhB), and Coumarin 47 solutions. Their TPA cross-sections are well known. RhB and Coumarin 47 were dissolved in methanol, R6G was dissolved in DMSO (dimethyl sulfoxide) in concentration of 5.4 mmol/L. The measured cross-section is 26 ± 5 GM for Rh6G in a methanol solution. (1 GM is equal to 10^{-50}cm^{4}s/photon/ molecule). It agrees with the value measured in [147]. A detailed study of Rh6G TPA cross-section at 780–806 nm has been reported [148], it varies from 8 to 134 GM.

The sample thickness is 3 or 5mm, which is smaller than the Rayleigh parameter. In this case, we can with good accuracy take intensity to be approximately the same along the beam within the sample cell. To fit z-scans curves, the analytical expressions describing the transmission of Gaussian laser pulses through a two-photon absorbing medium, which are valid for arbitrary absorber thickness [149] are used.

To confirm that the change in the transmission is due to the TPA, the power dependence of the change was measured regularly. There is a number of nonlinear effects, as, for example, Kerr-lensing and thermal lensing, which can affect the measurements. They influence the collection of the transmitted signal on the detector and can be interpreted as a change in the transmitted power. Typically, dependence of the absorption on the power was close to quadratic if the relative nonlinear absorption does not exceed 10–15%. For higher absorptions, the dependence deviates from quadratic because of saturation effect.

The nonlinear absorption coefficient β and the TPA cross section σ_2 can be calculated from the transmittance, as mentioned in the Chapter 2 (see Eqs.2.9 and 2.8).

The measurements of small changes in transmission require rather stable laser sources because we measure low variation of large signal. This method is useful to calibrate the data and to determine-absolute of the TPA cross-sections. But it is more convenient and precise to obtain

TPA spectra by measuring the corresponding intensity of two-photon excited fluorescence while tuning the OPA's output wavelength.

The fluorescence-based method is suitable for all compounds studied in this work. The method was first proposed by M. D. Galanin and Z. A. Chizhikova [150] and later used with some modifications in a number of studies [151-153].

The intensity of the fluorescence is measured as a function of the excitation wavelength. Since for large organic molecules, including tetrapyrroles, the quantum yield of fluorescence is independent of the excitation wavelength, the resulting fluorescence spectrum, in effect, represents two-photon absorption spectrum in some arbitrary units. To get the absolute magnitudes, one needs to calibrate measurements.

Applying the fluorescence-based methods, one should account for the re-absorption.

TPA induced fluorescence is a sensitive technique for the determination of TPA cross-sections, because we measure signal variation starting from zero. Our results show that the quadratic-intensity dependence of the two-photon fluorescence intensity is valid only at low excitation intensity. When increasing the intensity of the laser beam, we observe that, the two-photon fluorescence amplitude deviates greatly from the square law. This is due to the effects of saturation and re-absorption.

Fig.5.4 shows the square dependence of the fluorescence intensity versus excitation laser power at 1050 nm. It provides reliable evidence that the fluorescence emission originates from the TPA process.

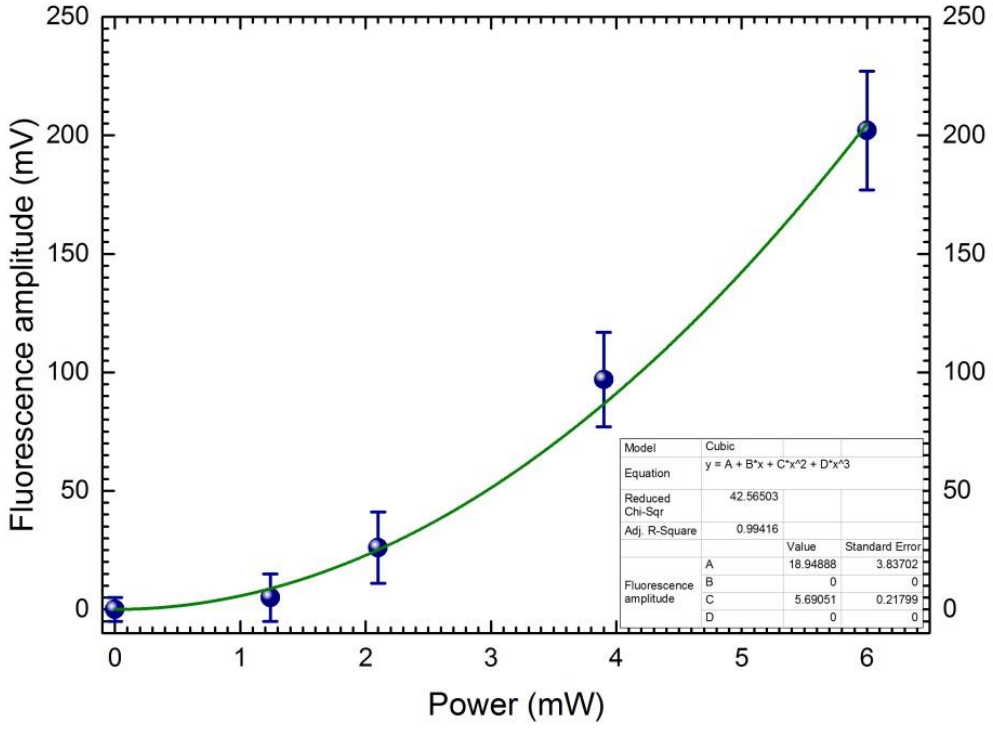

***Figure 5.4**: Two-photon excited fluorescence intensity for Rh6G in MeOH versus excitation intensity of the laser showing a quadratic dependence.*

5.2 Sample Preparation

The $Al(tpfc)_1$ and $(Al(tpfc)(py)_2$ samples were synthesized as reported previously [142, 145]. They are dissolved in toluene (C_7H_8) at the concentration of 2.8- 4 mmol/L. A maximal linear absorption is of about 0.6 OD in the Q-band (Fig.4.5).

The samples m-THPC, m-THPP, m-THPP-PD, and m-TCP-PD were obtained from biolitec AG. They were dissolved in DMSO (dimethyl sulfoxide) at typical concentrations of 1.8–6 mmol/L. m-THPC was also dissolved in methanol and in mixture of 50% ethanol with 50% acetonitrile solvents to study the solvent effect.

5.3 Two-Photon Excited Fluorescence Spectra of Porphyrin and Its Derivatives

The linearly polarized exciting laser beams at 1030 nm or 1300 nm were focused with an f = 40 cm lens into the 5 mm or 10 mm cuvettes with the samples positioned at the focal point of the lens. The TPEF signal in the perpendicular to the beam direction with the lens (f = 2.5 cm) and further focused on the Ocean-Optics spectrometers with other lens. The laser polarization is adjusted to be in a vertical plane with the help of a half-wave plate.

The one-photon fluorescence is measured with the Fluorlog-3 Spectrofluometer (Horiba Jobin Yvon).

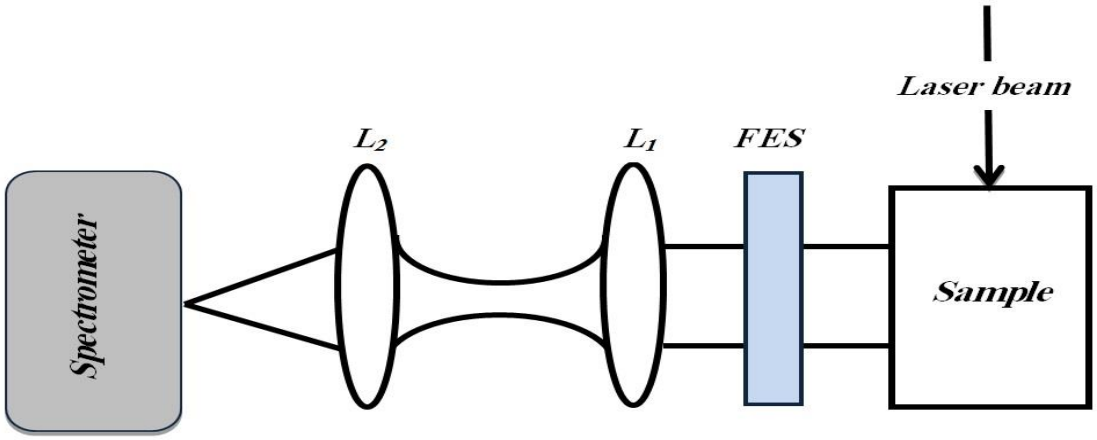

Figure 5.5*: Two-photon excited fluorescence measurements scheme, L1 and L2 are lenses with focal length of 2.5 cm each, FES short pass filter 750 nm.*

From Fig.5.6 one can see that there is a shift between one and two-photon fluorescence spectra for the four investigated samples.

For m-THPP-PD the first peak in one-photon fluorescence at λ_{max}=650 nm is dominating in comparison with the two-photon excited fluorescence. We assumed that this is because of the re-absorption in the sample.

There is primary absorption processes when the pump radiation is absorbed and there is secondary processes when the fluoresced radiation is absorbed. The primary absorption processes, which are independent of all of the other photophysical and instrumental factors, reduce the intensity of the excitation radiation and, as a result, reduce the amount of the observed fluorescence [154, 155, 156].

In order to remove or minimize deviation that can arise from using two different instrument systems for the absorption and the fluorescence measurements, Parker and Barnes [157] propose the use of a correction factor [158, 159, 160]. It corrects the absorption of the excitation radiation [161, 162].

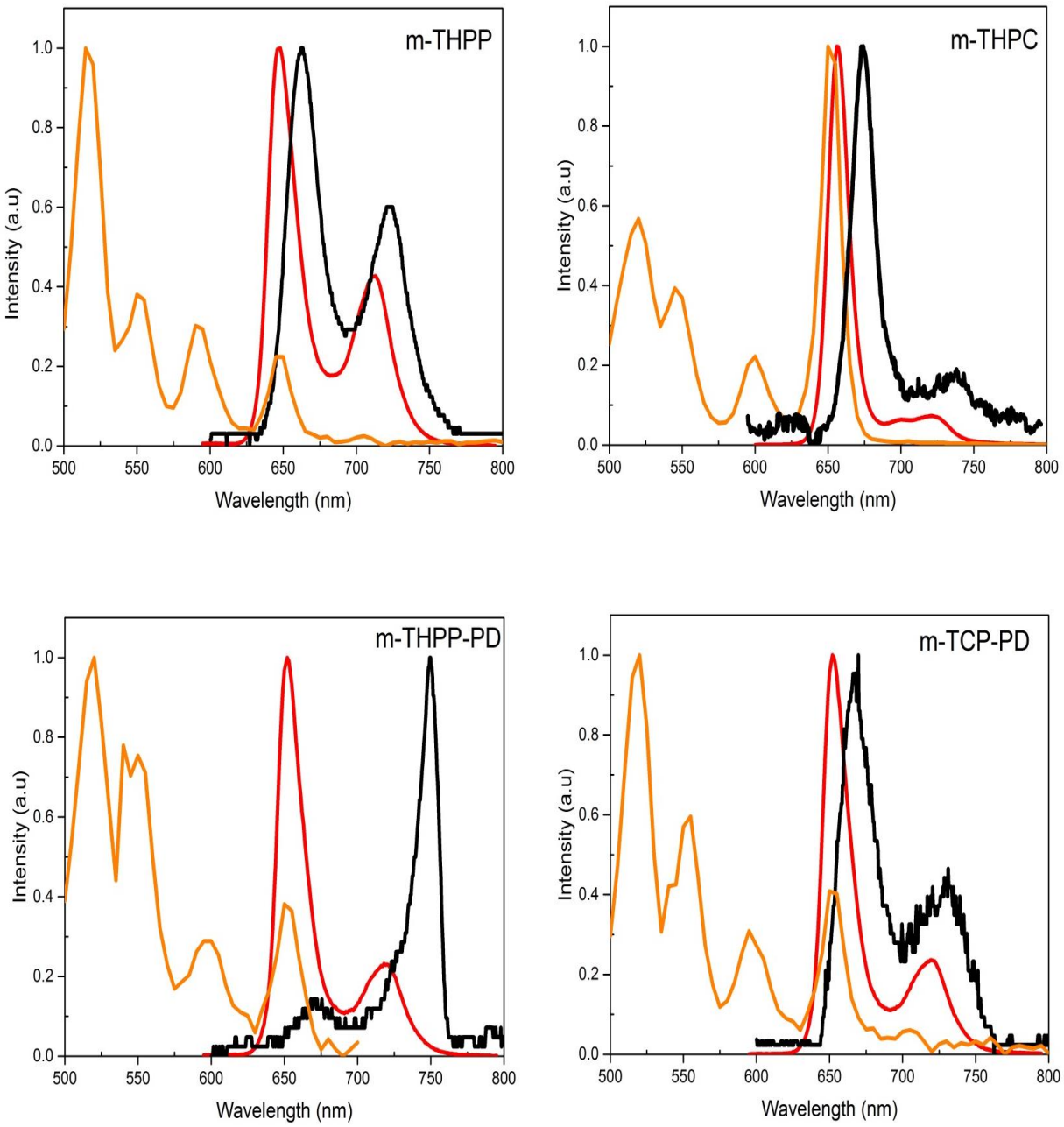

Figure 5.6: *One-photon (red lines) two-photon (black lines) fluorescence spectra and one-photon absorption spectra (orange lines) of m-THPP, m-THPC, m-THPP-PD and m-TCP-PD.*

5.4 TPA Properties of Tetrapyrrolic Molecules

Here we present the measurement of the TPA cross-sections and two-photon excited fluorescence (TPEF) of six photosensitizer.

The following figures (Fig.5.7, Fig.5.8 and Fig.5.9) show the measured absolute TPA spectra. The laser excitation wavelengths is tuned in the range λ_{ex} = 1040 – 1400 nm. Also the SPA spectra are shown in the corresponding transition region of (λ_{tr} = 520 – 700 nm). The solid line show the SPA, the filled circles with the solid lines show the TPA cross-section spectra, and filled squares with solid lines show the TPEF spectra. The x-axis presents the transition wavelength.

Our measurements of TPA cross-sections at 775 nm for *m-THPC*, *m-THPP*, *m-THPP-PD* and *m-TCP-PD* dissolved in DMSO give the magnitudes of 28 $\pm$ 8 GM, 60 $\pm$ 20 GM, 120 $\pm$ 40 GM and 50 $\pm$ 20 GM, respectively. The value reported in the literature [122] is σ_2 = 18 GM at 800 nm for the m-THPC dissolved in 20% ethanol, 30% polyethylene glycol and 50% distilled water. TPA cross-sections of about 2000 GM have been reported for other potential tetrapyrrole-based PDT agents– tetraphenylporphycenes [163]. These significantly enhanced TPA cross-sections are due to near one-photon resonance with the Q-band transition around 650 nm [163-165]. This effect is supported by a Soret-band absorption at wavelengths shorter than 400 nm and is reduced by red shifted Soret-band absorption at wavelengths longer than 400 nm [163]. For m-THPP and m-THPC the Soret-band absorption is red shifted and peaks at about 420 nm, gives a negligible resonance enhancement of TPA at 775 nm.

The two- and one-photon absorption spectra of *m-THPC*, *m-THPP*, *m-THPP-PD* and *m-TCP-PD* are presented in Fig.5.7 and Fig.5.8. The TPA spectra are plotted against half the excitation wavelength value to allow comparison with the one-photon absorption spectra. It can be seen that the transition features for the one- and two-photon absorptions are very similar, and if we could more precisely determine the maxima of the TPA spectra, they would most probably be the same for *m-THPC*, and *m-THPP*. It is possible that one- and two-photon excitations may reach the same excited state if a molecule is not centrosymmetric like in Foscan (*m-THPC*)or through relaxation of symmetry rules by vibronic coupling [148,166–

168], or due to conformational effects [163]. As a result, the same band could appear in both, one- and two-photon absorption spectra, although with different relative intensities. The molecule in this study m-THPP is centrosymmetric, whereas the m-THPC is not. In the m-THPC the symmetry is broken by the reduced double bond. The decrease in symmetry results in higher intensity of the long wavelength Q-band in the absorption spectrum of chlorins. The reduced symmetry increases the TPA probability for the symmetry-forbidden transitions. The observation of the relatively high and not resonance enhanced TPA in the Q-band region between 500 and 700 nm for both symmetric and not symmetric molecules shows that the vibronic coupling [168] and conformation [163] could play an important role here.

The TPEF spectrum differs from two-photon absorption cross-sections spectrum. It does not follow exactly the two-photon absorption spectra for *m-THPC*, and *m-THPP* (Fig.5.7). The main difference is not in the peak's positions but in the peak's intensity. We attribute these differences not to photophysical properties of the samples, but to some factors or parameters, which we did not manage to control properly. Between such factors could be re-absorption of emitted fluorescence light as well as changes in geometry of fluorescence collection and transmitted light detection when tuning the OPA's output wavelength.

From Fig.5.8 it can be seen that, the TPEF spectra follow the two-photon cross-section measured with the z-scan technique for *m-THPP-PD* and *m-TCP-PD.*

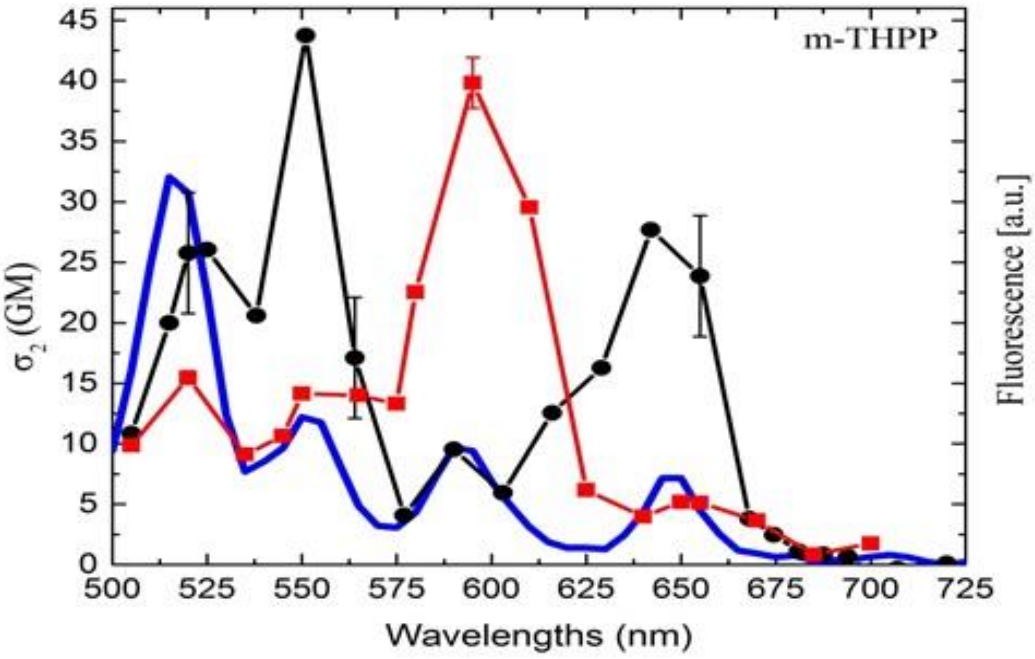

(a)

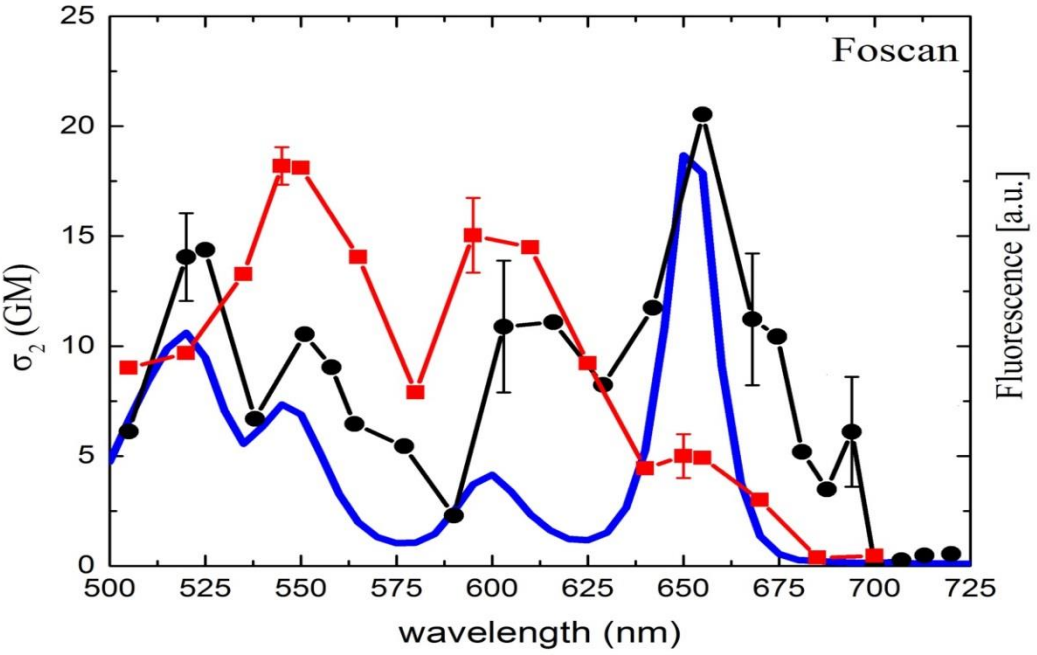

(b)

Figure 5.7*: Two-photon absorption (black), fluorescence (red) and one-photon absorption spectra (blue) for (a) m-THPP and (b) m-THPC dissolved in DMSO. The TPA spectra are plotted against half the excitation wavelength.*

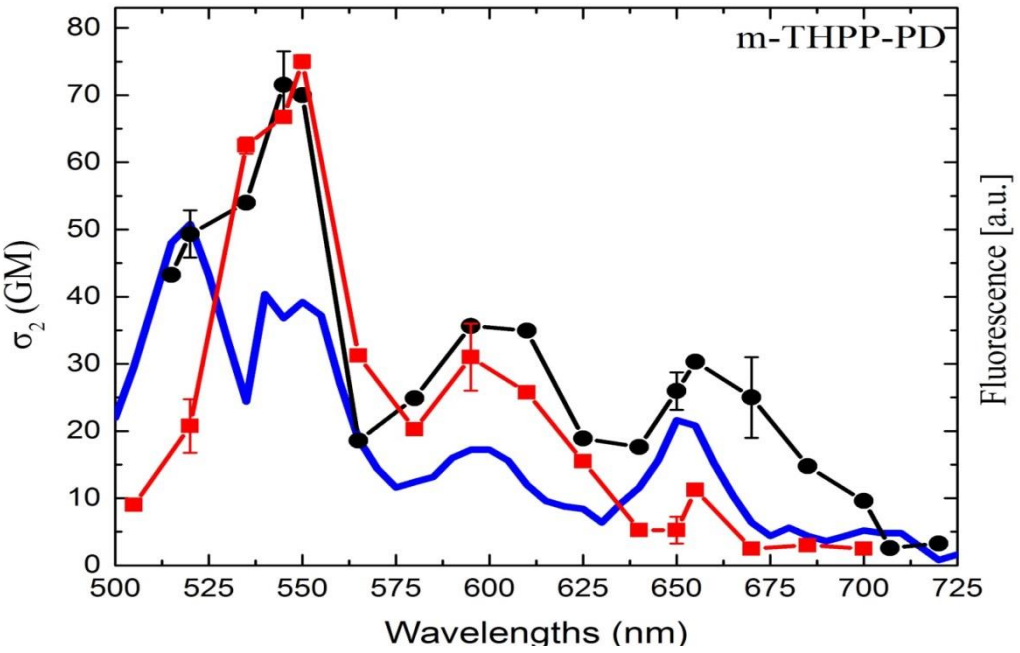

(a)

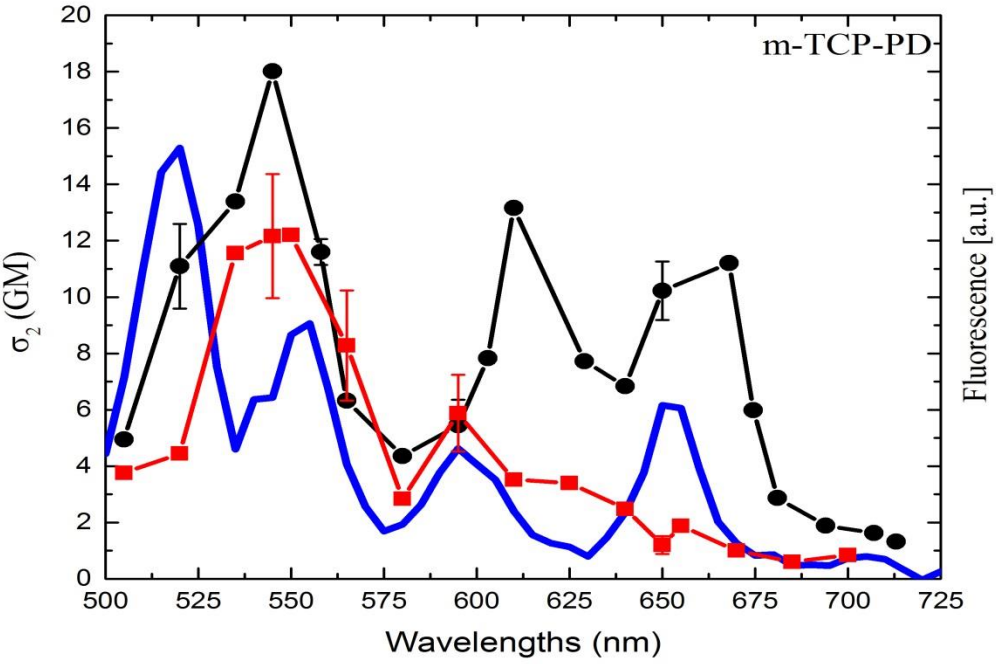

(b)

Figure 5.8*: Two-photon absorption (black), fluorescence (red) and one-photon absorption spectra (blue) for (a) m-THPP-PD and (b) m-TCP-PD dissolved in DMSO. The TPA spectra are plotted against half the excitation wavelength.*

TPA cross-sections and spectra of two corroles Al (tpfc)$(py)_1$ and Al(tpfc)$(py)_2$ in the spectral range of 1040–1400nm were studied . In contrast to symmetrically-substituted porphyrins, the TPA spectrum of corrole contains a distinct peak at the laser wavelength close to twice the wavelength of maximum of the Soret-band (850 nm). The corrole has a quite significant cross section, σ_2 = 60–130 GM [169]. Lowering of the symmetry relaxes the parity selection rules for TPA, thus making the Soret-band allowed for two-photon transition.

SPA spectra of Al (tpfc)$(py)_1$ and Al(tpfc)$(py)_2$ show strong bands around 580 nm and 622 nm. In analogy to porphyrins, one usually keeps the notations Soret and Q-band for the short and long-wavelength bands, respectively.

In both Soret and Q- band, the TPA transition wavelengths do not coincide with the corresponding one-photon transition wavelengths. This indicates that, in contrast to centro-symmetric porphyrins [170–173], the corroles are non-centrosymmetric. Fig.5.9 shows TPA spectra with at least four distinct peaks, one in the Soret- and three in the Q- band.

Our measurements of TPA cross-sections at 775 nm for Al(tpfc)$(py)_1$ and Al(tpfc)$(py)_2$ give the magnitudes of 133 $\pm$ 40 GM and 300 $\pm$ 90 GM, respectively.

The TPEF spectra do not follow the two-photon absorption spectra for Al(tpfc)$(py)_1$, while in Al(tpfc)$(py)_2$ both spectra are rather identical.

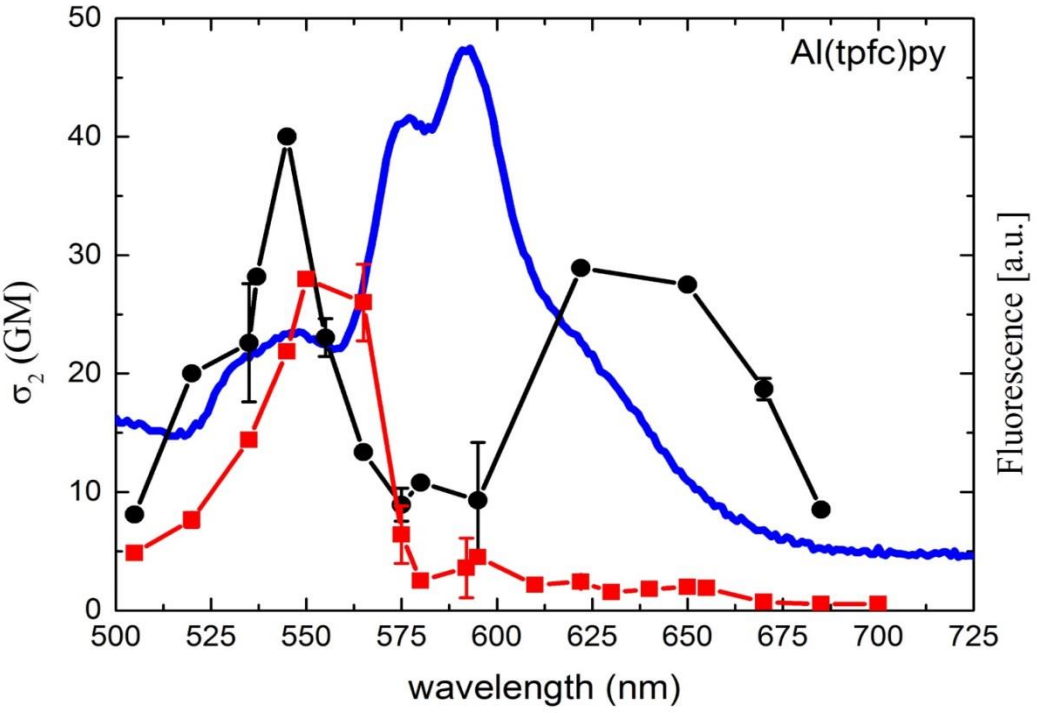

(a)

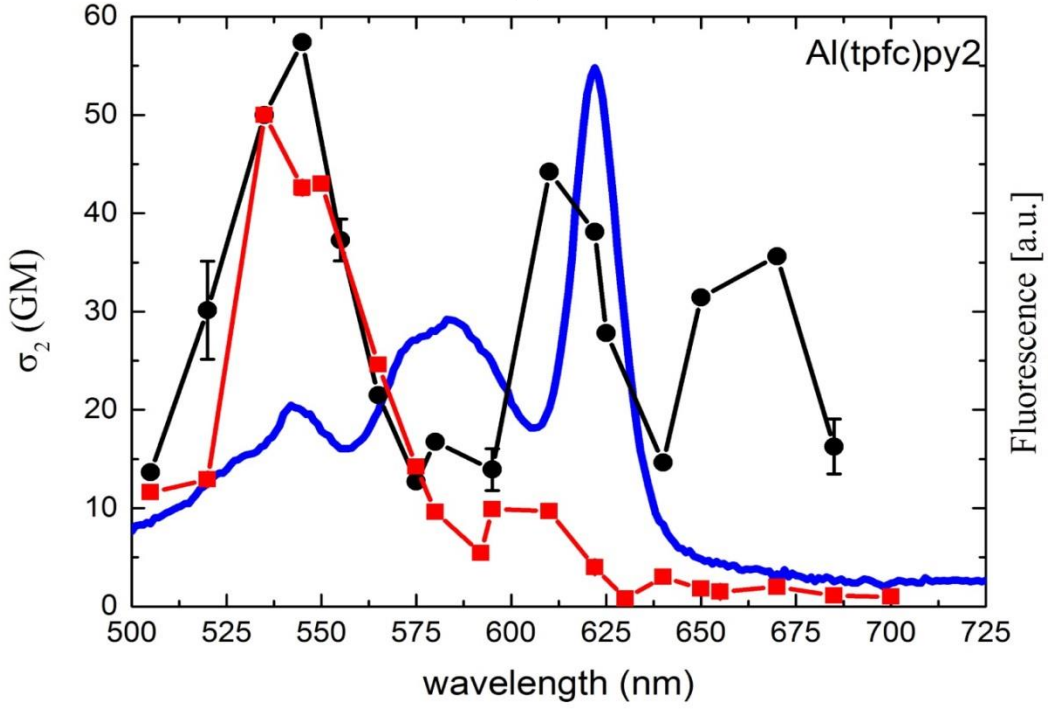

(b)

Figure 5.9*: Two-photon absorption, fluorescence and one-photon absorption spectra for (a)* Al (tpfc)$(py)_1$ *and (b)* Al (tpfc)$(py)_2$ *dissolved in toluene. The TPA spectra are plotted against half of the excitation wavelength.*

5.5 TPA Cross-Section for Linear and Circular Light Polarization

The polarization effects can reveal important information about photophysical properties of the organic compounds. It can provide information about the angle between dipole moments [174], symmetry of excited states [175]. In chiral samples, it allows to obtain information on magnetic-dipole and transition electric-quadrupole moment [176, 177].

Synthesis and design of molecules with large σ_2 has received a lot of attention [178-180], for applications such as the two-photon imaging microscopy [181] photodynamic therapy [182], optical limiting [183], all-optical switching and signal processing [184] etc.

Generally, the TPA and TPEF measurements are performed with linearly polarized light. McClain and co-workers [185, 186] have laid the early foundation for describing the polarization dependence of TPA of isotropic liquid samples. They have basically used combination of photons with different polarizations for assigning the two-photon transition rates for different symmetry states. Then, Nascimento [187] discussed theoretically the polarization dependence of the TPA efficiency for randomly oriented molecules in a single-beam regime. Circular dichroism of the TPA is also well-known theoretically for chiral molecules [188, 189].

Recently, TPA spectroscopy with polarization control has drawn great attention due to the possibility of exploring optical effects beyond the electric dipole approximation and also been shown to be a powerful tool in study of complex molecular structures. For example, Olesiak-Bańska [190] and Mojzisova [191] used the polarized two-photon microscopy to investigate the organization of liquid crystalline DNA. Luo and co-workers [192, 193] have also done theoretical studies of polarization effect in TPA for different organic molecules by using *ab initio* response theory. Recently Wanapun *et al.* [194] described a very interesting theoretical method to determine secondary structures in proteins from the differences in TPA for circular versus linear polarizations (circular-linear dichroism). De Boni *et al.* [195] reported anovel L-scan method which allows experimental measurement of polarization dependent TPA effects in chiral molecules.

We measured ratio (**Ω**) of TPA cross-sections and TPEF signals for linear and circular polarizations at different spectral peaks. As it was shown, it is an important parameter for randomly oriented molecules characterization [187], and helps to determine whether a particular transition has a change in symmetry or not. The **Ω** is governed by the tensor patterns of the two-photon transition matrix elements for circularly and linearly polarized beams [187,196]. The tensor pattern is a property of the states involved in the transition and is merely determined by the symmetry of initial and final states, with no role of the intermediate virtual state.

It is stated that the ratio of the cross section for circularly polarized light to that for linearly polarized light $\boldsymbol{\Omega_{CLD}}=(\sigma_{2\,CP}/\sigma_{2\,LP}) < 1$ for any transition involving two states of the same symmetry on any point group with some rare exceptions [187]. For example, if the molecule belongs to a well-defined symmetry point group, we can anticipate that if $\boldsymbol{\Omega_{CLD}} < 1$ the symmetry of the ground and final excited state are the same. In contrast, if $\boldsymbol{\Omega_{CLD}} > 1$, they have different symmetry [187].

An example of different transmittance and fluorescence curves for linear and circular polarizations is shown in Fig.5.10. The quantitative results are presented in Table 5.1. As it can be seen, $\boldsymbol{\Omega_{CLD}}$ does not exceed one for all peaks in the measured TPA spectra for all studied samples, indicating that the excited Q-band states, responsible for the TPA allowed band, have the same symmetry of the ground state. The averaged value for a number of measured peaks in our experiment is $70 \pm 20\%$. It indicates that in our measurements ground and excited states have the same symmetry.

To guarantee the same experimental condition for the measurements, the quarter-wave plate is kept in the setup in both experiments (linear and circular polarization). We oriented the axes of the λ/4-wave plate at 0° angle relative to the original direction of the light polarization in experiments with linear and at 45° angle with circular polarizations. The TPEF experiments also show that the fluorescence signal increases as the polarization changes from circular to linear (Fig.5.10b).

(a)

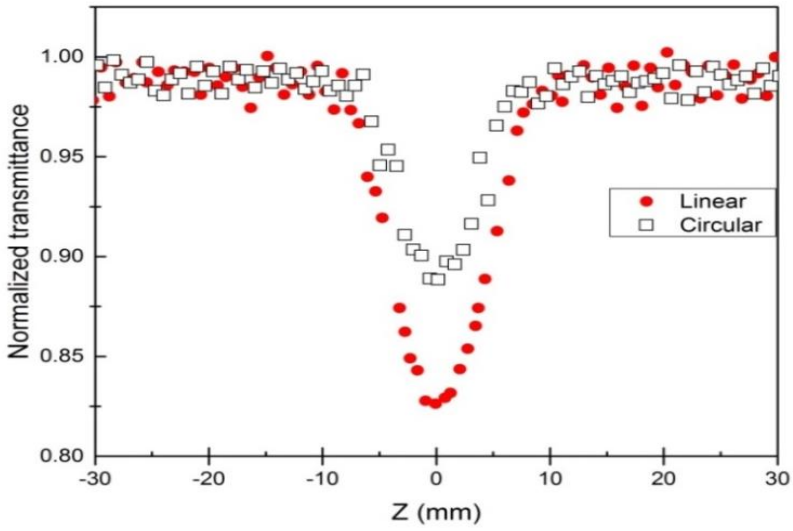

(b)

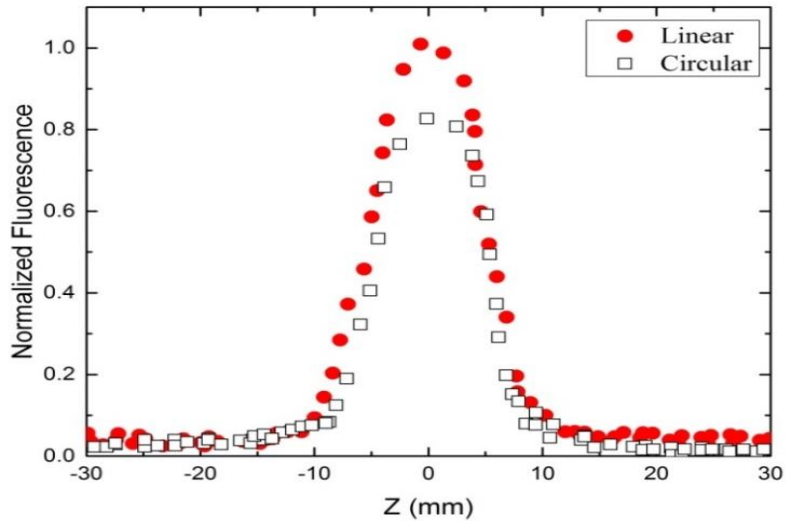

***Figure 5.10**: (a) Transmittance and b) fluorescence curves for linear and circular polarization for m-THPP (porphyrin) in DMSO solvent at 1258 nm.*

Table 5.1 TPA cross-sections for linear and circular polarizations for the six studied photosensitizers.

Wavelength (nm)	*Samples*	σ_2 *-Linear polarization*	σ_2 *-Circular polarization*	Ω_{CLD}
1050 (525)	*m-THPC/ DMSO*	27 ± 5	21 ± 4	0.78 ± 0.2
1076(538)	*m-THPC/ DMSO*	13 ± 3	11 ± 2	0.85 ± 0.2
	m-THPC/ Mix	7 ± 2	4 ± 1	0.57 ± 0.2
1102(551)	*m-THPC/ DMSO*	47 ± 10	33 ± 7	0.70 ± 0.2
	m-THPC/ Mix	31 ± 6	25 ± 5	0.81 ± 0.2
	m-THPP/DMSO	45 ± 9	42 ± 8	0.93 ± 0.2
	m-THPP-PD/DMSO	90 ± 20	60 ± 20	0.70 ± 0.2
	m-TCP-PD/ Meth	4 ± 1	3 ± 1	0.75 ± 0.2
	Al(tpfc)py$_1$	13 ± 3	10 ± 2	0.77 ± 0.2
	Al(tpfc)py$_2$	16 ± 4	4 ± 1	0.25 ± 0.1
1128(564)	*m-THPC/ DMSO*	4 ± 1	3 ± 1	0.75 ± 0.2
1154(577)	*m-THPC/DMSO*	12 ± 3	6 ± 1	0.5 ± 0.1
1180(590)	*m-THPC/ DMSO*	19 ± 4	13 ± 3	0.68 ± 0.2
	m-THPC/ Mix	3 ± 1	2 ± 1	0.67 ± 0.2
	m-THPP/DMSO	11 ± 2	4 ± 1	0.36 ± 0.2
	m-THPP-PD/DMSO	21 ± 5	12 ± 3	0.57 ± 0.2
1258 (629)	*m-THPC/ Mix*	4 ± 1	3 ± 1	0.75 ± 0.2
	m-THPP/DMSO	17 ± 4	11 ± 2	0.65 ± 0.2
	m-THPP-PD/DMSO	41 ± 8	31 ± 6	0.77 ± 0.2
1310 (655)	*m-THPC/ DMSO*	6 ± 1	2 ± 1	0.33 ± 0.1
	m-THPC/Mix	3 ± 1	2 ± 1	0.67 ± 0.2
	m-THPP/DMSO	25 ± 5	14 ± 3	0.56 ± 0.2
	m-THPP-PD/DMSO	30 ± 6	25 ± 5	0.83 ± 0.2
	m-TCP-PD/ Meth	3 ± 1	0.5 ± 0.2	0.17 ± 0.2
	Al(tpfc)py$_1$	16 ± 3	4 ± 1	0.25 ± 0.1
	Al(tpfc)py$_2$	20 ± 4	18 ± 4	0.90 ± 0.2
1362(681)	*m-THPC/Meth*	4 ± 1	3 ± 1	0.75 ± 0.2
	m-TCP-PD/ Meth	4 ± 1	3 ± 1	0.75 ± 0.2

5.6 Study of Solvent Effect in Foscan (Chlorin)

It has been shown that effect of solvent polarity can play an important role in the modulation of σ_2 of the chromophores [197–203]. However, there is a lack of systematic study in this direction. Extensive theoretical and experimental research has been devoted to understanding the solvent dependence in linear spectroscopy [204–206] but the efforts were limited to address solvent effects on TPA of conjugated molecules. Theoretical studies on push-pull molecule [197, 200] show strong dependence of the molecular geometry in solution associated with the solvent polarities, and therefore, polar solvents lead to higher σ_2. The studies of solvent effect on the TPA of $D-\pi-A$ systems [198] displayed a nonmonotonic behavior of σ_2 regarding the solvent polarity. Other theoretical studies with more developed models [200], have found that for charge-transfer molecules σ_2 is more dependent on the optical dielectric constant rather than the static dielectric constant of the solvent. Consequently, a very polar solvent, such as water, does not necessary yields a higher σ_2.

The experiments that have been performed [201–203], confirmed the theoretical predictions [198, 199] that the σ_2 do not show a monotonic dependence on the polarity of the solvent. It was found for distyrylbenzene chromophores [201], that the σ_2 in tetrahydrofuran is higher than in water. However, using the TPA fluorescence method with femtosecond pulses for a series of fluorene and carbazole-core molecules [202], the maximum σ_2 was for a solvent of intermediate polarity (acetophenone). While, the TPA study of the novel dibenzothiophene core-branched structures [203], shows the highest σ_2 in polar solvents.

The influence of the solvent on electronic and geometric properties of compounds is an important aspect and affects their optical properties as well as one/two-photon absorption properties. Almost all the experimental measurements of organic molecules have been carried out in solutions. Parallel different computational calculations have been done [207-209].

It is important to consider the solvent effect, when performing the measurements on the samples which are in solution. Sometimes an enhancement of the TPA is due to the solvent effect.

Methanol (MeOH), DMSO and mixture of ethanol and acetonitrile were used as solvents for the m-THPC samples to study the solvent effect

Solvents of different polarity shift the two-photon absorption spectra of m-THPC. The TPA cross sections show an increasing trend with the increase of solvent polarity. In general, for centrosymmetric molecules, TPA is forbidden for single-photon allowed transitions. However, for non-centrosymmetric molecules due to symmetry relaxations, the SPA and TPA peaks may coincide. Our study shows that in polar solvents the relative intensities of the peaks in the TPA and SPA spectra are similar.

Possible explanation for this phenomenon can be that the weak single-photon peaks at 400nm may be due to the vibronic subbands coupled with electronic states. The coupling of the odd parity component in the electronic state with odd parity component of vibrational state may give rise to even parity component [210], which can be accessible from ground state via two-photon transition. In nonpolar solvents this efficient vibronic coupling may be responsible for increase of TPA peaks.

So, one could resume that one and two-photon excitations may reach the same excited state due to relaxation of symmetry rules via vibronic coupling. In polar solvents DMSO, mixture and MeOH, the vibronic coupling is stronger than for nonpolar solvent. Thus the solvents change the TPA properties of these chromophores through a change in the dielectric constant of the medium, which in turn can change the chromophore electronic structure; or by inducing geometrical distortions like a change in the torsional angle between the aromatic rings of the chromophores. However, it is not possible to specifically identify how the solvent is affecting the vibronic coupling.

With nonpolar solvents the TPA peaks do not coincide with SPA S_2 peak. The peaks are clearly red-shifted. But with the DMSO, the mixture solvents and MeOH the TPA peak actually coincide with the S_2 peak indicating that polar solvents actually assist the two-photon absorption process to reach the pure two-photon allowed state in this particular case.

Table 5.2 shows the TPA cross-sections measurements for chlorin in three solvents (DMSO, methanol and mixture of ethanol and acetonitrile) in the excitation range of 1.01-1.3μm. It can be seen that the higher σ_2 is for high polar solvent DMSO.

Table 5.2 TPA cross-sections for m-THPC (Foscan) in different solvents.

Wavelengths(nm)	***DMSO*** Polarity = 7.2	***Ethanol /Acetonitrile*** Polarity ~ 5.5	***Methanol*** Polarity = 5.1
505	6 ± 2	4 ± 2	1.0 ± 0.3
520	14 ± 4	5 ± 2	2.0 ± 0.6
545	23 ± 7	8 ± 3	4 ± 2
565	9 ± 3	3 ± 1	2.0 ± 0.6
595	13 ± 4	4 ± 2	4 ± 2
650	15 ± 5	5.0 ± 2	3 ± 1

At the end we should note that there are several factors which influence the quality of our measurements. One of them is the cuvette type.

Generally the solvents which are used to prepare the samples are volatile, so it is important to have cuvette which can shut tightly to ensure that the sample concentration remains constant and well known during the measurements. The material of the cuvette is also important. The cuvette must have negligible effect on the transmitted light and do not contribute to the fluorescence.

One of the important experimental considerations is the sample thickness. This thickness must be less than Rayleigh length of the focused laser beam. Then by processing the measured data, we can use approximation that the pump intensity is the same along the sample (so called thin sample).

One should pay attention to the stability of the pump pulses. Unstable light source reduces the accuracy, especially when we should be able to measure about 10% change in the transmission of the sample. Our reference detector and normalization of the informative signal decreases fluctuations, but it does not help against pulse-length and spatial beam fluctuations. In such case, we accumulate and average pulse signal from the photodiodes to reach required accuracy.

5.7 Conclusions

In conclusion, TPA spectra of the transitions of tetrapyrrolic molecules in the visible part of spectrum are obtained. Measured two-photon cross-sections are relatively small. This is explained by the lack of strong two-photon allowed $g \leftarrow g$ transitions in this spectral region.

The measured fluorescence intensity is normalized to the square of the excitation photon flux to be able to compare signals at different pump beam intensities and at different wavelengths. Absolute TPA cross-sections were measured within a broad range of laser wavelengths, 1040–1450 nm (520–725 nm transition wavelengths). We measured the TPA cross-sections of promising photosensitizers for photodynamic therapy m-THPC, m-THPP, m-THPP-PD, m-TCP-PD, Al (tpfc) py_1, and Al (tpfc) py_2. The TPA in the Q-band is comparable with the TPA at 775nm. The question under study now is how effectively the triplet state is populated by the excitation of the Q-band and its vibronic components.

We measured the TPA cross-section for the mentioned above photosensitizers for linear and circular polarized exciting pulses. For all peaks in the measured TPA spectra the ratio of the cross section for circularly polarized light to that for linearly polarized light does not exceed 1. It means that the ground and excited Q-band states are of the same symmetry.

The influence of solvents on TPA process in chlorin was studied. The TPA cross section increases with increasing the polarity of solvents. However, a quantitative description of the solvent effect on TPA and TPEF is perhaps one of a challenging task in spectroscopy because of the unavailability of a good model.

5.7 Zusammenfassung

Zweiphotonenabsorptionsspektren von Übergängen von tetrapyrrolischen Molekülen wurden aufgenommen. Gemessene Zwei-Photonen-Querschnitte sind relativ klein. Dieser Sachverhalt wird durch das Fehlen von starken für Zweiphotonenanregung erlaubten $g \leftarrow g$ Übergängen in diesem Spektralbereich erklärt.

Die gemessene Fluoreszenzintensität wird auf das Quadrat des Erregungsphotonenflusses normiert, um sie bei unterschiedlichen Pumpstrahl-Intensitäten und bei unterschiedlichen Wellenlängen vergleichen zu können. Absolute TPA-Querschnitte wurden in einem breiten Laserwellenlängenbereich 1040 nm - 1450 nm (520 nm - 775 nm Übergangswellenlänge) bestimmt.

Wir haben die TPA-Querschnitte einiger hoffnungsvollen Photosensibilisatoren für die photodynamische Therapie gemessen: m-THPC, m-THPP, m-THPP-PD, m-TCP-PD, $Al(tpfc)(py)_1$, und $Al(tpfc)(py)_2$. Die Zweiphotonenabsorption in der Q-Bande ist vergleichbar mit der bei 775 nm. Die zu untersuchende Fragestellung war, wie effektiv der Triplett-Zustand bevölkert wird, wenn die Q-Bande und ihre vibronischen Anteile angeregt werden.

Wir haben die Zweiphotonenquerschnitte der oben genannten Photosensibilisatoren für linear und zirkular polarisierte Anregung bestimmt. Für alle Linien der gemessenen Zweiphotonenabsorptionsspektren überschreitet das Verhältnis des Querschnittes für den zirkular polarisierten zu den linear polarisierten Strahl nicht die Eins. Das heißt, der Grundzustand und die angeregten Q-Banden-Zustände besitzen die gleiche Symmetrie.

Der Einfluß von Lösungsmitteln auf den Zweiphotonenprozeß wurde für Chlorin untersucht. Der Zweiphotonenquerschnitt wächst mit zunehmende Polarität des Lösungsmittels. Jedoch gehört die guantitative Beschreibung des Lösungsmitteleffektes auf TPA und TPEF zu den größten Herausforderungen der Spektroskopie, da es kein gutes Modell gibt.

Summary

In photodynamic therapy (PDT) m-Tetra (hydroxyphenyl) chlorin (m-THPC, Foscan, Temoporfin) has proven to possess high photodynamic efficacy. This molecule is one of the rare photosensitizers approved for medical application on humans. In comparison I investigated similar molecules and compared them to Foscan. The benefit of two-photon absorption (TPA) is to be able to achieve deeper penetration into tissues. Four promising photosensitizers for photodynamic therapy (in cooperation with biolitec AG) of the porphyrin type: 5,10,15,20-tetrakis (m-hydroxyphenyl) porphyrin (m-THPP), chlorin 5,10,15,20-tetrakis (m-hydroxyphenyl) chlorin (m-THPC, temo-porfin) (Foscan), palladium 5,10,15,20-tetrakis (3-hydroxyphenyl)-porphyrinato-palladium-(II) (m-THPP-PD), and 5,15-Bis-(4-carboxphenyl)-10,20-dihexyl-porphyrin (m-TCP-PD) were studied. Furthermore the TPA cross-sections and spectra of $Al(tpfc)(py)_1$ and $Al(tpfc)(py)_2$ type 5,10,15 tris (pentafluorophenyl) corrole were studied, testing the usage for PDT.

The PDT can be done with one-photon or two-photon excitation. The main disadvantage of single photon PDT is the limited penetration depth of the visible light into the tissue. It is possible to overcome this problem by using two-photon excitation with near-infrared (IR) light.

In order to work with widely tunable light and tune the excitation wavelength, we built an optical parametric amplifier (OPA). The mode-locked Ti:sapphire laser (CPA-2001, Clark-MXP, Inc.) having full-width at half-maximum (FWHM) pulse-length of 150 fs at the fundamental wavelength of 775 nm was used to pump the OPA, generated white light, as well as to carry out some of the TPA measurements. The tuning range of the OPA with a pulse-width of 100–125 fs is from 1040 to 1450 nm. Two-photon processes are proportional to the square of the pump intensity.

Two different techniques were used for measuring TPA spectra and TPA cross sections. One of them is based on the measurement of the change in the transmittance of a sample when it is

scanned along the focused intense pump beam. It is so called open aperture z-scan method. The other one is the two-photon excited fluorescence (TPEF) technique. In this case the integral fluorescence induced due to the TPA is measured. The setup allows to measure the two-photon absorption and the two-photon excited fluorescence, simultaneously.

Absolute TPA cross-sections were measured in the range of 1040 –1450 nm (520–725 nm transition wavelengths) and at 775 nm. Our measurements of TPA cross-sections at 775 nm for m-THPC, m-THPP, m-THPP-PD and m-TCP-PD dissolved in DMSO give the values of 28 $\pm$ 8 GM, 60 $\pm$ 20 GM, 120 $\pm$ 40 GM and 50 $\pm$ 20 GM, respectively.

We found that TPA in the Q-band of studied compounds are smaller compared to the TPA at 775 nm, where the transition is close to the Soret band. Our measurements of TPA cross-sections at 775 nm for Al(tpfc)$(py)_1$ and Al(tpfc)$(py)_2$ give the magnitudes of 130 $\pm$ 40 GM and 300 $\pm$ 90 GM, respectively. In general TPA cross-sections in the range of 60 - 130 GM were reported for corroles.

We measured the TPA cross-section for the mentioned organic molecules for linear and circular polarized exciting pulses. For all peaks in the measured TPA spectra the ratio of the cross section for circularly polarized light to that for linearly polarized light does not exceed 1. This indicates that the ground and excited Q-band states are of the same or similar symmetry.

We studied the influence of solvents of different polarity on the TPA process in m-THPC (chlorin). The measurements show that the TPA cross-section increases by a factor of about 4 with increasing the polarity of solvents start from 5 to 7. We explained this by the change in the dielectric constant of the solution, influencing the TPA properties of the investigated molecule.

Comparison of TPA with single-photon absorption can indicate differences in the symmetry of electronic transitions. In Fig.5.9b the TPA and TPEF at 550 nm is higher than for 590 nm, in contrast to the single-photon absorption. This could be explained by the pyramidalic structure of the corrole ring changing the symmetry for the two transitions.

Moreover, differences in TPEF and TPA could point to different relaxation pathways. In Fig.5.7a the TPEF at 600 nm is much higher than at 550 nm or at 650 nm. This could be explained by a higher quantum yield of the fluorescence at 1200 nm excitation. In turn we expected a higher triplet quantum yield at 550 nm and 650 nm.

My work shows that Foscan and related molecules are potiential photosensitizers, but an increase in TPA cross-section would greatly enhance their applications.

List of Publications

1. Baidaa Hamed , Theodore von Haimberger , Valeri Kozich , Arno Wiehe, Karsten Heyne

   Two-photon cross-sections of the photosensitizers m-THPC and m-THPP in the 1.05–1.45 μm range; Journal of Photochemistry and Photobiology A: Chemistry 295 (2014) 53–56

Appendix A

TPA Image Processing

1. Contrast and Lightness Enhancement Algorithms

Significant discrepancy is existing between the image captured from any digital devices and the observation of real scenes. This is owing to the fact that the captured image consists of the information given by the physical values of light whereas the human perception has nature of dynamic range compression and color rendition on the scenes.
Many algorithms are suggested to enhance color images from any type of distortion (such as noise, lightness change, inverse transform for any operation and color shift) ,in this section we introduce two enhancement methods such as Multi scale retinex algorithm and Histogram equalization, these algorithm are used to enhance both contrast and lightness in the color image.

The idea behind considering the retinex as model of lightness and color perception of the human vision first was proposed by Land [211] and many researchers [211, 212, 213]. MSR is a method for image enhancement that proved color constantly and dynamic range compression. Nevertheless , there are many problems with the original MSR method, one of them is that the main practical consequence of this is not appropriate for application which is sensitive to color [213] and extreme luminance (very dark or very bright regions) in digital image . We use adaptive algorithm which does not change the color in the image because the processing which done on the light component and colors components are conserved and so effective in night images enhancement.

1.1 Multi Scale Retinex Algorithm

The multiscale retinex (MSR) is explained from single-scale retinex (SSR) we have [214, 215]:

$$R(x, y,c) = \log[I(x, y)] - \log[F(x, y,c) \otimes I(x, y)] \quad (A.1)$$

Where $R(x, y,c)$ the Gaussian shaped surrounding space constant at position x, y , c , $I(x, y)$ is the image value and symbol $\otimes$ denoted the convolution . $F(x, y,c)$ Gaussian surrounds function that is calculated by [214]:

$$F(x, y, c) = (k) \exp(\frac{-(x^2 - y^2)}{c^2}) \quad (A.2)$$

k is determined by [216]:

$$\iint F(x, y, c)dx, dy = 1 \quad (A.3)$$

The output of multi scale is then simply a weighted sum of the outputs of several different SSR output where [214,215]

$$R_{MSR}(x, y, w, c) = \sum_{n=1}^{N} w_n R \quad (x, y, c_n) \quad (A.4)$$

Where $R_{MSR}(x, y, w, c)$ the i'th spectral component of the MSR output, N is the number of the scales, $Ri(x, y,cn)$ the i'th component of the n'th scale, and n w_n is the weight associated with the n'th scale. And we insist that (Σw_n =1). The result of the above processing will have both positive and negative RGB values, and the histogram will typically have large tails. Thus a final gain-offset is applied as mentioned in [215] and discussed in more detail below. This processing can cause image colors to go towards gray, and thus an additional processing step is proposed in [214]:

$\grave{R} = R_{MSR} \, . I'_i(x, y, a)$, Where I' given by

$$I'_i(x,y,a) = \log\left[1 + a\,\frac{I_i(x,y)}{\sum_{i=1}^{3} I_i(x,y)}\right] \qquad (A.5)$$

where we have taken the liberty to use log *(1+x)* instead of log(x) to ensure the positive result. In [215] a value of 125 is suggested for (a) second. And the final step is gain-offset by 0.35 and 0.56 respectively [216]. In this work we used *(w_1=w_2=w=1/3)* and (*c_1=250, c_2=120, c_3=80)*. This algorithm done by using the following steps:

1. Input gray image I(x, y).
2. Calculate Gaussian surrounds function $F(x,y,c_n) = (k)\exp\left(\frac{-(x^2-y^2)}{{c_n}^2}\right)$, where k is the normalization constant,c_n, n=3, {c_1=250, c_2=120, c_3=80}.
3. Compute SSR from $R(x,y,c) = \log[I(x,y)] - \log[F(x,y,c_n) \otimes \mathrm{I}(x,y)]$

4. Compute MSR from $R_{MSR}(x,y,w,c) = \sum_{i=1}^{N} w_n R(x,y,c_n)$, N=3, *{$w_1$=$w_2$=$w_3$=1/3}.*

1.2 Adaptive retinex algorithm

We can increase efficiency of the retinex (AR) algorithm by transform the normalized intensity of the gray image by sigmoid function that is given by:

$$\mathrm{S_n} = \frac{1}{1 + \sqrt{\frac{1-\mathrm{I_n}}{\mathrm{I_n}}}} \qquad (A.6)$$

Figure (A.1) is illustrated the relationship between the sigmoid function $\mathrm{S_n}$ and the normalized intensity $\mathrm{I_n}$. This function increases the low lightness levels. And then apply retinex algorithm.

We do this by the following steps:

1. Input gray image C(x,y).

2. Normalized Y component by $\mathrm{I_n} = \frac{\mathrm{C}}{255}$

3. Transform lightness component by using $S_n = 1/(1 + \sqrt{\frac{1-I_n}{I_n}})$ getting processed lightness component Yp.

4. Apply R algorithm on S_n to get the output image.

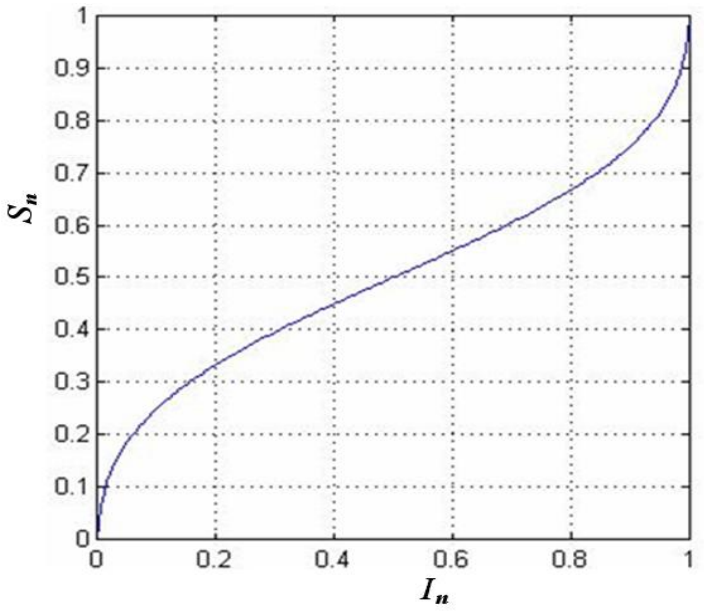

***Figure A.1**: sigmoid function as a function of normalized intensity.*

1.3 Histogram Equalization

Histogram equalization (HE) and its variations have conventionally been used to correct for the uniform lighting and exposure problems. This technique is based on the idea of remapping the histogram of the scene to a histogram which has a near uniform probability density function. This produces in reassigning dark regions to brighter values and bright regions to darker values. The histogram equalization works well for the scene that has unimodal histogram, and the same thing for the scene that has weakly bi-modal histogram (i.e. very bright, or very dark), but it does not work so well for those images with strongly bimodal

histograms (i.e. scenes that contain very bright and very dark regions) [211]. Histogram equalization is a global technique that works well for a wide variety of images. If lightness levels are continuous quantities normalized to the range (0, 1), $p_r(r)$ which denote the probability density function (PDF) of the lightness levels in a given image, where the subscript is use for differentiating between the PDFs of the input and output images. Suppose that we perform the following transformation on the input levels to obtain output (processed) intensity levels [212],

$$s = T(r) = \int_0^r p_r(w)dw \qquad (A.7)$$

Where *w* is a dummy variable of integration, that the probability density function of the output levels is uniform, that is [212]:

$$p_r(s) = \begin{cases} 1 & for \quad 0 \leq s \leq 1 \\ 0 & else \end{cases} \qquad (A.8)$$

When dealing with discrete quantities we work with histograms and call the Preceding technique histogram equalization, where [213]:

$$s_k = \sum_{j=0}^{k} p_r(r_j) = \sum_{j=0}^{k} \frac{n_j}{N} \qquad (A.9)$$

$k = 0,1,2, \ldots \ldots L$

L =255 for lightness band with 8 bit/pixel), s_k corresponding normalized intensity level of the output image and $n_j$being the number of pixel with intensity level *j* and *n* is the total number. The Eq. (A.9) is represent the cumulative probability density function (CPDF). r_j is normalized intensity level of the input image corresponding to the (un–normalized) intensity level this algorithm summarized by using the following steps:

1.Input color image C(n,m,i), i=1,2,3 (red ,green, blue) components.

2. Normalize each component r_j(i) = C(x,y,i)/ 255 and calculated frequency of Occurrence each gradual level n_j(i) , where j=0,1,..255.

3. Compute histogram from P (r_j(i)) = n_j(i) /N, where N being the size of image.

4. Calculate cumulative histogram by:

$$s_k(i) = \sum_{j=0}^{k} \frac{n_j}{N} \qquad (A.10)$$

where $k = 0,1,2, \ldots \ldots 255$

5. Replace each normalized component r_j(i) by value of s_k(i) we get the output image.

1.4 Adaptive histogram equalization (AHE) algorithm

As in AR algorithm the first step is transform the normalized lightness value by using sigmoid function that is given by:

$$S_n = 1/(1 + \sqrt{\frac{1 - I_n}{I_n}}) \qquad (A.11)$$

Where S_n is the output lightness, and I_n is the input lightness. By applying HE on modify lightness component. This can be achieved by the following steps:

1. Input gray image C(x,y).

2. Normalized Y component by $I_n = \frac{C}{255}$.

3. Transform lightness by using $S_n = 1/(1 + \sqrt{\frac{1-I_n}{I_n}})$.

4. Applied HE on transformed lightness component S_n getting processed lightness component get out put image.

2. Results

In this work, four algorithms MSR, AR, HE, and AHE have been used to enhance images with different lightness and contrast level, these images are skin samples measured at 1030 nm with resolution about 2.1 μm. The images have been enhanced as follows:

There is a similarity between HE and AHE algorithms except in the high intensity level of images enhanced by AHE Figures (A.2, A.3, A.4, A.5), this distribution will be increase and will become more fluctuated.

The distribution for the images enhanced by AR algorithm in Figures (A.2, A.3, A.4, A.5), will be increased in the moderate and high lightness level, this mean that the enhancement of lightness became the best. All algorithms have been succeeded to enhance the images.

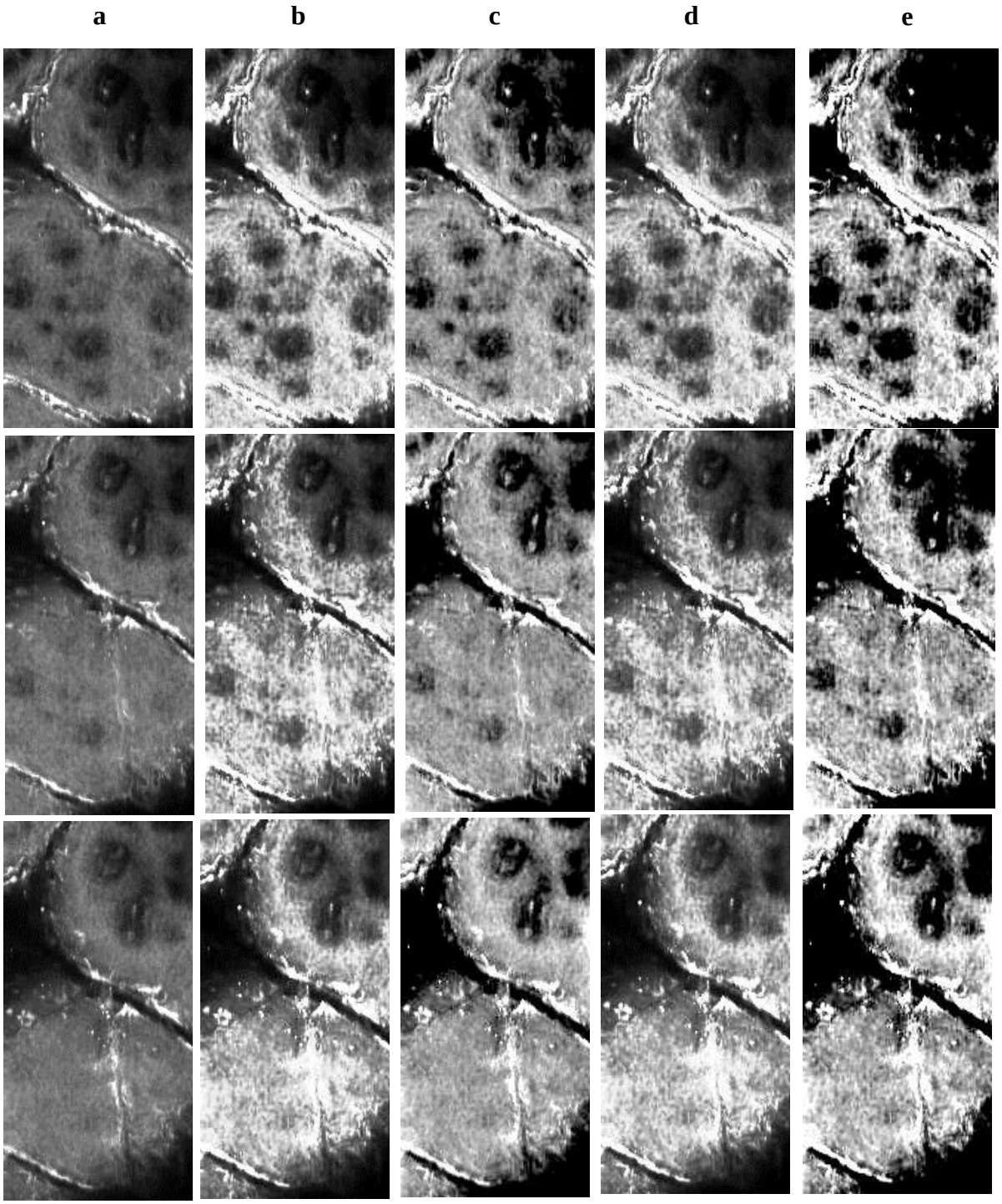

Figure A.2*: Image enhancement. a) Original images, b) images enhanced using AHE, c) Images enhanced using MR, d) Images enhanced using HE, and e) Images enhanced using MSR.*

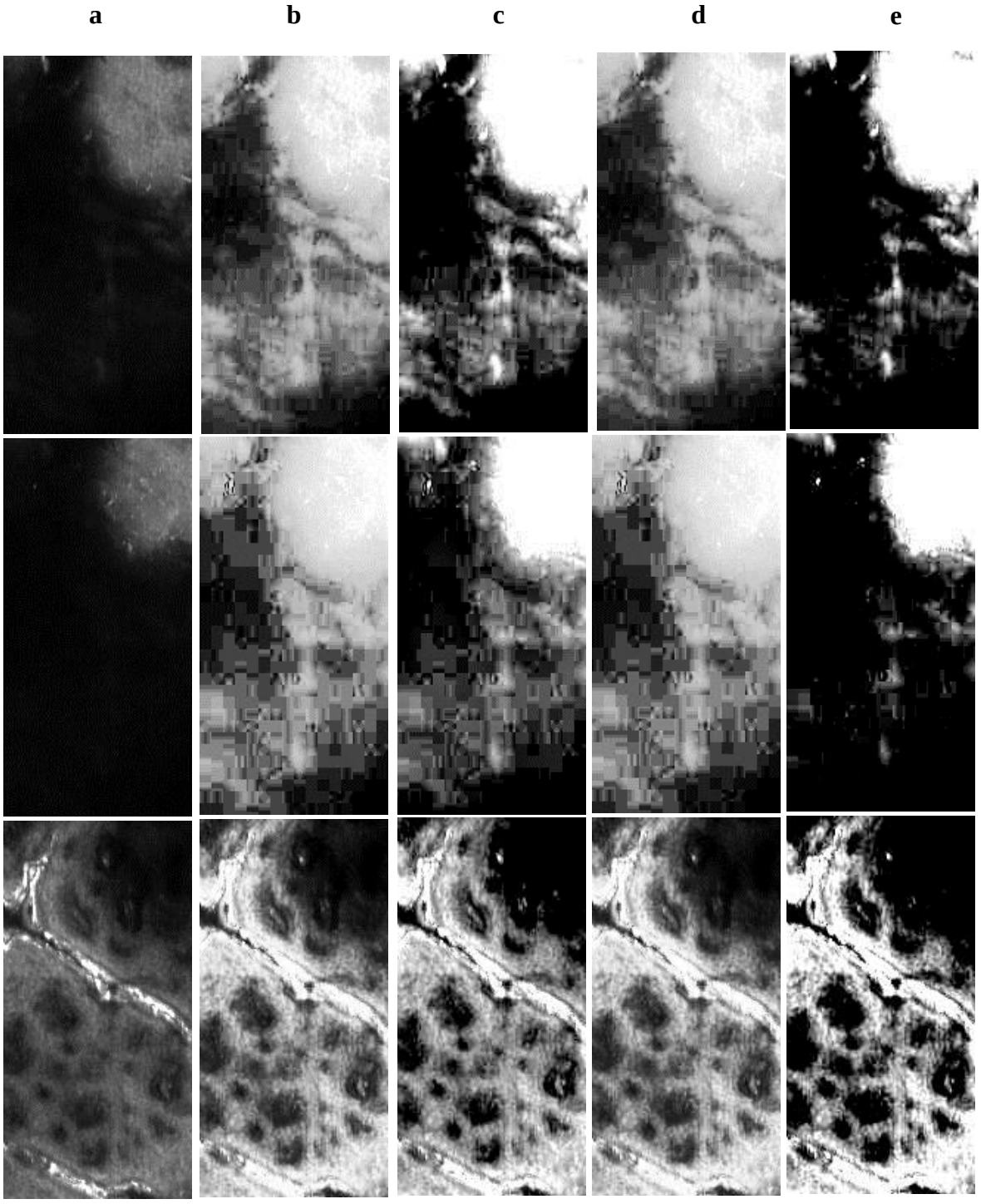

***Figure A.3**: Image enhancement. a) Original images, b) images enhanced using AHE, c) Images enhanced using MR, d) Images enhanced using HE, and e) Images enhanced using MSR.*

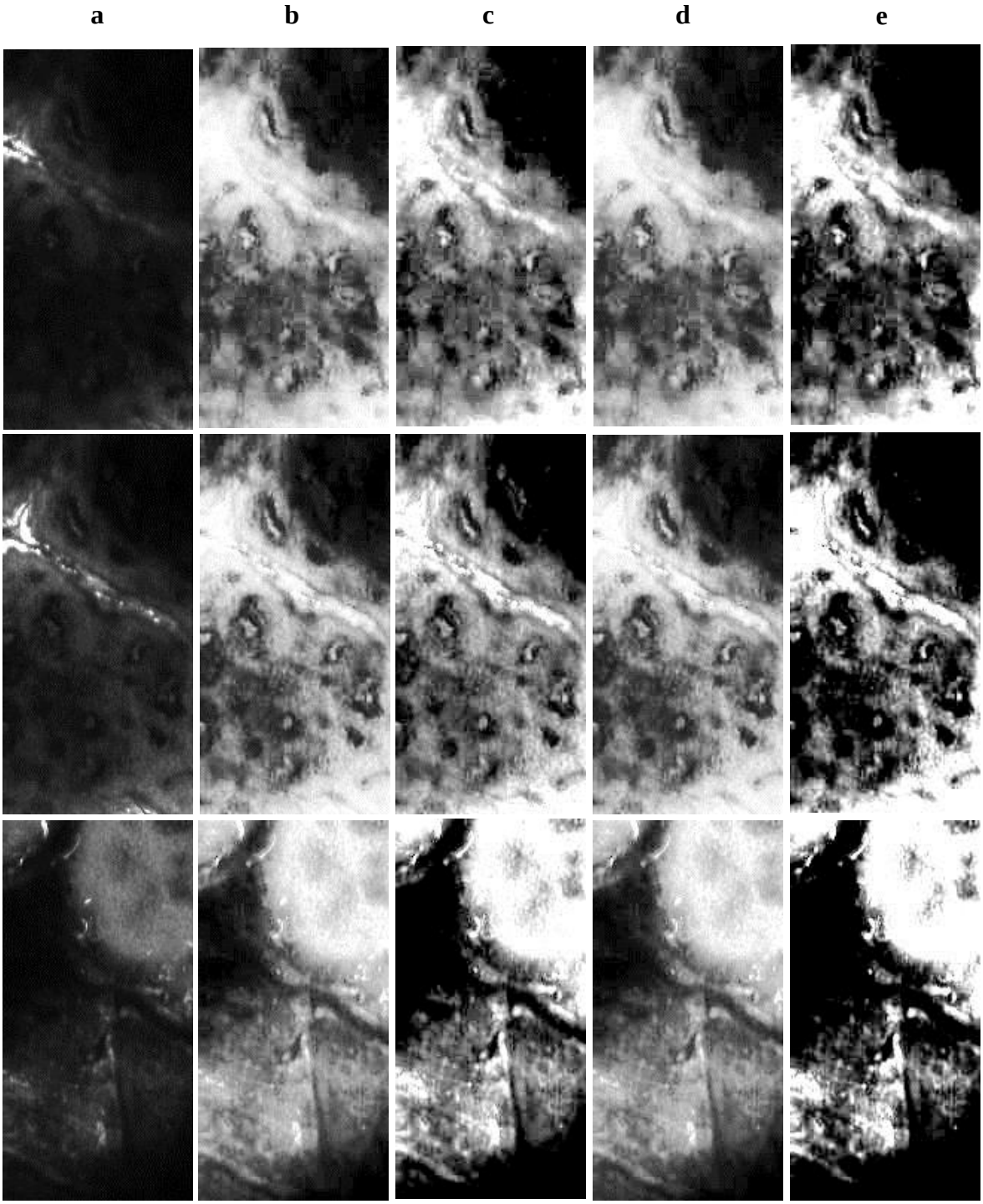

***Figure A.4**: Image enhancement. a) Original images, b) images enhanced using AHE, c) Images enhanced using MR, d) Images enhanced using HE, and e) Images enhanced using MSR.*

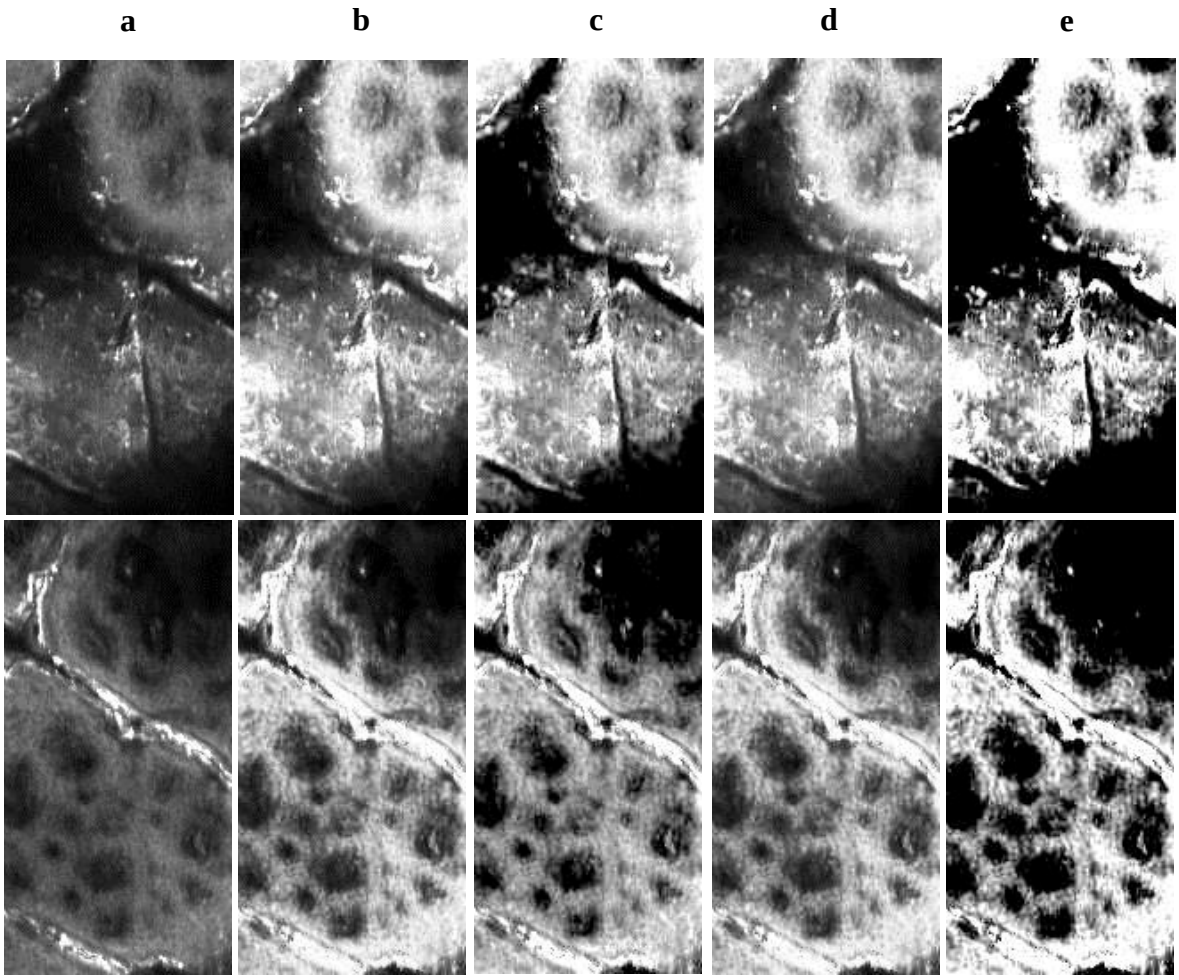

Figure A.5*: Image enhancement. a) Original images, b) images enhanced using AHE, c) Images enhanced using MR, d) Images enhanced using HE, and e) Images enhanced using MSR.*

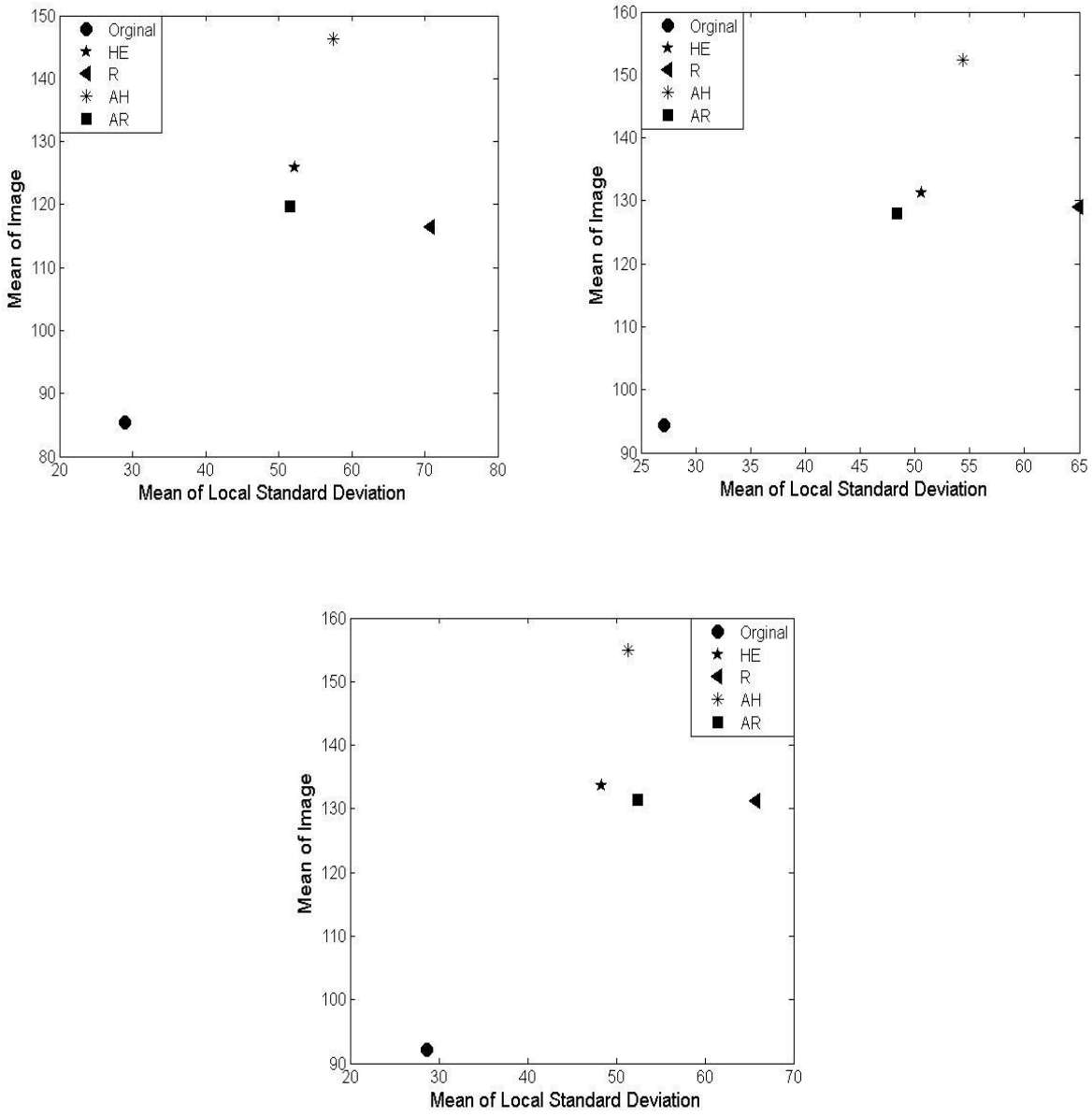

***Figure A.2**: Continue*

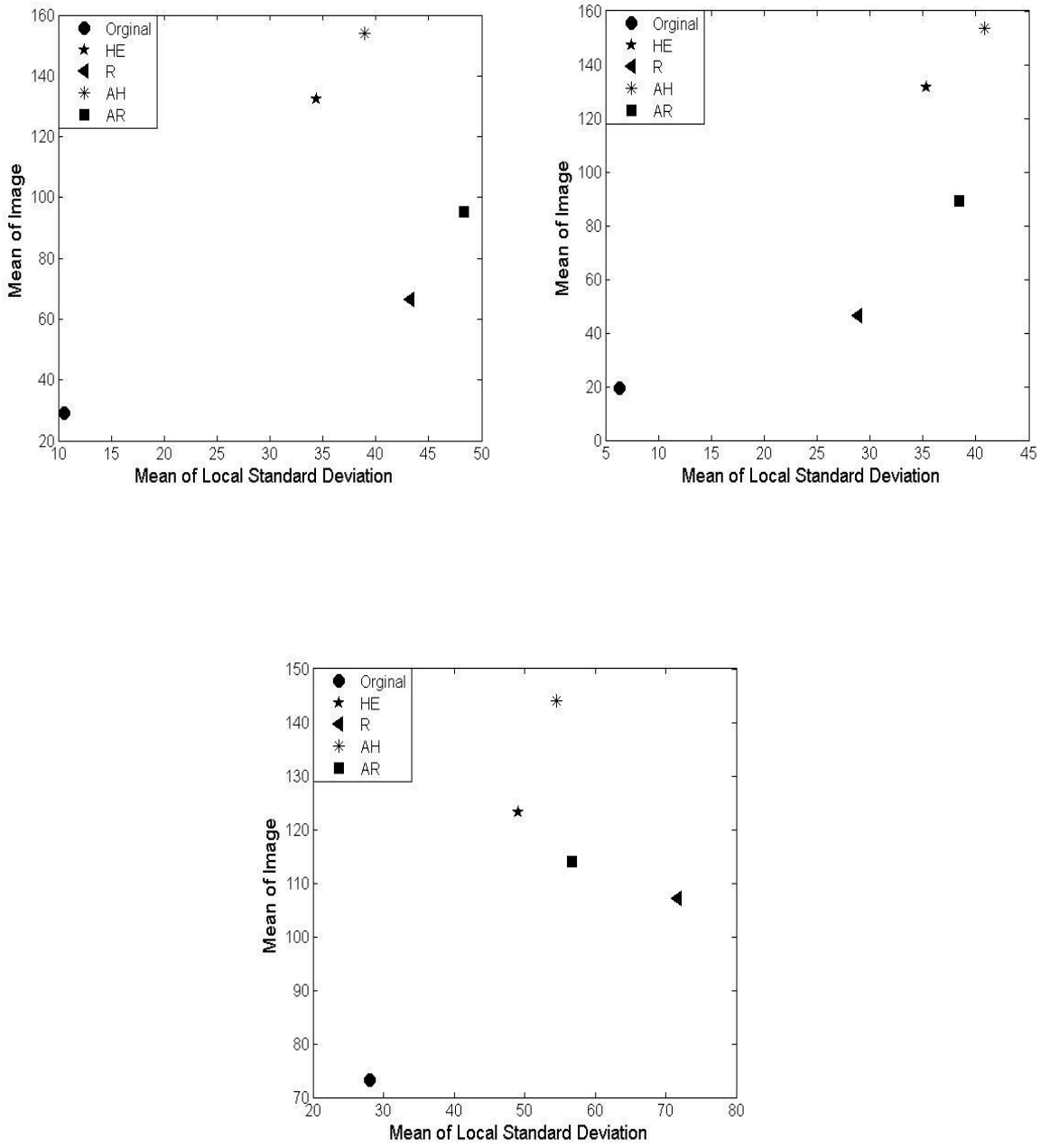

***Figure A.3**: Continue*

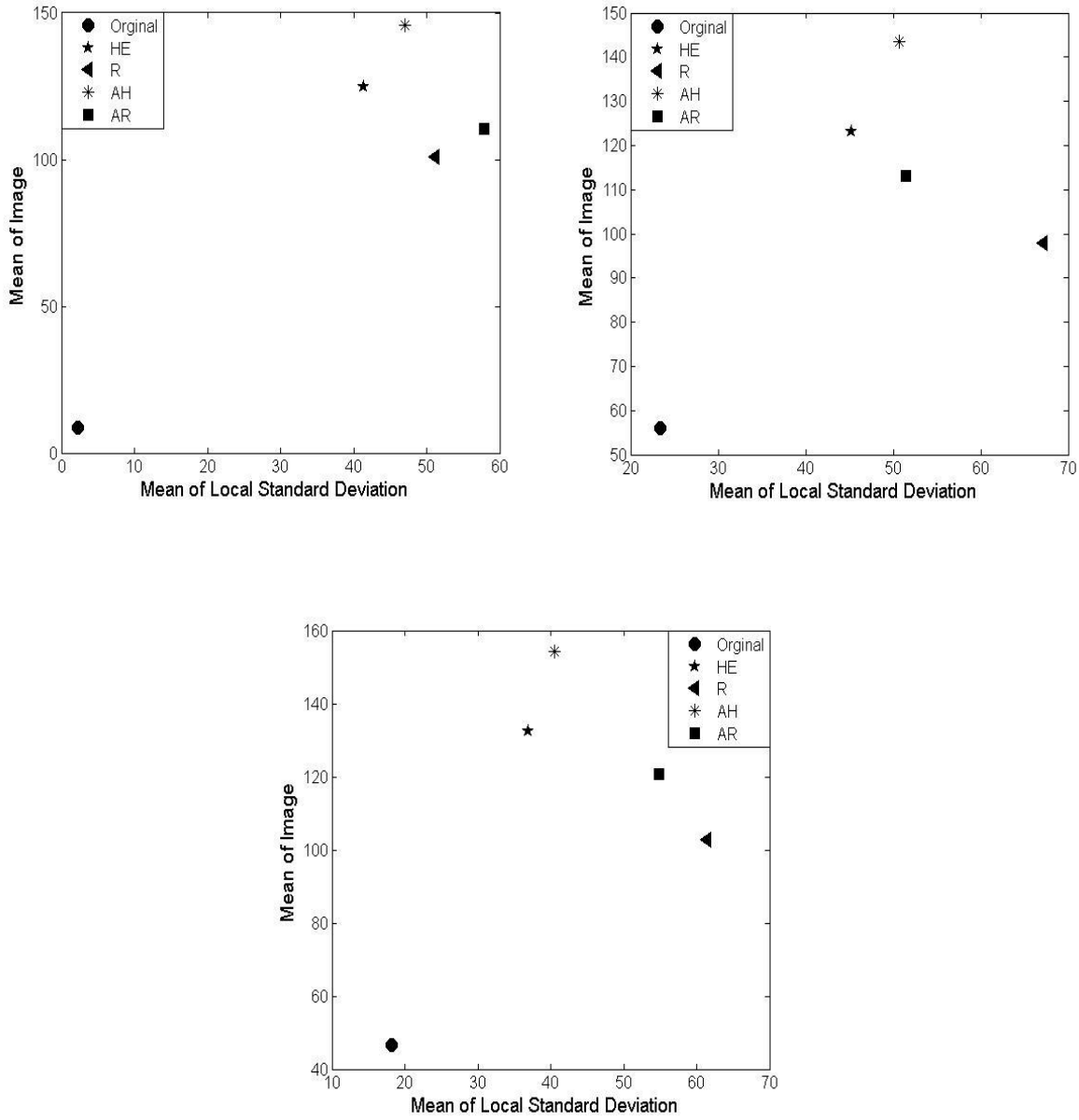

***Figure A.4**: Continue*

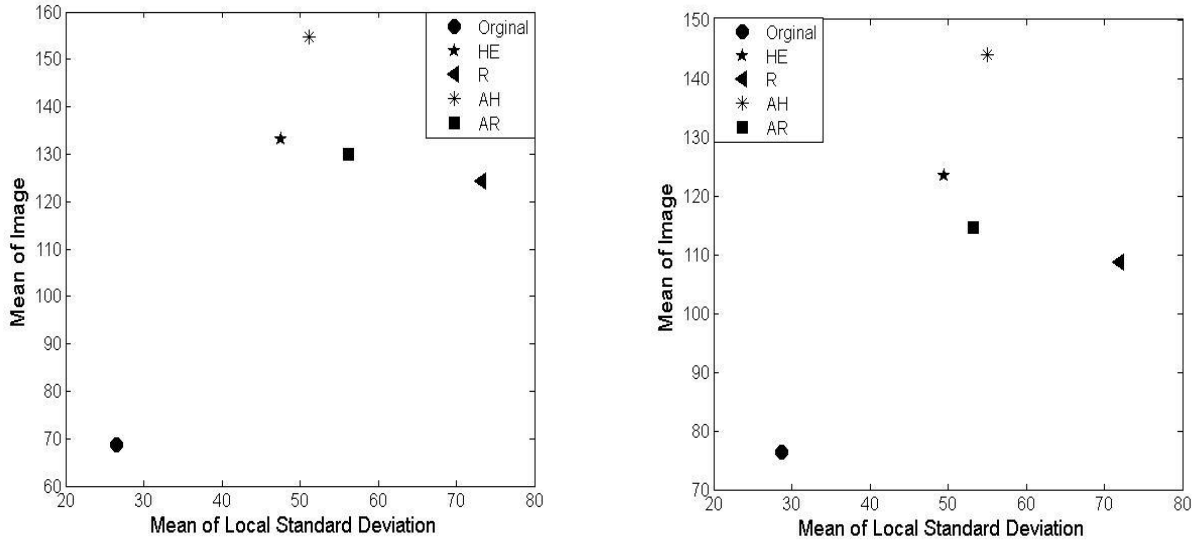

***Figure A.5**: Continue*

The mean of locally model (μ, σ) has been illustrated in Figures continue (A.2, A.3, A.4, A.5) continue for images with low and moderate lightness, which are enhanced by different algorithms. We can see, the most points in the optimal regions (increase in contrast and lighting) belong to AH algorithm then it follows by MR algorithm. This indicated that the AH algorithm is enhanced the lightness well, whereas the MR is enhanced the contrast. In the images which captured at good lightness levels the best enhancement appears in the R algorithm due to higher value of σ and mean of the image.

Bibliography

1. O. Lammel and A. Penzkofer, “Femtosecond Pulse Duration Measurement by Two-Photon Fluorescence Detection”, Opt. Quant. Electr., 32, pp. 1147-1160, 2000.
2. M. Müller, J. Squier, and G. J. Brakenhoff, “Measurement of Femtosecond Pulses in the Focal Point of a High-Numerical-Aperture Lens by Two-Photon Absorption”, Opt. Lett., 20, pp.1038-1040, 1995.
3. W. Schade, J. Preusser, D. L. Osborn, Y. Y. Lee, J. deGouw, S. R. Leone, “Spatially Resolved Femtosecond Time Correlation Measurements on a GaAsP Photodiode”, Opt. Commun., 162, pp. 200-204, 1999.
4. J. A. Giordmaine, P. M. Rentzepis, S. L. Shapiro, and K. W. Wecht, “Two-Photon Excitation of Fluorescence by Picosecond Light Pulses”, Appl. Phys. Lett., 11, pp.216-218, 1967.
5. F. G. Omenetto, W. A. Schroeder, K. Boyer, J. W. Longworth, A. McPherson, and C. K. Rhodes, “Measurement of 160-fs, 248-nm Pulses by Two-Photon Fluorescence in Fused-Silica Crystals”, Appl. Opt., 36, pp. 3421-3424, 1997.
6. A. Tünnermann, H. Eichmann, R. Henking, K. Mossavi, and B. Wellegehausen, “Single-Shot Autocorrelator for KrF Subpicosecond Pulses Based on Two-Photon Fluorescence of Cadmium Vapor at $\lambda = 508$ nm”, Opt. Lett., 16, pp. 402-404, 1991.
7. B. Luther-Davies, M. Samoc, J. Swiatkiewicza, A. Samoc, M. Woodruff, R.Trebino, and K. W. Delong, “Diagnostics of Femtosecond Laser Pulses Using Films of Poly(p-phenylenevinylene)”, Opt. Commun., 131, pp. 301-306, 1996.
8. A. Reuther, A. Laubereau, and D. N. Nikogosyan, “A Simple Method for the in Situ Analysis of Femtosecond UV Pulses in the Pump-Probe Spectroscopy of Solutions”, Opt.Commun., 141, pp. 180-184, 1997.
9. M. Rasmusson, A. N. Tarnovsky, E. Åkesson, and V. Sundström, “On the Use of Two-Photon Absorption for Determination of Femtosecond Pump-Probe Cross-Correlation Functions”, Chem. Phys. Lett., 335, pp. 201-208, 2001.

10. J. I. Dadap, G. B. Focht, D. H. Reitze, and M. C. Downer, “Two-Photon Absorption in Diamond and Its Application to Ultraviolet Femtosecond Pulse-Width Measurement”, Opt. Lett. 16, pp. 499-501, 1991.

11. GS. He, R. Signorini, and PN. Prasad, “Two-Photon-Pumped Frequency-Upconverted Blue Lasing in Coum arin Dye Solution”, Appl. Opt., 37, pp. 5720-5726, 1998.

12. GS. He, PP. Markowicz, TC. Lin, and PN. Prasad, “Observation of Stimulated Emission by Direct Three-Photon Excitation”, Nature 415, pp. 767-770, 2002.

13. A. Mukherjee, “Two-Photon Pumped Upconverted Lasing in Dye Doped Polymer waveguides”, Appl. Phys. Lett. 62, pp. 3423-3425, 1993.

14. W. Denk, JH. Strickler, and W. W. Webb, “Two-Photon Laser Scanning Fluorescence Microscopy”, Science 248, pp. 73-76, 1990.

15. RM. Williams, DW. Piston, and WW. Webb, “Two-Photon Molecular Excitation Provides Intrinsic 3-Dimensional Resolution for Laser-Based Microscopy and Microphotochemistry”, FASEB J. 8, pp. 804-813, 1994.

16. W. Denk and K. Svoboda, “Photon Upmanship: Why Multiphoton Imaging is More Than a Gimmick”, Neuron 18, pp. 351-357, 1997.

17. BR. Masters, PT. C. So, KH. Kim, C. Buehler, and E. Gratton, “Multiphoton Excitation Microscopy, Confocal Microscopy, and Spectroscopy of Living Cells and Tissues; Functional Metabolic Imaging of Human Skin in Vivo”, in Methods of Enzymology: Confocal Microscopy, Academic Press, San Diego, ed. P. M. Conn,307, pp. 513-536, 1999.

18. DA. Parth enopoulos and PM. Rentzepis, “Three-Dimensional Optical Storage Memory”, Science 245, pp. 843-845, 1989.

19. A. Toriumi, JM. Herrmann, and S. Kawata, “Nondestructive Readout of a Three-Dimens ional Photochromic Optical Memory with a Near-Infrared Differential Phase-Contrast Microscope”, Opt. Lett. 22, pp. 555-557, 1997.

20. A. Toriumi, S. Kawata, and M. Gu "Reflection Confocal Microscope Readout System for Three-D imensional Photochromic Optical Data Storage", Opt. Lett. 23,pp. 1924-1926, 1998.

21. S. Maruo, and S. Kawata, "Two-Photon-Absorbed Near-Infrared Photopolymerization for Three-Dimensional Microfabrication", J.Microelectromech. Syst. 7, pp. 411-415, 1998.

22. HB. Sun, T. Kawakami, Y. Xu, JY. Ye, S. Matuso, H. Misawa, M. Miwa, and R. Kaneko, "Real Three-Dimensional Microstructures Fabricated by Photopolymerization of Resins through Two-Photon Absorption", Opt. Lett. 25,pp. 1110-1112, 2000.

23. JD. Bhawalkar, JN.D. Kumar, CF. Zhao, and PN. Prasad, "Two-photon photodynamic therapy", J. Clin. Laser Med. Surg. 15, pp. 201–204, 1997.

24. WG. Fischer, WP. Patridge, C. Dees, EA. Wachter, "Simultaneous two-photon activation of Type-I photodynamic agents", Photochem. Photobiol. 66, pp.141–155, 1997.

25. M. Atif, PE. Dyer, TA. Paget, HV. Snelling, and MR. Stringer, "Two-photon excitation studies of m-THPC photosensitizer and photodynamic activity in an ephithelial cell line", Photodiagn. Photodyn. Ther. 4, pp. 106–11, 2007.

26. CW. Spangler, "Recent Development in the Design of Organic Materials for Optical Power Limiting", J. Mater. Chem. 9, pp. 2013-2020, 1999.

27. G. Zhou, X. Wang, D. Wang, Z. Shao, and M. Jiang, "Upconversion Fluorescence and Optical Power Limiting Effects Based on the Two- and Three-Photon Absorption Process of a New Organic Dye BPAS", Appl. Opt. 41, pp. 1120-1123,2002.

28. C. Desroches, S. Parola, F. Vocanson, N. Ehlinger, P. Miele, R. Lamartine, J. Bouix, A. Eriksson, M. Lindgren, and C. Lop es, "Synthesis, Characterization and Optical Power Limiting Behavior of Phenylazo- and 4-Nitrophenylazo-Tetrahydroxytetrathiacalix[4]arene", J. Mater. Chem. 11, pp. 3014-3017, 2001.

29. (a) LB. Josefsen, and RW. Boyle,"Unique diagnostic and therapeutic roles of porphyrins and phthalocyanines in photodynamic therapy imaging and theranostics", Theranostics 2, pp. 916–966, 2012. (b) RR. Allison, and CH. Sibata, "Oncologic

photodynamic therapy photosensitizers: a clinical review", Photodiagn. Photodyn. Ther., 7, pp. 61–75, 2010.

30. M. Pawlicki, HA. Collins, RG. Denning, HL. Anderson, "Two-photon absorption and the design of two-photon dyes",Angew. Chem. Int. Ed. 48, pp. 3244–3266, 2009.
31. Goeppert-Mayer M (1931). "Über Elementarakte mit zwei Quantensprüngen", Annals of Phys., 9, pp. 273–294, 1931, German.
32. W. Kaiser and CG.B. Garrett, "Two-photon excitation in $CaF_2:Eu^{2+}$", Physical Review Lett.7, pp. 229–232, 1961.
33. A.Volkmer, DA. Hatrick, and DJ.S. Birch, "Time-resolved nonlinear fluorescence spectroscopy using femtosecond multiphoton excitation and single-photon timing" Meas.Sci.Technol.8, pp. 1339-1349, 1997.
34. I.Gryczynski, H. Malak, and JR. Lakowicz, "Three-photon induced fluorescene of 2.5-diphenyloxaxole with a femtosecond Ti:sapphire laser", Chem. Phys. Lett., 245, pp.30-35, 1995.
35. DJ. Bradley, MH. R. Hutchinson, H. Koetser, T. Morrow, GH. C. New, and MS. Petty, "Interactions of Picosecond Laser Pulses with Organic Molecules.I.Two-Photon Fluorescence Quenching and Singlet States Excitation in Rhodamine Dyes", Proc.R.Sco.Lond. A 329, 97, 1972.
36. P. Sengupta, J. Balaji, S. Banerjee, R. Philip, RG. Kumar, S. Maiti, "Sensitive measurement of absolute two-photon absorption cross sections", J. Chem. Phys. 112, pp. 9201-9205, 2000.
37. JD. Bhawalkar, J.N.D. Kumar, CF. Zhao, PN. Prasad, "Two-photon photodynamic therapy", J. Clin. Laser Med. Surg. 15. pp. 201-204, 1997.
38. WG. Fischer, WP. Patridge, C. Dees, and EA.Wachter, "Simultaneous two-photon activation of Type-I photodynamic agents. Photochem", Photobiol. 66, pp. 141-155, 1997.

39. M. Atif, P.E. Dyer, TA. Paget, HV. Snelling, and MR. Stringer. "Two-photon excitation studies of m-THPC photosensitizer and photodynamic activity in an ephithelial cell line. Photodiagn", Photodyn. Therapy, 4, pp. 106-111, 2007.
40. H. Stiel, K.Teuchner, A. Paul, W. Freyer, and D. Leupold," Two-photon excitation of alkyl-substituted magnesium phthalocyanine: radical formation via higher excited states", J. Photochem. Photobiol., A, 80, pp. 289-298, 1994.
41. M. Calvete, GY. Yang, and M. Hanack, "Porphyrins and phthalocyanines as materials for optical limiting", Synth. Met.141, pp.231-243, 2004.
42. JR. Lakowicz, "Topics in fluorescence spectroscopy", Plenum Press Newyork, 2003.
43. W. Denk, "Two-photon scanning photochemical microscopy: Mapping ligand-gated ion channel distributions", Proc. Natl. Acad. Sci. U.S.A., 91, pp. 6629-6633, 1994.
44. DA.Parth enopoulos, and PM. Rentzepis, "Three-Dimensional Optical Storage Memory", Science 245, pp.843-845, 1989.
45. JH. Strickler and WW. Webb, "Three-Dimensional Optical Data Storage in refractive Media by Two-Photon Point Excitation", Opt. Lett.16, pp.1780-1782, 1991.
46. JA. Reyes-Esqueda, L. Vabre, R. Lecaque, F. Ramaz, BC. Forget, A. Dubois, B. Briat, C. Boccara, G. Roger, M. Canva, Y. Levy, F. Chaput, and JP. Boilot, "Optical 3D-Storage in Sol-Gel Materials with a Reading by Optical Coherence Tomography-Technique", Opt. Commun. 220, pp.59-66, 2003.
47. T. Yu, CK. Ober, SM. Kuebler, W. Zhou, SR. Marder, and JW. Perry, "Chemically Amplified Positive Resists for Two-Photon Three-Dimensional Microfabrication", Adv. Mater., 15, pp.517-521, 2003.
48. HB. Sun and S. Kawata, "Two-Photon Laser Precision Microfabrication and Its Applications to Micro-Nano Devices and Systems", J. Lightw. Tech., 21, pp.624-633, 2003.
49. S. Maruo, K. Ikuta, and H. Korogi, "Submicron Manipulation Tools Driven by Light in a Liquid", Appl. Phys. Lett., 82, pp. 133-135, 2003.
50. HB. Sun, V. Mizeikis, YXu, S. Juodkazis, JY. Ye, S. Matsuo, and H. Misawa, "Microcavities in Polymeric Photonic Crystals", Appl.Phys. Lett., 79, pp.1-3, 2001.

51. I.Wang, M. Bouriau, PL. Baldeck, C. Martineau, and C. Andraud, "Three - Dimensional Microfabrication by Two-Photon Initiated Polymerization with a Low-Cost Microlaser", Opt. Lett., 27, pp.1348-1350, 2002.
52. CW. Spangler, "Recent Development in the Design of Organic Material for Optical Power Limiting", J. Mater.Chem., 9, pp.2013-2020, 1999.
53. G. Zhou, X. Wang, D. Wang, Z. Shao, and M. Jiang, "Upconversion Fluorescence and Optical Power Limiting Effects Based on the Two- and Three-Photon Absorption Process of a New Organic Dye BPAS", Appl. Opt., 41, pp.1120-1123,2002.
54. MG. Silly, L. Porrès, O. Mongin, PA. Chollet, and M. Blanchard-Desce, "Optical Limiting in the Red-NIR Range with Soluble Two-Photon Absorbing Molecules, "Chem. Phys. Lett., 379, pp.74-80, 2003.
55. N. Izard, C. Ménard, D. Riehl, E. Doris, Ch. Mioskowski, E. Anglaret, "Combination of carbon nanotubes and two-photon absorbers for broadband optical limiting",Chem. Phys. Lett., 391, pp. 124-128, 2004.
56. PN. Prasad, "Introduction to Biophotonics", John Wiley and Sons, Inc., Hoboken, New Jersey, 2003.
57. J. Scrimgeour, DN. Sharp, ChrF. Blanford, OM. Roche, RG. Denning, and AJ. Turberfield, "Three-dimensional Optical Lithography for photonic Microstructures", Adv. Mater., 18, pp. 1557-1560, 2006.
58. W. Denk, JH. Strickler, and WW. Webb, "Two-Photon Laser Scanning Fluorescence Microscopy," Science, 248, pp.73-76, 1990.
59. RM. Williams, WR. Zipfel, and WW. Webb, "Multiphoton Microscopy in Biological Research," Curr. Opin. Chem. Biol. 5, pp. 603-608, 2001.
60. DR. Larson, WR. Zipfel, RW. Williams, SW. Clark, MP. Bruchez, FW. Wise, WW. Webb, "Water-Soluble Quantum Dots for Multiphoton Fluorescence Imaging in Vivo," Science, 300, pp. 1434-1436, 2003.
61. M. Albota, C. Xu, W. Webb, "Two-photon fluorescence excitation cross sections of biomolecular probes from 690 to 960nm" Appl. Opt. 37, pp. 7352-7356, 1998.
62. Ch. Xu, and W. Webb, "Measurement of two-photon excitation cross sections of fluorophores with data from 690 to 1050nm," J.Opt. Soc., 13, pp. 481-491, 1996.

63. M. Rumi, JE.Ehrlich, AA. Heikal, JW. Perry, S. Barlow, Z. Hu, D. McCord-Maughon, TC. Parker, H. Rockel, S. Thayumanavan, SR. Marder, D. Beljonne, and JL. Bredas, "Structure-property relationships for two-photon absorbing chromophores: bis donor diphenyl polyene and bis (styryl) benzene derivatives", J. Am. Chem. Soc., 122, pp. 9500-9510, 2000.
64. C. Xu, J. Guild, W. Webb, and W. Denk, "Determination of absolute two-photon excitation cross sections by in situ second-order autocorrelation" Opt. Lett. 20, 23 pp. 2372-2374, 1995.
65. LA. Padilha, S. Webster, H. Hu, OV. Przhonska, DJ. Hagan, EW. Van Stryland, MV. Bondar, IG. Davydenko, YL. Slominsky, and AD. Kachkovski, " Excited state absorption and decay kinetics of near IR polymethine dyes", Chem. Phys., 352, pp. 97-105, 2008.
66. A. Ulises Acuña, F. Amat-Guerri, P. Morcillo, , M. Liras, and B. Rodríguez, "Structure and Formation of the Fluorescent Compound of Lignum nephriticum", Org. Lett., 11, pp. 3020–3023, 2009.
67. A. Skoog Douglas, F. James Holler, and R. Crouch Stanley, "Principles of Instrumental Analysis", 6th Edition, Cengage Learning, 2006.
68. Lakowicz, and R. Joseph "Principles of Fluorescence Spectroscopy (second edition) ". Kluwer Academic / Plenum Publishers, pp.10, 1999.
69. Valeur, Bernard, Berberan-Santos, and Mario, "Molecular Fluorescence: Principles and Applications 2nd ed.," Wiley-VCH, pp. 64, 2012.
70. http://pharmaxchange.info/press/2013/03/animation-for-the-principle-of-fluorescence-and-uv-visible-absorbance/.
71. A.Nag, S. Singh, and D. Goswami, "Structure property correlations in alcohols through two-photon absorption cross-section measurements", Chem. Phys. Lett., 430, pp.420-423, 2006.
72. B.H. Cumpston, S.P. Ananthavel, S. Barlow, D.L. Dyer, J.E. Ehrlich, et al., "Two-photon polymerization initiators for three-dimensional optical data storage and microfabrication", Nature, 398, pp. 51-54,1999.

73. N.S. Makarov, M. Drobizhev, and A. Rebane, “Two-photon absorption standards in the 550–1600 nm excitation wavelength range,” Opt. Express, 16, pp. 4029–4047, 2008.
74. H. Rath, J. Sankar, V. Prabhuraja, T.K. Chandrashekar, A. Nag, and D.Goswami, “Core-modified Expanded Porphyrins with Large Third Order Nonlinear Optical Response”, J. Am. Chem. Soc., 127, pp. 11608-11609, 2005.
75. D. Y. Kim, T. K. Ahn, 1. H. Kwon, D. Kim, T. Ikeue, N. Aratani, A. Osuka, M. Shigeiwa, and S. Maeda, J. Phys. Chem., 109, pp. 2996-2999, 2005.
76. CH. Wang, OY. Tai, Y. Wang, TH. Tsai, and NC. Chang. “Non-quadratic-intensity dependence of two-photon absorption induced fluorescence of organic chromophores in solution”, J. Chem. Phys., 122, pp. 084509-084516, 2005.
77. A.Nag, S. Singh, D. Goswami. “Structure property correlations in alcohols through two-photon absorption cross-section measurements” Chem. Phys.Lett.430, pp. 420-423, 2006.
78. S. E. Harris, M. K. Oshman, and R. L. Byer, “Observation of tunable optical parametric fluorescence,” Phys. Rev. Lett., vol. 18, pp. 732–734, 1967.
79. E. Pontecorvo, S. M. Kapetanaki, M. Badioli, D. Brida, M. Marangoni, G. Cerullo, and T. Scopigno, "Femtosecond stimulated Raman spectrometer in the 320-520nm range," Optics Express, 19, pp. 1107-1112, 2011.
80. A. V. Egorysheva, and V. M. Skorikov, “Efficient nonlinear optical material BiB3O6 (BIBO)”, Inorg. Mater, 45, pp. 1461-1476, 2009.
81. Kummrow, M. Wittmann, F. Tschirschwitz, G. Korn, and E. T. J. Nibbering, "Femtosecond ultraviolet pulses generated using noncollinear optical parametric amplification and sum frequency mixing", App. Phys. B-Lasers and Opt., 71, pp. 885-887, 2000.
82. Shirakawa, I. Sakane, M. Takasaka, and T. Kobayashi, "Sub-5-fs visible pulse generation by pulse-front-matched noncollinear optical parametric amplification" , App. Phys. Lett., 74, pp. 2268-2270, 1999.
83. M. Nisoli, S. Stagira, S. De Silvestri, O. Svelto, G. Valiulis, and A. Varanavicius, "Parametric generation of high-energy 14.5-fs light pulses at 1.5 mu m", Opt. Lett., 23, pp. 630-632, 1998.

84. J. C. Diels, and W. Rudolph, “Ultrashort Laser Pulse Phenomena”, Academic Press, Albuquerque, 2006.
85. G. Cerullo, and S. De Silvestri, "Ultrafast optical parametric amplifiers", Review of Scientific Instruments, 74, pp. 1-18, 2003.
86. W. Zinth, and U. Zinth, “Optik Lichtstrahlen – Wellen – Photonen”, Oldenbourg Verlag, Munich, 2009.
87. D. N. Nikogosyan, "Beta barium borate (BBO)", Appl. Phys., 52, pp. 359-368, 1991.
88. M. E. Klein, D.-H. Lee, J.-P. Meyn, K.-J. Boller, and R. Wallenstein, “Singly resonant continuous-wave optical parametric oscillator pumped by a diode laser”, Opt. Lett. 24, pp. 1142-1144, 1999.
89. R. Pottier, and TG. Truscott, “The photochemistry of haematoporphyrin and related systems”, Int. J. Radiat. Biol., 50, pp. 421-452, 1986.
90. B. Chen, BW. Pogue, PJ. Hoopes, and T. Hasan, “Vascular and cellular targeting for photodynamic therapy”, Crit. Rev. Eukaryot. Gene. Expr., 6, pp. 279-305, 2006.
91. D. Kessel, Y. Luo, Y. Deng, and CK.Chang, “The role of subcellular localization in initiation of apoptosis by photodynamic therapy”, Photochem. Photobiol. , 65, pp. 422-426, 1997.
92. A.K. Haylett, F. I. McNair, D. McGarvey, N. J. F. Dodd, E. Forbes, T. G. Truscott and J. V. Moore, “Singlet oxygen and superoxide characteristics of a series of a novel asymmetric photosensitizers ”, Cancer Lett., 112, pp. 233-238, 1997.
93. K. Ogawa, A. Ohashi, Y. Kobuke, K. Kamada, and K. Ohta, “Two-photon absorption properties of self-assemblies of butadiyne-linked bis (imidazolylporphyrin)”, J. Phys. Chem. , 109, pp. 22003-22012 , 2005.
94. Rebane and J. Feinberg, “Time-Resolved Holography”, Nature, 351, pp. 378-380, 1991.
95. V. SY. Lin, S. G. DiMagno, and M. J. Therien, “Highly Conjugated, Acetylenyl Bridged Porphyrins: New Molecules for Light-Harvesting Antenna Systems”, Science, 264, pp. 1105-1111, 1994.
96. M. S. Choi, T. Aida, T. Yamazaki, and I. Yamazaki, “Dendritic multiporphyrin arrays as light-harvesting antennae: Effects of generation number and morphology on intramolecular energy transfer”, Chem.Eur. J., 8, pp. 2668-2678, 2002.

97. H. Imahori, Y. Mori, and Y. Matano, “Nanostructured Artificial Photosynthesis”, J.Photoch. Photob., 4, pp. 51-83, 2003.
98. Rebane, R. Kaarli, P. Saari, A. Anijalg, and K. Timpmann, “Photochemical Time-Domain Holography of Weak Picosecond Pulses”, Opt. Commun., 47, pp. 173-176, 1983.
99. Rebane, “Femtosecond Time-and-Space Domain Holography”, in Trends in Optics:Research, Developments and Applications, ed. A. Consortini, Academic Press, San Diego, pp. 165-188, 1996.
100. K. K. Rebane, “Spectral Hole Burning and Optical Information Processing in Current Trends in Optics”, ed. J. C. Dainty, Academic Press, London, pp. 177-194, 1994.
101. Rebane, M. Drobizhev, and C. Sigel, “Single Femtosecond Exposure Recording of an Image Hologram by Spectral Hole Burning in an Unstable Tautomer of a Phthalocyanine Derivative”, Opt. Lett. 25, pp. 1633-1635, 2000.
102. H. Schwoerer, D. Erni, and A. Rebane, “Holography in Frequency-Selective Media.3. Spectral-Synthesis of Arbitrary Time-Domain Pulse Shapes”, J. Opt. Soc. Am., 12, pp. 1083-1093, 1995.
103. M. Drobizhev, C. Sigel, and A. Rebane, “Photo-tautomer of Br-porphyrin: a new frequency-selective material for ultrafast time-space holographic storage”, J. Lumin., 86, pp. 391-397, 2000.
104. M. P. O’Neil, M. P. Niemczyk, W. A. Svec, D. Gosztola, G. L. Gaines III, and M. R. Wasielewski, “Picosecond Optical Switching Based on Biphotonic Excitation of an Electron Donor-Acceptor-Donor Molecule”, Science, 257, pp. 63-65, 1992.
105. R. W. Wagner, J. S. Lindsey, J. Seth, V. Palaniappan, and D. F. Bocian, “Molecular Optoelectronic Gates”, J. Am. Chem. Soc., 118, pp. 3996-3997, 1996.
106. D. Holten, D. F. Bocian, and J. S. Lindsey, “Probing Electronic Communication in Covalently Linked Multiporphyrin Arrays. A Guide to the Rational Design of Molecular Photonic Devices”, Acc. Chem. Res., 35, pp. 57-69, 2002.
107. M. Drain, “Self-Organization of Self-Assembled Photonic Materials into Functional Devices: Photo-Switched Conductors”, Proc. Nat. Ac. Sc., 99, pp. 5178-5182, 2002.
108. W. Henderson and T. J. Dougherty, “How does Photodynamic Therapy work”, Photoch. Photob., 55, pp. 147-157, 1992.

109. R. Bonnett, “Chemical Aspects of Photodynamic Therapy”, Gordon and Breach Science Publishers, Amsterdam, Netherlands, 2000.
110. RK. Pandey and G. Zheng, “Porphyrins as Photosensitizers in Photodynamic Therapy”, in the Porphyrin Handbook: Applications: Past, Present and Future, eds. K. M. Kadish, K. M. Smith, and R. Guilard, 6, Academic Press, 2000.
111. B. Chen, BW. Pogue, PJ. Hoopes, and T. Hasan,” Critical Reviews™ in Eukaryotic Gene Expression”, Rev. Eukaryot. Gene. Expr., 16, pp. 279-306, 2006.
112. Claes af Klinteberg, “On the use of light for the characterization and treatment of malignant tumours”, Dissertation thesis, Lund Institute of Technology, Lund, Sweden, 245, pp. 302, 1999.
113. Yu. P. Meshalkin, EE. Alfimov, NE. Vasil’ev, AN. Denisov, VK. Makukha, and AP. Ogirenko, “Two-Photon Excitation of Aluminium Phthalocyanines”, Quant. Electron., 29, pp. 1066-1068, 1999.
114. NN. Vsevolodov, LP. Kostikov, LP. Kayushin, and VI. Gorbatenkov, “Two-Photon Absorption of Laser Radiation by Chlorophy ll a and Some Organic Dyes”, Biofizika., 18, pp. 755-757, 1973.
115. RL. Goyan and DT. Gramb, “Near-Infrared Two-Photon Excitation of Protoporphyrin IX: Photodynamics and Photoproduct Generation”, Photochem. Photobiol., 72, pp. 821-827, 2000.
116. TC. Wen, LC. Hwang, WY. Lin, CH. Chen, and CH. Wu, “Nonlinear Absorption of Light: Two-Photon Absorption and Optical Saturation in Metalloporphyrin - Doped Boric Acid Glass”, Chem. Phys., 286, pp. 293-302, 2003.
117. Wachter, WP. Partridge, WE. G. Fisher, HC. Dees, and MG. Petersen, “Simultaneous Two-Photon Excitation of Photodynamic Therapy Agents”, in Procee dings of the SPIE, 3269, pp. 68-75, 1998.
118. Suzuka, M. Kozawa, and Y. Numata, “Two-Photon Absorption Spectra of Porphyrins First Observation of the Hidden g-Excited State”, presented at the XVIII International Union of Pure and Applied Chemistry Simposium on Photochemistry, Dresden, Germany, pp. 19-22, 2000.
119. J. Rodriguez, C. Kirmaier, and D. Holten, “Optical properties of metalloporphyrin excited states”, J. Am. Chem. Soc., 111, pp. 6500-6506, 1989.

120. H. Gratz and A. Penzkofer, “Singlet-Singlet Excited-State Absorption and Triplet-Triplet Absorption of Meso-Tetraphenylporphine”, Chem. Phys., 254, pp. 363-374, 2000.
121. M. Pawlicki, HA. Collins, RG. Denning, and HL. Anderson, “Two-photon absorption and the design of two-photon dyes”, Angew. Chem. Int. Ed., 48, pp. 3244–3266, 2009.
122. M. Atif, PE. Dyer, TA. Paget, HV. Snelling, and MR. Stringer, “Two-photon excitation studies of m-THPC photosensitizer and photodynamic activity in an ephithelial cell line”, Photodiagn. Photodyn. Ther., 4, pp. 106-111, 2007.
123. M. Schneider, G. Graschew, TA. Roelofs, E. Balanos, S. Rakowsky, HJ. Sinn, and P. Schlag,”Multiphoton excitation and photodynamic activity of macromolecular derivatized mTHPC”, Proc. SPIE, 3909, pp. 60-65, 2000.
124. L. R. Milgrom, “The Colours of Life: An Introduction to the Chemistry of Porphyrins and Related Compounds,” Oxford Univ. Press, 1997.
125. R. Bonnett, P. Charlesworth, BD. Djelal, S. Foley, DJ. McCarvey, and T.G. Truscott, “Photophysical properties of m-THPP, m-THPC and m-THPBC: a comparative study,” J. Chem. Soc. Perkin Trans. 2, pp. 325–328, 1999.
126. R. Bonnett, BD. Djelal, and A. Nguyen, “Physical and chemical studies related to the development of m-THPC (FOSCAN) for the photodynamic therapy (PDT) of tumours,” J. Porphyrins Phthalocyanines 5, pp. 652–661, 2001; (b) R. Bonnett, R.D. White, UJ. Winfield, MC. Berenbaum, “Hydroporphyrins of the meso-tetra(hydroxyphenyl) porphyrin series as tumor photosensitizers”, Biochem. J. 261, pp. 277–280, 1989.
127. AW. Johnson, and IT. Kay, J. Chem. Soc., pp.1620-1629, 1965.
128. DT. Gryko, “Recent Advances in the Synthesis of Corroles and Core-Modified Corroles”, Eur. J. Org. Chem., pp. 1735–1743, 2002.
129. AE. Meier-Callahan, AJ. Di Bilio, L. Simkhovich, A. Mahammed, , I. Goldberg, HB. Gray, and Z. Gross, “Chromium corroles in four oxidation States”, Inorg. Chem., 40, pp. 6788-6793, 2001.
130. E. Van Caemelbecke, S. Will, M. Autret, VA. Adamian, J. Lex, JP. Gisselbrecht, M. Gross, E. Vogel, and KM. Kadish, “Electrochemical and Spectral Characterization of

Iron Corroles in High and Low Oxidation States: First Structural Characterization of an Iron(IV) Tetrapyrrole pi Cation Radical", Inorg. Chem., 35, pp. 184-192, 1996.

131. S. Will, J. Lex, E. Vogel, VA. Adamian, E. Van Caemelbecke, and KM. Kadish," Synthesis, Characterization, and Electrochemistry of sigma-Bonded Cobalt Corroles in High Oxidation States", Inorg. Chem., 35, pp. 5577-5583, 1996.
132. D. Aviezer, S. Cotton, M. David, A. Segev, N. Khaselev, N. Galili, Z. Gross, and A. Yayon, "Porphyrin Analogues as Novel Antagonists of Fibroblast Growth Factor and Vascular Endothelial Growth Factor Receptor Binding That Inhibit Endothelial Cell Proliferation, Tumor Progression, and Metastasis", Cancer Research, 60, pp. 2973-2980, 2000.
133. A. Mahammed, HB .Gray, JJ. Weaver, K. Sorasaenee, and Z. Gross, "Amphiphilic corroles bind tightly to human serum albumin", Bioconj.Chem., 15, pp.738-746, 2004.
134. R. Paolesse, in: K.M. Kadish, K.M. Smith, R. Guilard (Eds.), "The Porphyrin Handbook," vol. 2, Academic Press, New York, pp. 201, 2000.
135. R. Guilard, J.-M. Barbe, C. Stern,and K.M. Kadish, in: K.M. Kadish, K.M. Smith, R. Guilard (Eds.), "The Porphyrin Handbook", vol. 18, Elsevier Science, USA, pp.351, 2000.
136. DT. Gryko, JP. Fox, DP. Goldberg, ," Recent advances in the chemistry of corroles and core-modified corroles", J. Porphyrins Phthalocyanines, 8, pp. 1091-1105, 2004.
137. M. Drobizhev, F. Meng, A. Rebane, Y. Stepanenko, E. Nickel, CW. Spangler, "Strong Two-Photon Absorption in New Asymmetrically-Substituted Porphyrins: Interference between Charge-Transfer and Intermediate-Resonance Pathways", J. Phys. Chem., 110, pp. 9802-9814, 2006.
138. M. Morone, et al.," Enhancement of Two-Photon Absorption Cross-Section and Singlet-Oxygen Generation in Porphyrins upon β-Functionalization with Donor−Acceptor Substituents", Org. Lett., 8, pp. 2719-2722, 2006.
139. M. Drobizhev, NS. Makarov, A. Rebane, G. de la Torre, T. Torres," Strong two-photon absorption in push-pull phthalocyanines: role of resonance enhancement and permanent dipole moment change upon excitation", J. Phys. Chem., 112, pp. 848-859, 2008.

140. E. Collini, et al.," Large two photon absorption cross section of asymmetric Zn(II) porphyrin complexes substituted in the meso or b pyrrolic position by –C„C–C6H4X moieties (X = NMe2, NO2)", Chem. Phys. Lett., 454, pp. 70-74, 2008.
141. A. Rebane, et al.," Quantitative prediction of two-photon absorption cross section based on linear spectroscopic properties",J. Phys. Chem., 112, pp. 7997-8004, 2008.
142. A. Mahammed, and Z. Gross, "Aluminum corrolin, a novel chlorophyll analogue", J. Inorg. Biochem., 88, pp. 305-309, 2002.
143. D. Kowalska, et al. "Ground- and Excited-State Dynamics of Aluminum and Gallium Corroles ",Inorg. Chem., 48, pp. 2670-2676, 2009.
144. X. Liu, A. Mahammed, U. Tripathy, Z. Gross, and RP. Steer, "Photophysics of Soret-excited tetrapyrroles in solution. III. Porphyrin analogues: Aluminum and gallium corroles ", Chem. Phys. Lett., 459, pp.113-118, 2008.
145. L. Wagnert, et al., "Exploring the photo excited triplet states of aluminum and tin corroles by time-resolved Q-band EPR ", Applied Magnetic Resonance, 30, pp.591-604, 2006.
146. Galvez, and J. Enrique, "Gaussian beams in the optics course", Am. J. Phys., 74, pp. 355- 361, 2006.
147. R. Sailaja, PB. Bisht, CP. Singh, KS. Bindra, and SM. Oak, "Influence of multiphoton events in measurement of two-photon absorption cross-section and optical nonlinear parameters under femtosecond pumping", Opt. Commun., 277, pp. 433–439, 2007.
148. N.S. Makarov, M. Drobizhev, and A. Rebane, "Two-photon absorption standards in the 550–1600 nm excitation wavelength range", Opt. Express, 16, pp. 4029–4047, 2008.
149. P. Sengupta, J. Balaji, S. Banerjee, R. Philip, R.G. Kumar, and S. Maiti, "Sensitive measurement of absolute two-photon absorption cross sections", J. Chem. Phys., 112, pp. 9201–9205, 2000.
150. MD. Galanin, and ZA. Chizhikova, "Effective Cross Sections of Two-Photon Absorption in Organic Molecules", JETP. Lett., 4, pp. 27-28, 1966.
151. JP. Hermann and J. Ducuing, "Absolute Measurement of Two-Photon Cross Sections", Phys. Rev., 5, pp. 2557-2568, 1972.

152. JM. Song, T. Inoue, H. Kawazumi, and T. Ogawa, "Determination of Two-Photon Absorption Cross Section of Fluorescein Using a Mode locked Titanium Sapphire Laser", Anal. Sci., 15, pp. 601-603, 1999.

153. RR. Birge, JA. Bennett, BM. Pierce, and TM. Thomas, "Two-Photon Spectroscopy of the Visual Chromophores. Evidence for a Lowest Excited $^{1}Ag^{-}$ -Like ππ* St ate in all-trans-Retinol (Vitamin A)", J. Am. Chem. Soc. 100, pp. 1533- 1539, 1978.

154. G. Weber, DM. Hercules (Ed.), "Fluorescence and Phosphorescence Analysis: principles and applications", Inter. science, Wiley, New York, pp. 217-240, 1966.

155. F. Holland John, E. Teets Richard, M. Kelly Patrick, and Tlmnlck Andrew," Correction of Right-Angle Fluorescence Measurements for the Absorption of Excitation Radiation", Analyst. Chem., 49, pp.706-710, 1977.

156. J. W. Longworth, "Techniques for measuring fluorescence and phosphorescence of biological materials", Photochem. Photobiol., 8, pp.589- 599, 1968.

157. CA. Parker, and WJ. Barnes," Some Experiments with Spectrofluorimeters and Filter Fluorimeters", Analyst., 82. pp. 606-618, 1957.

158. H. Braunsberg, and SB. Osborn, "Some general aspects of fluorimetric determinations," Anal. Chim. Acta 6, pp. 84-95, 1952.

159. WE. Ohnesorge, " Effects of sample cell position and dimensions on the fluorescence intensity-concentration curve for "perpendicular-type" fluorimeters", Anal. Chim. Acta., 31, pp. 484-487, 1964.

160. J. E. Gill, "Measurement of relative quantum yields of strongly absorbing solutions", Appl. Spectrosc., 24, pp.588-590, 1970.

161. M. Ehrensberg, E. Cronvall, and R. Rigler," Fluorescence of proteins interacting with nucleic acids. Correction for light absorption", FEBS. Lett., 18, pp. 199-203, 1971.

162. JS. Franzen, I. Kuo, and AE. Chung," Binding ratios by fluorescence with self-compensation for optical inner filter effects", Anal. Biochem., 47, pp. 426-441, 1972.

163. J. Ambjerg, A. Jiménez-Banzo, MJ. Paterson, S. Nonell, JI. Borrell, O. Christiansen, and PR. Ogilby, "Two-photon absorption in tetraphenylporphy- cenes: are porphycenes better candidates than porphyrins for providing optimal optical properties for two-photon photodynamic therapy", J. Am. Chem. Soc. 129, pp. 5188–5199, 2007.

164. LTh. Bergendahl, and MJ. Paterson, "Two-photon absorption in porphycenic macrocycles: the effect of tuning the core aromatic electronic structure", J. Chem. Commun. 48, pp. 1544-1546, 2012.

165. M. Drobizhev, F. Meng, A. Rebane, Y. Stepanenko, E. Nickel, and ChW. Spangler, "Strong two-photon absorption in new asymmetrically subctituted porphyrins: interference between charge-transfer and intermediate-resonance pathways", J. Phys. Chem., 110, pp. 9802-9814, 2006.

166. M. Drobizhev, N.S. Makarov, S.E. Tillo, T.E. Hughes, A. Rebane, "Two-photon absorption properties of fluorescent proteins", Nature Meth., 8, pp. 393 – 399, 2011.

167. A.Nag, and D. Goswami, "Solvent effect on two-photon absorption and fluorescence of rhodamine dyes", J. Photochem. Photobiol., 206, pp. 188 –197, 2009.

168. P. Macak, Y. Luo, and H. Ågren, "Simulations of vibronic profiles in two-photon absorption", Chem. Phys. Lett. 330, pp. 447–456, 2000.

169. Rebane, M. Drobizhev, N. S. Makarov, B. Koszarna, M. Tasior, D. T. Gryko, "Two-photon absorption properties of meso-substituted A3-corroles", Chem. Phys. Lett.462, pp. 246 – 250, 2008.

170. A. Karotki, M. Drobizhev, M. Kruk, CW. Spangler, E. Nickel, N. Mamardashvili, and A. Rebane," Enhancement of two-photon absorption in tetrapyrrolic compounds ", J. Opt. Soc. Am., 20, pp. 321-332, 2003.

171. M. Drobizhev, A. Karotki, M. Kruk, and A. Rebane," Resonance enhancement of two-photon absorption in porphyrins", Chem. Phys. Lett., 355, pp. 175-182, 2002.

172. M. Drobizhev, A. Karotki, M. Kruk, N. Mamardashvili, and A. Rebane," Drastic enhancement of two-photon absorption in porphyrins associated with symmetrical electron-accepting substitution", Chem. Phys. Lett., 361, pp. 504-512, 2002.

173. M. Drobizhev, N.S. Makarov, Y. Stepanenko, and A. Rebane," Near-infrared two-photon absorption in phthalocyanines: enhancement of lowest gerade-gerade transition by symmetrical electron-accepting substitution", J. Chem. Phys., 124, pp. 224701-224712, 2006.

174. WJ. Meath, and EA. Power, "On the importance of permanent moments in multiphoton absorption using perturbation theory", J. Phys., 17, pp. 763–781, 1984.

175. MA. C. Nascimento, “The polarization dependence of 2-photon absorption rates for randomly oriented molecules”, Chem. Phys., 74, pp. 51–66, 1983.

176. EA. Power, “Two-photon circular dichroism”, J. Chem. Phys., 63, pp. 1348–1350, 1975.

177. I. Tinoco, “Two-photon circular dichroism”, J. Chem. Phys., 62, pp. 1006–1009, 1975.

178. M. Albota, D. Beljonne, JL. Brédas, JE. Ehrlich, JY. Fu, AA. Heikal, SE. Hess, T. Kogej, MD. Levin, SR. Marder, D. McCord-Maughon, JW. Perry, H. Röckel, M. Rumi, G. Subramaniam, WW.Webb, XL. Wu, and C. Xu,” Design of organic molecules with large two-photon absorption cross sections”, Science, 281, pp. 1653-1655, 1998.

179. T. Kogej, D. Beljonne, F. Meyers, JW. Perry, SR. Marder, and JL. Bredas,” Mechanisms for enhancement of two-photon absorption in donor–acceptor conjugated chromophores”, Chem. Phys. Lett., 298, pp. 1-6, 1998.

180. BR. Cho, KH. Son, SH. Lee, YS. Song, YK. Lee, SJ. Jeon, JH. Choi, H. Lee, and M. Cho,”Two photon absorption properties of 1,3,5-tricyano-2,4,6-tris(styryl)benzene derivatives”, J. Am. Chem. Soc., 123, pp.10039-10045, 2001.

181. W. Denk, JH. Strickler, and WW. Webb,” Two-Photon Laser Scanning Fluorescence Microscopy”, Science, 248, pp.73-76, 1990.

182. J. Arnbjerg, A. Jimenez-Banzo, MJ. Paterson, S. Nonell, JI. Borrell, O.Christiansen, and PR. Ogilby, “Two-photon absorption in tetraphenylporphycenes: Are porphycenes better candidates than porphyrins for providing optimal optical properties for two-photon photodynamic therapy”, J. Am. Chem. Soc., 129, pp.5188-5199, 2007.

183. TC. Lin, GS. He, Q. Zheng, and PN. Prasad, “Degenerate two-/three-photon absorption and optical power-limiting properties in femtosecond regime of a multi-branched chromophore”, J. Mater. Chem. 16, pp.2490-2498, 2006.

184. GI. Stegeman, in Handbook of Optics IV: Fiber Optics and Nonlinear Optics, 2nd ed., edited by M. Bass, JM. Enoch, EW. Van. Stryland, and WL. Wolfe, McGraw-Hill, New York, Chap. 21, 2001.

185. PR. Monson, and WM. McClain, “Polarization dependence of the two-photon absorption of tumbling molecule with application to liquid 1-chloronaphthalene and benzene”, J. Chem. Phys., 53, pp.29-37, 1970.

186. WM. McClain, “Two-photon molecular spectroscopy”, Acc. Chem. Res., 7, pp.129-135, 1974.

187. MAC. Nascimento, “The polarization dependence of two-photon absorption rates for randomly oriented molecules”, Chem. Phys., 74, pp. 51–66, 1983.

188. I. Tinoco, “Two-Photon Circular Dichroism”, J. Chem. Phys., 62, pp.1006-1009, 1975.

189. RW. Woody, “The excitation model and the circular dichroism of polypeptides”, Monatsh. Chem., 136, pp.347-366, 2005.

190. Olesiak-Banska, H. Mojzisova, D. Chauvat, M. Zielinski, K. Matczyszyn, P. Tauc, and J. Zyss, “Liquid crystal phases of DNA: evaluation of DNA organization by two-photon fluorescence microscopy and polarization analysis”, Biopolymers 95(6), pp. 365–375, 2011.

191. H. Mojzisova, J. Olesiak, M. Zielinski, K. Matczyszyn, D. Chauvat, and J. Zyss, “Polarization-sensitive two photon microscopy study of the organization of liquid-crystalline DNA”, Biophys. J. 97(8), pp. 2348–2357, 2009.

192. P. Macak, Y. Luo, P. Norman, and H. Agren, J. Chem. Phys., 113, pp.7055-7061, 2000.

193. CK. Wang, P. Macak, Y. Luo, and H. Agren,” Effects of π centers and symmetry on two-photon absorption cross sections of organic chromophores”, J. Chem. Phys., 114, pp.9813-9820, 2001.

194. D. Wanapun, RD. Wampler, NJ. Begue and GJ. Simpson,”Polarization-dependent two-photon absorption for determination of protein secondary structure: A theoretical study”, Chem.Phys. Lett., 455, pp.6-12, 2008.

195. L. De Boni, C. Toro, and FE. Hernandez,” Synchronized double L-scan technique for the simultaneous measurement of polarization-dependent two-photon absorption in chiral molecules”, Opt. Lett., 33, pp.2958-2960, 2008.

196. A. Nag, and D. Goswami, “Polarization induced control of single and two-photon fluorescence”, J. Chem. Phys., 132, pp.154508, 2010.

197. Luo, P. Norman, P. Macak, and H. Ågren, “Solvent-induced two-photon absorption of a push-pull molecule”, J. Phys. Chem., 104, pp. 4718–4722, 2000.

198. CK.Wang, K. Zhao, Y. Su, R. Yan, X. Zhao, and Y. Luo, “Solvent effects on the electronic structure of a newly synthesized two-photon polymerization initiator”, J. Chem. Phys., 119, pp. 1208–1213, 2003.

199. Frediani, Z. Rinkevicius, and H. Ågren, “Two-photon absorption in solution by means of time-dependent density-functional theory and the polarizable continuum model”, J. Chem. Phys., 122 , pp. 244104-1–244104-12, 2005.

200. K. Zhao, L. Ferrighi, L. Frediani, CK.Wang, and Y. Luo, “Solvent effects on two-photon absorption of dialkylamino substituted distyrylbenzene chromophore”, J. Chem. Phys., 126, pp. 204509-1–204509-6, 2007.

201. HY. Woo, B. Liu, B. Kohler, D. Korystov, A. Mikhailovsky, and GC. Bazan, “Solvent effects on the two-photon absorption of distyrylbenzene chromophores”, J. Am. Chem. Soc., 127, pp. 14721–14729, 2005.

202. Fitilis, M. Fakis, I. Polyzos, V. Giannetas, P. Persephonis, P. Vellis, and J. Mikroyannidis, “A two-photon absorption study of fluorene and carbazole derivatives. The role of the central core and the solvent polarity”, Chem. Phys. Lett., 447, pp. 300–304, 2007.

203. Y. Yan, B. Li, K. Liu, Z. Dong, X.Wang, S. Qian, “Enhanced two-photon absorption and ultrafast dynamics of a new multibranched chromophore with a dibenzothiophene core”, J. Phys. Chem., 111, pp. 4188–4194, 2007.

204. Reichardt, “Solvatochromic dyes as solvent polarity indicators”, Chem. Rev. 94, pp. 2319–2358, 1994.

205. J.R. Lakowicz, “Principles of Fluorescence Spectroscopy”, third ed., Springer Science Publishers, New York, pp. 205–235, 2006.

206. Buncel, S. Rajagopal, “Solvatochromism and solvent polarity scales”, Acc. Chem. Res. 23, pp. 226–231, 1990.

207. LM. Tao, K. Zhao, YH. Sun, and CK. Wang, J. At. Mol. Phys., 21, pp. 111, 2004.

208. K. Zhao, L. Ferrighi, L. Frediani, C. K. Wang, and Y. Luo "Solvent effect on two-photon absorption of dialkylamino substituted distyrylbenzene chromophore”, J. Chem. Phys. 126 (204509), 2007.

209. CK. Wang, K. Zhao, Y. Su, Y. Ren, X. Zhao, and Y. Luo, “Solvent effects on the electronic structure of a newly synthesized two-photon polymerization initiator“, J. Chem. Phys., 119, pp.1208-1213, 2003.
210. T. Wakebe, E.V. Keuren, “The excitation spectra of two photon induced fluorescence in xanthenes dyes”, Jpn. J. Appl. Phys., 38, pp. 3556–3561, 1999.
211. J. Jobson, Z. Rahman, and G. A. Woodell, "A Comparison of the Multiscale Retinex with Other Image Enhancement Techniques”, Proceedings of the IS&T’s 50th P Annual Conference, Cambridge, MA, 1997.
212. Rafael C. Gonzales, and Richard E. Woods," Digital Image Processing", second edition, Prentice Hall, 2002.
213. Li. Tao and V. Asari, "An integrated neighborhood dependent approach for nonlinear enhancement of color images", International Conference on Information Technology: Coding Computing; ITCC, pp. 138-139, 2004.
214. D. Jabson, Z. Rahman, and GA. Woodel, “A multi-scale retinex for bridging the gap between color images and the human observation of scenes”, IEEE Trans. Image Process.6, pp. 965 - 976, July 1997.
215. J. Jobson, Z. Rahman, and GA. Woodell, "Properties and performance of a center/surround retinex", IEEE Trans. on Image Processing 6, pp. 451–462, March 1996.
216. K. Barnard, and B. Funt, "Analysis and Improvement of Multi-ScaleRetinex" In Proceedings of the IS&T/SID Fifth Color Imaging Conference: Color Science, Systems and Applications“, Scottsdale, Arizona, pp. 221-226, 1997.

Erklärung der Selbstständigkeit

Hiermit versichere ich, die vorliegende Arbeit selbstständig verfasst und anderen als die angegebenen Quellen und Hilfsmittel benutzt sowie die Zitate deutlich kenntlich gemacht zu haben. Die Arbeit ist weder in einem früheren Promotionsverfahren angenommen noch als ungenügend beurteilt worden.

Berlin, den 24.07.2015

Baidaa Hamed